The Development of a New Lightning-Frequency Parameterization and its Implementation in a Weather Prediction Model

Dissertation

Fakultät für Physik
Ludwig-Maximilians-Universität
München

Dipl.-Met. Johannes M. L. Dahl,
Berlin

Eingereicht am 24.02.2010

Gutachter der Dissertation:

1. Gutachter: apl. Prof. Dr. U. Schumann
2. Gutachter: Prof. Dr. G. C. Craig

Tag der mündlichen Prüfung: 23.03.2010

Contents

Zusammenfassung

Basierend auf einem einfachen physikalischen Modell wurde eine neue Blitz-Parametrisierung entwickelt. Hierbei repräsentiert ein Plattenkondensator die grundlegende Dipol-Ladungsstruktur einer Gewitterwolke. Dieser Kondensator wird kontinuierlich durch einen Generator-Strom aufgeladen und durch Blitzentladungen entladen. In dem hier verfolgten Ansatz werden der Generatorstrom sowie die Stärke der Entladungen mithilfe des Graupelmasse-Feldes parametrisiert. Aus diesen beiden Größen kann die Blitzfrequenz eindeutig bestimmt werden, wenn sich Generator- und Entladungs-Strom im Gleichgewicht befinden. Mit diesem Ansatz können Unzulänglichkeiten früherer theoretischer Überlegungen, bei der die Blitzrate beispielsweise mit der Leistung des Gewitters in Verbindung gesetzt wird, behoben werden.

Um diesen Ansatz zu testen, wurden polarimetrische Doppler-Radar-Daten benutzt, mittels derer die Graupelverteilung in beobachteten Gewittern ermittelt werden konnte. Die Blitz-Aktivität wurde mithilfe des LINET-Netzwerks bestimmt. Der Vergleich zwischen theoretisch vorhergesagten und beobachteten Blitzraten ist ermutigend: Für isolierte Gewitterzellen liefert der theoretische Ansatz genaue Ergebnisse. Zwei bereits existierende Parametrisierungen, in denen die vertikale Wolkenmächtigkeit zur Beschreibung der Blitzrate verwendet wird, zeigen deutlich weniger Güte.

Diese beiden existierenden Ansätze, der im Kontext dieser Arbeit neu entwickelte Ansatz sowie ein weiterer, welcher auf der Vertikalgeschwindigkeit im Aufwind des Gewitters beruht, wurden in das Wettervorhersagemodell COSMO-DE implementiert. Mit diesem Modell wurden reale Gewitter-Szenarios simuliert. Die Güte der Parametrisierungen anhand modellierter Konvektion zu testen ist schwierig, da es generell keine eindeutige Zuordnung zwischen beobachteten und modellierten konvektiven Wolken gibt. Für Fälle, in denen ein direkter Vergleich zwischen simulierten und beobachteten Gewitterzellen möglich war, waren die Ergebnisse ebenfalls vielversprechend. Ein Vergleich der gesamten Blitzaktivität in einem Gebiet, das v.a. den Süden Deutschlands beinhaltet, zeigt, dass keiner der implementierten Ansätze die Blitzaktivität zufriedenstellend widerspiegelt. Dies ist v.a. darin begründet, dass im COSMO-DE die Gewitterzellen nicht in der korrekten Anzahl und zur korrekten Zeit entstehen.

Abstract

Based on a straightforward physical model, a new lightning parameterization has been developed: A two-plate capacitor represents the basic dipole charge structure of a thunderstorm, which is charged by the generator current and discharged by lightning. In this approach, the generator current as well as the discharge strength are parameterized using the graupel-mass field. If these two quantities are known, and if the charging and discharging are in equilibrium, then the flash rate is uniquely determined. This approach remedies shortcomings of earlier theoretical approaches that relate the flash rate e.g., to generator power. No distinction is made between intracloud and cloud-to-ground discharges.

In order to test this approach, polarimetric radar data were used, from which the graupel distribution in observed thunderstorms could be inferred. The lightning activity was detected using the LINET network. The comparison between theoretically-predicted and measured flash rates is encouraging: Over a wide range of flash rates, the theoretical approach yields accurate results for isolated thunderstorms. Two existing parameterizations, which only use the depth of the clouds as predictor, produce substantially less accurate forecasts.

These two existing approaches, the one developed in this study, as well as a fourth one based on updraft velocity, were implemented in the convection-resolving COSMO-DE numerical weather prediction model. With this model, real-world convective scenarios were simulated. The output of the lightning scheme includes the location and time of every simulated discharge. Testing the performance of the parameterizations with modeled convection is difficult as there is no one-to-one correspondence between observed and modeled convective clouds. Where a comparison between modeled and observed flash rates of individual clouds was possible, the results for individual cells were promising.

The comparison of the bulk lightning activity over an area comprising southern Germany and adjacent countries suggests that none of the four parameterizations captures the overall lightning activity well. This is mainly because COSMO-DE does not simulate the observed number of cells at the correct times.

Chapter 1

Introduction

Atmospheric lightning is associated with a variety of meteorological and geophysical phenomena, deep moist convection arguably being the most common among these. Besides, lightning is known to accompany volcanic ash plumes and dust storms (Uman, 2001, p. 26), and it may even be associated with piezoelectric effects preceding earthquakes (Finkelstein and Powell, 1970). However, these types of lightning shall not be the subject of this study, but only those that are associated with thunderstorms. Given the spectacular visual and acoustic manifestation of thunderstorm discharges, as well as the threat to life and property posed by them, they have always fascinated mankind and they have been a persisting subject of research efforts.

With the advent of numerical models, deep convective clouds could be simulated (Klemp and Wilhelmson, 1978) and soon electrification models were included. In 1982, Rawlins (1982) first considered charging and discharging processes but no lightning channels yet. Helsdon and Farley (1987) simulated channel propagation using a two-dimensional model. Nowadays, advanced three-dimensional cloud models are equipped with sophisticated electrification schemes (e.g., Mansell, 2000; MacGorman et al., 2001; Barthe et al., 2005). These make use of the results from laboratory experiments (e.g., Takahashi, 1978; Jayaratne, 1998; Saunders and Peck, 1998), which determine the magnitude and direction of charge transfers during hydrometeor collisions. Dielectric breakdown is modeled explicitly by initiating lightning channels which exhibit realistic branching and propagation (Mansell, 2000).

These parameterizations were implemented in cloud models and more recently in convection-resolving mesoscale models (Barthe et al., 2005).

A sophisticated analytical model involving a basic dipole charge structure was developed by Driscoll et al. (1992). In their model, the generator current, the lightning current, and other parameters need to be prescribed to determine the average current towards the ionosphere.

Another approach was stimulated by Vonnegut (1963), who suggested that the

electrical power of a storm can be determined if the flash rate and the flash energy are known. This idea was further developed by Williams (1985) who proposed that the flash rate varies linearly with storm power. After several assumptions mainly about storm geometry, he found that the lightning rate varies as the 5th power of the cloud-top height. This result was condensed into a separate parameterization by Price and Rind (1992). Similarly, the lightning frequency has been linearly related to the charging current (Blyth et al., 2001; Deierling et al., 2008; Yoshida et al., 2009). Other investigators have found correlations between the lightning rate and the convective rainfall rate (e.g., Chéze and Sauvageot, 1997; Tapia et al., 1998). In their essence, all these are "single-parameter" approaches as they relate the flash rate to a single predictor.

These approaches only consider the charging of the cloud while making implicit and partly unphysical assumptions about the neutralization of the charge during a lightning flash. By employing a straightforward physical model in this study, this shortcoming is remedied. This model involves a two-plate capacitor which is applied to convective clouds. Since the charging is parameterized by merely considering the graupel-mass field, this model is less sophisticated than those by Barthe et al. (2005) and Mansell (2000). Also, the lightning channels are not explicitly modeled and only the instantaneous lightning rate is determined. Moreover, no distinction is made between cloud-to-ground and intra-cloud discharges. However, the location and time of each flash are determined, so that an accurate display of the simulated flashes is possible, directly comparable to measurements by lightning-detection networks. As such, the underlying physical model as well as the products yielded by the lightning scheme, may be considered to be a compromise between the highly sophisticated approaches and the single-parameter approaches. The latter ones are usually implemented such that a flash-rate value is depicted for each gridbox (e.g., Price and Rind, 1992). These approaches were intended mostly for applications on the global scale (Price and Rind, 1992; Tost et al., 2007; Yoshida et al., 2009) and the highly-sophisticated schemes are mostly used either in cloud models or in idealized studies with convection-resolving mesoscale models. Since the main application of the scheme developed herein is real-world scenarios, the intermediate degree of sophistication seems to be an appropriate choice.

Apart from the obvious purpose of general thunderstorm forecasting, which is the basis for warnings, the lightning forecasts are useful in other respects, as well: A lightning scheme that is capable of realistic predictions of the lightning activity of individual convective cells, may be used to assess the skill of the model's microphysics scheme. Also, the accuracy of modeled convective initiation may be revealed by lightning simulations. The lightning activity integrated over an entire day comfortably reveals a summary of that day's convective activity at one glance

(in convection-resolving models, there is no distinction between convective and non-convective precipitation; thus the accumulated precipitation field would not provide such a clear picture).

Lightning plays an important role in atmospheric chemistry. Chemical reactions in the lightning channel result in the creation of nitrogen oxides, NO_x (Schumann and Huntrieser, 2007; Grewe, 2009; Pickering et al., 2009). Schumann and Huntrieser (2007) estimate the total equivalent mass of lightning-produced NO_x to be 5 ± 3 Tg per year. Lightning NO_x (often referred to as LNO_x) affects the free-atmospheric ozone production, which in turn acts as greenhouse gas. LNO_x may thus be considered as indirect greenhouse gas, and its emission is an important factor in climate-change scenarios.

The simulations may also provide insight into the thermodynamic and kinematic environments of thunderstorms in relation to their electrical activity. Apart from that, there has been a long discussion about the processes that govern the flash rate (e.g., Boccippio, 2002; Yoshida et al., 2009). With the straightforward approach pursued in this work, some of these question could be answered (e.g., is the flash rate proportional to the electric power that the storm generates, or to the charging current?).

1.1 Thesis goals and outline

The specific goals of this study are to

- develop a new method to diagnose the flash rate in a thunderstorm cloud,

- implement this method in the COSMO-DE model,

- implement three existing parameterizations in COSMO-DE,

- test the new method with observed thunderstorm clouds and compare the predictions with results from existing parameterizations,

- apply all parameterizations to simulations of real-world scenarios,

- compare the simulation results based on the different parameterizations.

In chapter 2, a brief overview of dynamics of convective storms, charging processes, and lightning discharges will be provided. Also, approaches to diagnosing the flash rate will be presented. Chapter 3 is devoted towards the new parameterization of the lightning frequency. Chapter 4 deals with the implementation of the parameterization into COSMO-DE. In chapter 5, the parameterization will be tested using radar data. Results of COSMO-DE simulations are shown in chapter 6. The results

of the test and the simulations will be discussed in chapter 7. A summary and suggestions for future work are offered in chapter 8.

The units of all variables appearing in the equations are SI units unless stated otherwise. Following the convention in lightning research, a cloud is said to be "electrified" when it produces lightning.

Chapter 2

Background

2.1 Thunderstorm structures

A thunderstorm is a complex phenomenon, which involves updrafts, downdrafts, and precipitation processes which are all interacting with each other. Arguably, the heart of a thunderstorm is its updraft: Hydrometeor and downdraft formation, as well as all other processes accompanying a thunderstorm are secondary effects which would not occur if no updraft had existed previously. Hence, this section will focus on the physics of deep, free convective updrafts.

2.1.1 Deep moist convection

The necessary, albeit not sufficient condition for such a moist buoyant updraft to arise, is the existence of conditional instability and moisture. These may be combined in a single quantity, the *convective available potential energy* (CAPE). CAPE is the potential energy of a parcel due to thermal buoyancy,

$$\text{CAPE} = R \int_{p(z_2)}^{p(z_1)} T_v{'} \, d(\ln p), \tag{2.1}$$

where R is the individual gas constant of dry air, $T_v{'}$ is the virtual temperature perturbation due to the parcel, p is pressure, and the heights z_1 and z_2 bound the region where free ascent occurs.

Usually, the air parcels making up the convective cell have to be lifted somewhat before becoming positively buoyant. This stable region is characterized by the *convective inhibition*, CIN, which is the energy required to overcome this layer. The level at which the free ascent commences is referred to as *level of free convection* (LFC). The level where the parcel's temperature equals the environmental temperature, is called *equilibrium level* (EL). It follows, that for a deep, moist convective updraft to develop, conditional instability, moisture, and lift need to coincide (Doswell, 1987;

Johns and Doswell, 1992). An example of a sounding with positive CAPE is shown in Fig. 2.1.

2.1.2   Organization of convection

Once a convective updraft has formed, precipitation particles develop and fall through the updraft, which gradually weakens and eventually completely diminishes as a consequence. The life cycle of such a convective system was categorized into three stages, i.e., the cumulus stage, the maturity stage, and the dissipation stage by Byers and Braham (1949). These authors defined the maturity stage to commence as precipitation begins reaching the ground. In the dissipation stage, merely the cool, precipitation-laden downdraft is left. The time scale of this entire process is on the order of 30 min. Though rarely met in nature, this single-cellular form of storm structure represents the archetype of a weakly-organized convective system.

At the other end of the spectrum, there are well-organized, long-lived and often quite severe thunderstorms. A key to storm organization is vertical wind shear. There are at least three reasons that wind shear is supportive of storm organization: i) Updrafts and downdrafts become laterally separated, reducing the demise of the updrafts as precipitation forms and falls within them (e.g., Houze, 1993); ii) a vertically-sheared flow contains horizontal vorticity, which may be tilted into the vertical by updrafts (e.g., Davies-Jones, 1984), and rotation of the thunderstorm cell may ensue. In many circumstances, this vorticity is thought to reduce the turbulent energy cascade within the updraft, and hence increase its longevity and strength (e.g., Lilly, 1986); iii) a non-hydrostatic pressure field develops in and around updrafts in sheared environments (Rotunno and Klemp, 1982; Davies-Jones, 2002). A dramatic example of a storm in strong shear is the supercell (Rotunno, 1993; Doswell and Burgess, 1993), which possesses a long-lived, rotating updraft, and whose dynamics is dominated by dynamic perturbation pressure gradient forces (Rotunno, 1993). An example of a supercell storm is shown in Fig. 2.2. The reflectivity as well as the doppler velocity fields are shown, nicely displaying the supercell's hook echo as well as the mesocyclonic circulation.

The dynamics of linearly-organized storms, like squall lines, is dominated by the pressure field that develops in and around the precipitation-generated cold pool (Trapp and Weisman, 2003; Weisman, 2001; Weisman et al., 1988). Though the gustfront also plays a role in supercell dynamics, a supercell can be sustained in the absence of gustfronts[1], while squall lines cannot.

This spectrum is continuous, with structures like squall lines and supercells

---

[1]So-called low-precipitation supercells (Bluestein and Parks, 1983) are an example of this.
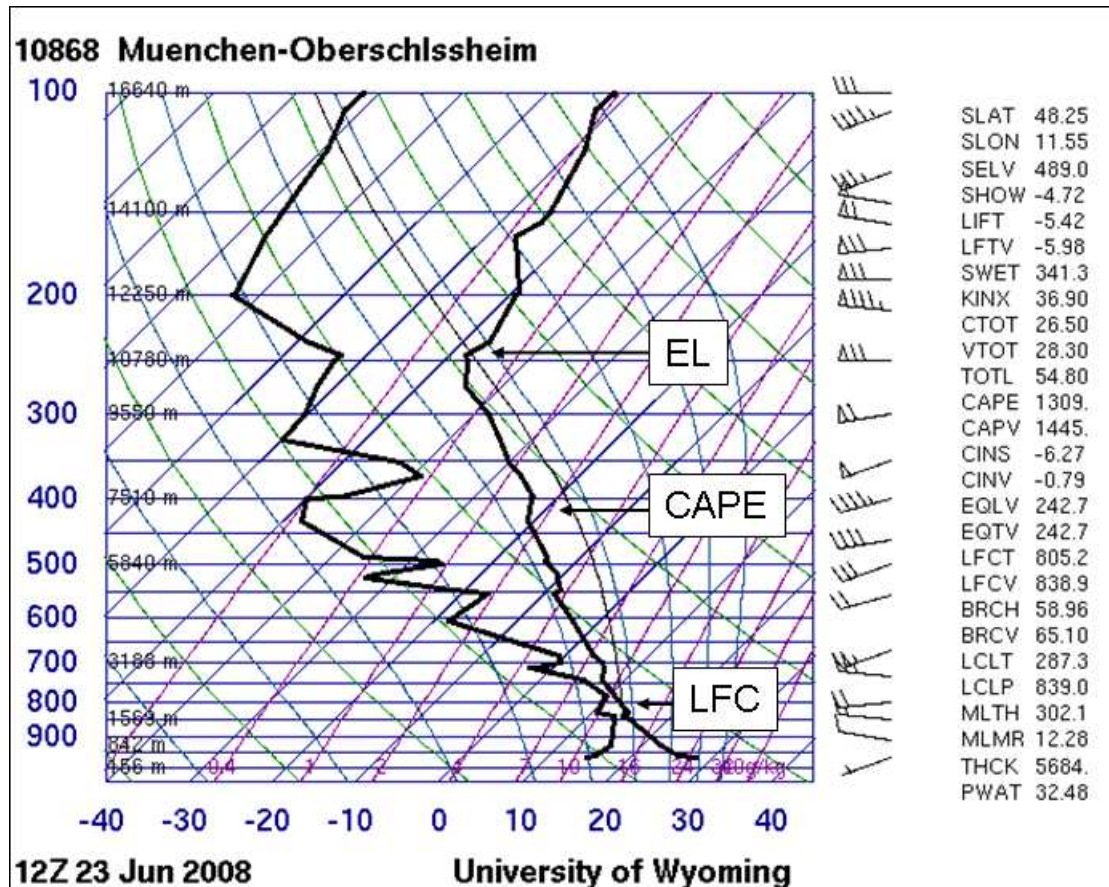
Figure 2.1: Skew T-log p diagram from München-Oberschleissheim on 23 June 2008, 12 UTC. Wind barbs: pennant = 25 ms^{-1}; long barb = 5 ms^{-1}; short barb = 2.5 ms^{-1}. The list on the right shows several convective parameters, including the virtual-temperature corrected mixed-layer CAPE (CAPV) and the corresponding CIN value (CINV). The sampled air mass is minimally capped (CINV = -0.79 J kg^{-1}), rather unstable (CAPV = 1,445 J kg^{-1}) and strongly sheared (about 40 knots ($\approx$ 20 ms^{-1}) in the lowest 6 km). Supercells that produced large hail formed later that day in this air mass. Image courtesy of the University of Wyoming.

placed at the well-organized end, and the short-lived single cell at the weakly-organized end of the spectrum. Multicellular storms that share a common gust-front and that are organized in the mesoscale are referred to as *mesoscale convective system* (MCS) (NCAR, 1984). The most prominent type of MCS is a squall line.
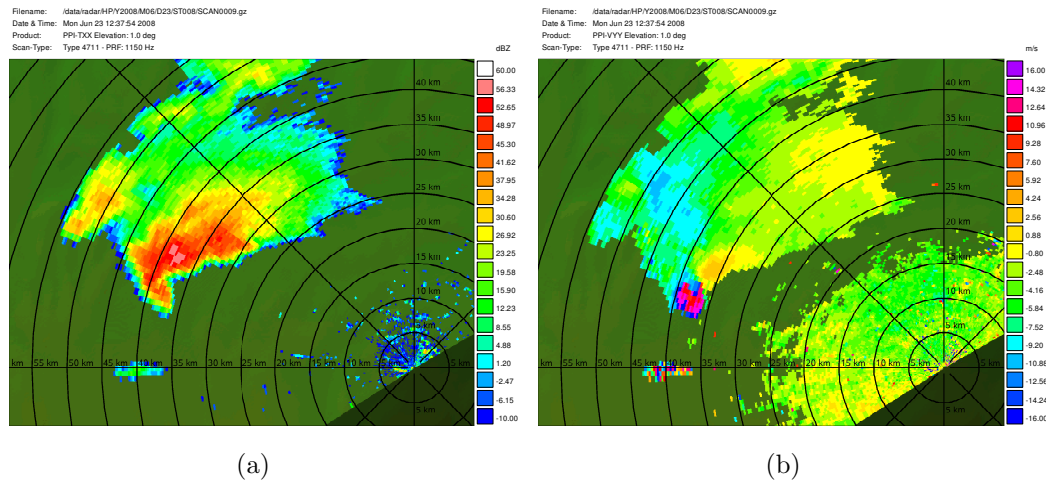
Figure 2.2: POLDIRAD PPI images of a supercell on 23 June 2008. (a) shows the reflectivity field, displaying a well-pronounced hook echo (appendage to the southwest of the main echo). (b) shows the radial-velocity signature of a mesocyclone where the hook echo is located.

2.2   Charging mechanisms of thunderclouds

Non-inductive charging   The basic charging process is believed to occur during collisions between graupel pellets with ice crystals and subsequent sedimentation that results from the different terminal fall velocities of both hydrometeor classes (e.g., Takahashi, 1978). The underlying theory is called *relative growth rate* (RGR) theory (Baker et al., 1987): Charge transfer during hydrometeor collisions proceeds according to the following rule: Of two colliding particles, the one with the larger depositional growth rate charges positively due to the loss of negative charge. The one with the lower depositional growth rate charges negatively (Dash et al., 2001; Saunders, 2008). The reason for the surface charge is the formation of an electric double layer which forms as a result of ion defects in the lattice structure during depositional growth. The stronger this growth, the more surface charge accumulates. The ion defects are associated with broken bonds of the H_2O molecules. As the H^+ ions are rather mobile, they diffuse towards the interior of the particle while the OH^- ions remain close to the surface owing to their remaining hydrogen bond (e.g., Saunders, 2008). Note that the riming of graupel pellets also affects its depositional

growth rate as only part of a captured supercooled droplet freezes because of latent-heat release. This may locally increase the degree of ice supersaturation.

Transferring this rule to a natural deep convective cloud, the result is a selective charge transfer between riming graupel pellets and ice crystals. This charge transfer changes sign at a certain temperature, the so-called *charge-reversal temperature*. The typical configuration of a natural deep convective cloud is such that the graupel attains negative charge roughly above the 263 K level (and the ice crystals gain positive charge), i.e., there is a transfer of negative charge from the ice crystals to the graupel pellets. Below this level, the charge transfer is opposite, and graupel charges positively (e.g., Saunders, 2008). Subsequent sedimentation allows for accumulation of space charge within the cloud. A basic electric "tripole" structure of a thunderstorm hence results, with a main positively charged region in the upper portions of the storm where ice crystals dominate, and a main negatively charged region somewhat above the 263 K isotherm where graupel dominates. A weaker positively charged region exists in the lower portions of the cloud (Williams, 1989). The cause of this charge region is not fully agreed upon. Aside from the graupel-ice collisions, possible mechanisms are ion capture, charge deposited by lightning, and inductive charging (Williams, 1989; Mansell, 2000). To gain insight into the hydrometeor distribution in a real-world cloud, Fig. 2.3 shows the hydrometeor classes derived from polarimetric radar data (Höller et al., 1994).

Inductive charging   The inductive charging mechanism requires a strong pre-existing electric field which results in a polarization of the hydrometeors. That is, inductive charging is considered to be a secondary effect after appreciable field strength has been achieved by the non-inductive charging process. The only viable collision partners are thought be cloud droplets and graupel particles (Saunders, 2008; Mansell, 2000). Other particles may coalesce or exhibit too weak a polarization for charge transfer to occur.

Convective charging   Grenet and Vonnegut suggested that positive fair-weather charge is ingested into the updraft, which results in a negative screening-layer charge (e.g., MacGorman and Rust, 1998). In this theory, the screening-layer charge is advected into the interior of the storm as descending motion at the updraft's flanks occurs. This hypothesis falls short of explaining observed charge structures and has largely been dismissed as initial electrification mechanism. However, it does have relevance in that it emphasizes the importance of convective motions that may redistribute charge that has previously been isolated by other processes (MacGorman and Rust, 1998).

The above-mentioned tripole structure of a convective storm is a strong over-
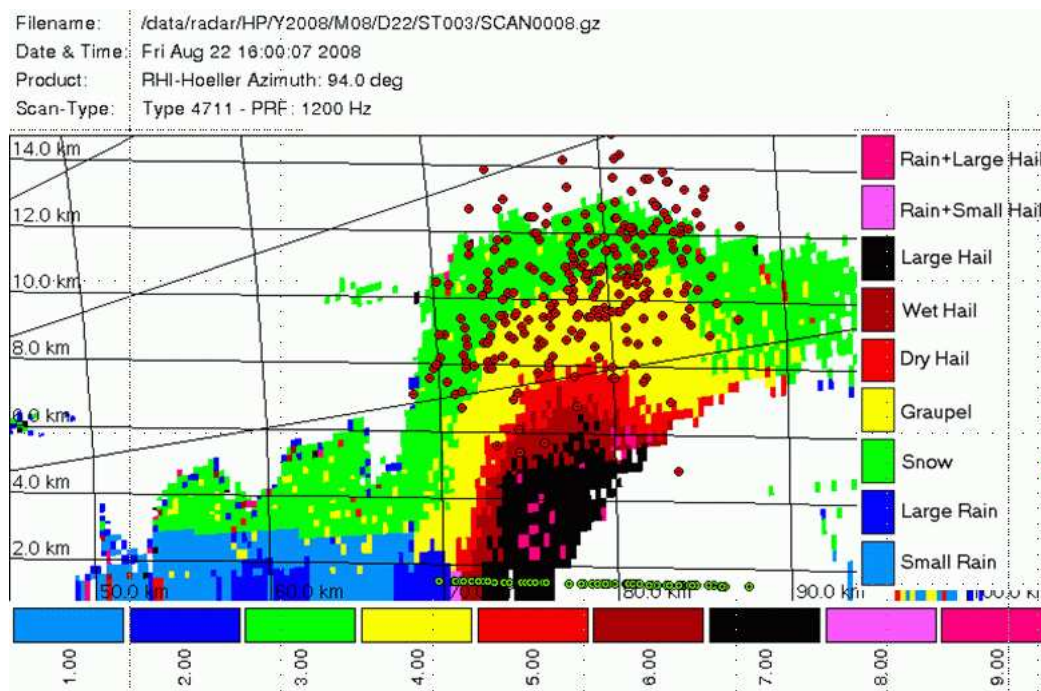
Figure 2.3: POLDIRAD RHI image of a severe hailstorm on 22 August 2008. Graupel (in this context, comprising the graupel and dry hail categories) is marked by yellow and red regions. Snow is shown in green. LINET (section 2.3.1) discharge positions are shown as red and green circles. Note the strong attenuation in the lower-right part of the image.

simplification. Even in the simplest setup, there are at least four charge layers, as a region of negative screening-layer charge forms at the top cloud boundary owing to ion attraction. As soon as the storm becomes organized, e.g., into an MCS with an extensive precipitation region behind or ahead of the convective line, multiple charge layers have been observed (Stolzenburg et al., 1998). Also, supercells where the main positive dipole was inverted have been observed, which may be explainable with unusual effective liquid water contents in the context of the RGR-hypothesis (Rust et al., 2005). Fig. 2.4 sketches the gross charge structure of a thunderstorm.

2.3 Lightning

2.3.1 Lightning detection with LINET

The lightning detection network, LINET, used in this study employs a time-of arrival (TOA) technique based on signals measured in the LF/VLF band (Betz et al., 2009). As of 2008, about 100 antennas were distributed across all of Europe. These antennas feature two orthogonally-aligned loops, so that the electric current induced by magnetic-field changes can be determined. This electromagnetic radiation is emitted by accelerating electrons in the lightning channel. The three-dimensional
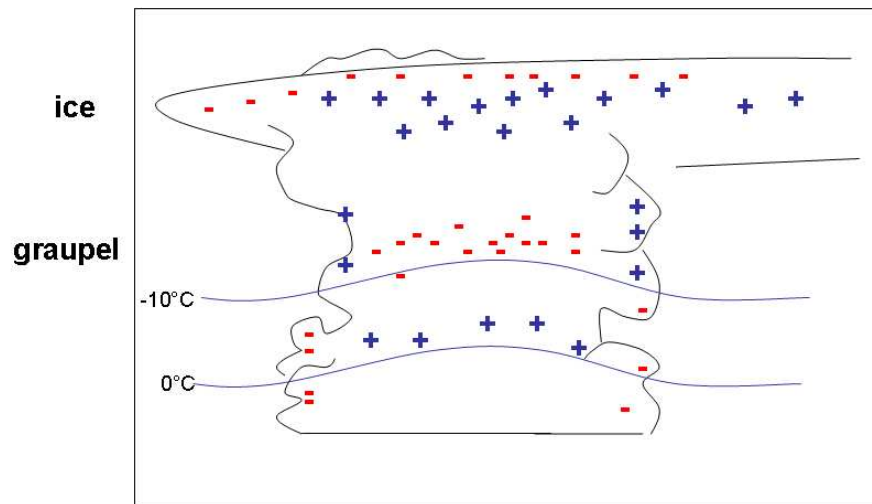
Figure 2.4: This sketch shows a convective cell and its basic charge structure, including screening-layer charge. Plus signs denote positive charge, minus signs denote negative charge.

position of a discharge is reported where the field emissions are strongest. In the case of a cloud-to-ground discharge, the most intense radiation follows the attachment process close to the ground, while radiation from IC-discharges originates at higher altitudes (Betz et al., 2009). This height of the discharge is also determined by the TOA technique, making any assumptions about wave forms that may belong to either intra-cloud or cloud-to-ground discharges unnecessary. The location accuracy is on the order of 100 m based on measurements on towers whose positions are well known.

2.3.2 Lightning initiation and lightning types

The details about streamer initiation and subsequent leader formation remain elusive, the main issue being that the electric-field strength necessary for field breakdown has never been observed in thunderclouds (e.g., Solomon et al., 2001). A possible explanation is that local field enhancements at the edges of hydrometeors allow for positive streamer initiation. Once a streamer system has developed, the field at the streamer origin increases beyond the critical field strength for breakdown. However, this process still requires fields higher than what has been observed (Petersen et al., 2008). Although it is possible that compact regions of enhanced field strength simply have not been sampled, evidence is accumulating that the existence of the conventional breakdown field strength of air is not necessary. Rather, high-energy seed electrons due to a cosmic-ray shower may trigger a so-called runaway breakdown (Gurevich et al., 1992; Marshall et al., 1995). The required field strength, called "breakeven" field strength, is an order of magnitude smaller than
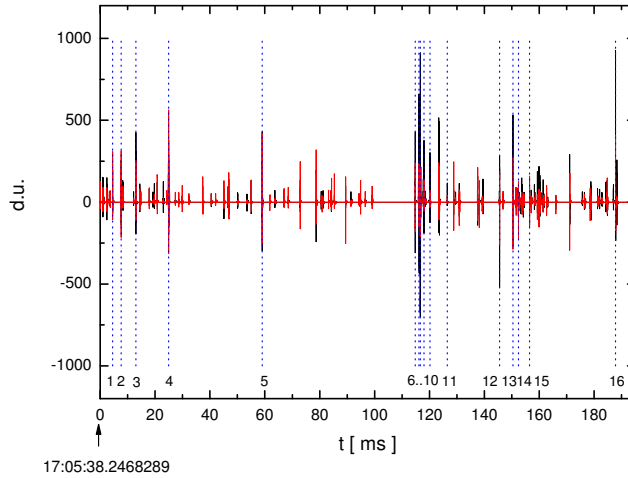
Figure 2.5: LINET measurements showing K-changes during an IC discharge. Only the highlighted pulses are reported by the system. Adapted from Schmidt (2007).

the conventional breakdown field strength (about 100 kV m^{-1} vs 1,000 kV m^{-1} in the mid-troposphere). The interaction of runaway electrons with air molecules may result in polarized plasma which enhances the electric field at its tips. This field enhancement could then initiate positive streamers from nearby hydrometeors. Petersen et al. (2008) suggest that a combination of both processes may occur. In any case, once a system of cool plasma streamers has developed, these are thought to combine into a hot and highly conductive leader channel (Petersen et al., 2008).

Intra-cloud (IC) lightning   The IC discharge consists of two phases (e.g., Rakov and Uman, 2003). The early phase begins as bidirectional leader between two charge centers, usually the upper positive and the central negative one. The positive leader propagates into the negative-charge region, and the negative leader propagates into the positive charge-region. In the second phase, the branches especially of the positive end of the leader are discharged by breakdown processes, accomplished by so-called recoil leaders. The LF/VLF signatures of these discharges are termed K-changes (Fig. 2.5). Several low- and high-amplitude discharge pulses are visible. Those pulses exceeding a certain strength at several stations are reported as a "stroke" by LINET. The signatures of strong recoil leaders and of return strokes (see next paragraph) are not discernible using the LF/VLF technique (Betz et al., 2009, p. 128) – only the height of the radiation source differs between measured cloud-to-ground and intracloud discharges. As the field weakens during this discharge process, the leader propagation into the space-charge region eventually ceases and the discharge pulses gradually wane, which completes the discharge.

Cloud-to-ground (CG) lightning It has been shown that in general the leader develops amidst the largest potential gradients between the space-charge regions and propagates into potential wells (Coleman et al., 2003). During a negative cloud-to-ground discharge (-CG), a bidirectional leader usually forms between the main negative charge and the lower positive charge regions. Usually, the negative leader propagates horizontally through the lower positive charge region during preliminary breakdown (Stolzenburg and Marshall, 2009). Once the leader reaches the ground, one or more upward connecting leaders are initiated from the surface. This attachment process short-cuts the circuit and allows the negative charge in the leader channel to be drained to the surface. This main, upward propagating discharge is known as return stroke. Once the charge is removed from the channel, a junction process (J-process) usually occurs, which involves recoil-leader discharges. This leads to the initiation of a second leader, the dart-leader, which usually retraces the residual channel of the previous discharge. Once this leader has attached to the ground, a subsequent return stroke may occur. This process may be repeated several times, so that most flashes exhibit several return strokes. Sometimes, a rather long-duration discharge (hundreds of milliseconds) follows the last return stroke, the so-called continuing current, which taps charge from the cloud, rather than the charge deposited in the channel. Only the return-stroke components of the CG discharge can be detected with LINET.

For more details about lightning discharges, see, e.g., Petersen et al. (2008), Stolzenburg and Marshall (2009), Ogawa (1995), or Rakov and Uman (2003).

2.3.3   Definition of a "flash"

The foregoing discussion implies that there is no single, well-defined discharge process. Rather, the discharge is a complicated, multi-stage phenomenon, involving electrical currents within multiple time and length scales. For the present purpose, a practical definition of a "discharge event" (= "flash") was needed:

> A flash includes all single discharges reported by LINET (called "stroke" independent of lightning type) that occur within one second and within a radius of 10 km.

Such grouping of discharge events into a single flash event is a widely-applied procedure (e.g., Shao et al., 2006), with spatial ranges usually being of order 10 km and temporal intervals of order 1 s. This choice ensures that discharges of separate cells are not binned into one flash. This would become increasingly likely if the radius was increased. The relation between strokes and flashes depends on the spatio-temporal

distribution of strokes. An impractical but more accurate method would be to select a radius that includes the convective system under consideration. However, a 10 km radius seems to be a reasonable compromise for most central-European storms. The advantage of such binning is that variations in detection efficiency are filtered out. The flash measurements thus are more robust to changes in the antenna coverage than stroke measurements. Also, in most studies flashes are considered rather than strokes, and to compare the results obtained in this study with other results, grouping the strokes into flashes seemed to be appropriate. Fig. 2.6 shows an example of the dependence of the flash number on the choice of the space and time intervals. As can be seen, the total number of flashes is quite strongly dependent upon the choice of the radius and time intervals.
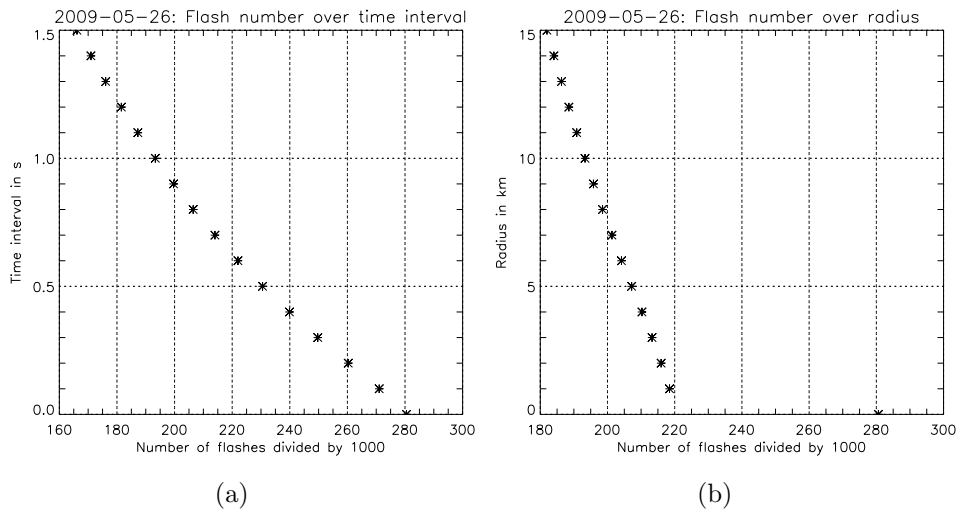
Figure 2.6: (a) Dependence of the number of accumulated flashes on the selected time interval at a radius of 10 km. (b) Dependence of the number of flashes on the selected radius at a time interval of 1 s. The abscissa is scaled to 1,000 flashes to improve readability. The number of accumulated strokes on 26 May 2009 was 280,614.

2.4 The flash rate

In this section, a theoretical framework is provided which yields a general expression for the flash rate based on a simple capacitor model.

2.4.1 General considerations

Once charge separation is occurring, an electrical field, E, builds between the space-charge regions. If the space charge reaches a critical strength, a discharge occurs. For the moment, it is assumed that no other discharge mechanisms than lightning discharges exist.

The time, T, for this initial charging is related to the rate at which the vertical component of the electric field, E, increases and to the critical electric field strength, E_c:

$$E_c = \int_0^T \frac{\partial E}{\partial t} dt. \tag{2.2}$$

At the time, T, the critical field strength is reached, and a discharge occurs. The strength of the discharge, i.e., the amount of charge transferred, determines the degree to which the electrostatic field has been neutralized. This is just the field strength that needs to be replenished before the next flash can occur. If $\bar{E}$ is the field strength after the discharge, the field strength that needs to be restored is given by

$$E_c - \bar{E} = \Delta E = \tau \frac{\partial E}{\partial t}, \tag{2.3}$$

where ΔE is the field strength that needs to be replenished for the next discharge to occur, and τ is the time required to rebuild the field. The charging rate, $\partial_t E$, has been assumed to be constant between two discharges. The discharge rate, f, is then given by

$$f = \frac{1}{\tau} = \frac{1}{\Delta E} \frac{\partial E}{\partial t}. \tag{2.4}$$

This equation may be re-written as

$$\frac{\partial E}{\partial t} - f \Delta E = 0, \tag{2.5}$$

which implies a balance between charging and discharging. I.e., the charging current constantly attempts to push the field strength beyond the critical threshold. This is prevented by the lightning current, which acts to weaken the electric field. This approach diagnoses an instantaneous flash rate with the assumption that the critical charge has been achieved already. This seems to be in contradiction to situations where a convective cell may become electrically charged, but the charging rate is so weak that the critical field strength is not reached before the cell dissipates. This contradiction is handled automatically in this approach: In such a situation, the convective cloud would be characterized either by a low charging rate or by a large field neutralization (ΔE), or both (see Eq. (2.4)). If these quantities are diagnosed correctly, this will result in a predicted time interval between two flashes that is smaller than the cell's lifetime. Although the flash rate is not zero, the cell would practically never produce a lightning discharge. This reasoning was also offered by Williams (1985, p. 6018).

Now ΔE may be expressed with the aid of a so-called *neutralization efficiency*[2], η, so that

$$\Delta E = \eta E_c, \tag{2.6}$$

where

$$\eta = \frac{E_c - \bar{E}}{E_c}. \tag{2.7}$$

Hence, the discharge rate is given by

$$f = \frac{1}{\eta E_c} \frac{\partial E}{\partial t}. \tag{2.8}$$

Obviously, the larger η, i.e., the stronger the discharge, the larger the electrostatic field that needs to be restored before the next flash can occur, and the smaller the flash frequency. E.g., $\eta = 1$ implies that the entire field has been neutralized during the discharge.

Instead of the electrostatic field, any other quantity may be chosen that uniquely describes when breakdown takes place. Apart from the electrostatic field, this could be the charge or the charge density. If this general quantity is denoted with Ψ, then the flash-rate equation may be written as

$$f = \frac{1}{\Delta \Psi} \frac{\partial \Psi}{\partial t}. \tag{2.9}$$

Eq. (2.5) then takes the form

$$\frac{\partial \Psi}{\partial t} - f \Delta \Psi = 0. \tag{2.10}$$

2.4.2   Application to a two-plate capacitor

To obtain quantitative results, specification of the space-charge distribution is necessary. In the following paragraphs, an analytical solution of Gauss' law for a two-plate circular capacitor will be used as basis for the new lightning-frequency parameterization. Fig. 2.7 summarizes the charge geometry. The lightning current, I_L (shown in yellow), is given by

$$I_L = \Delta Q f, \tag{2.11}$$

i.e., the product of lightning rate, f, and lightning charge, ΔQ. This current is balanced by the generator current (black arrows in Fig. 2.7). This balance between

---

[2]Introducing this quantity was stimulated by Boccippio (2002), who used a so-called charge-removal efficiency.
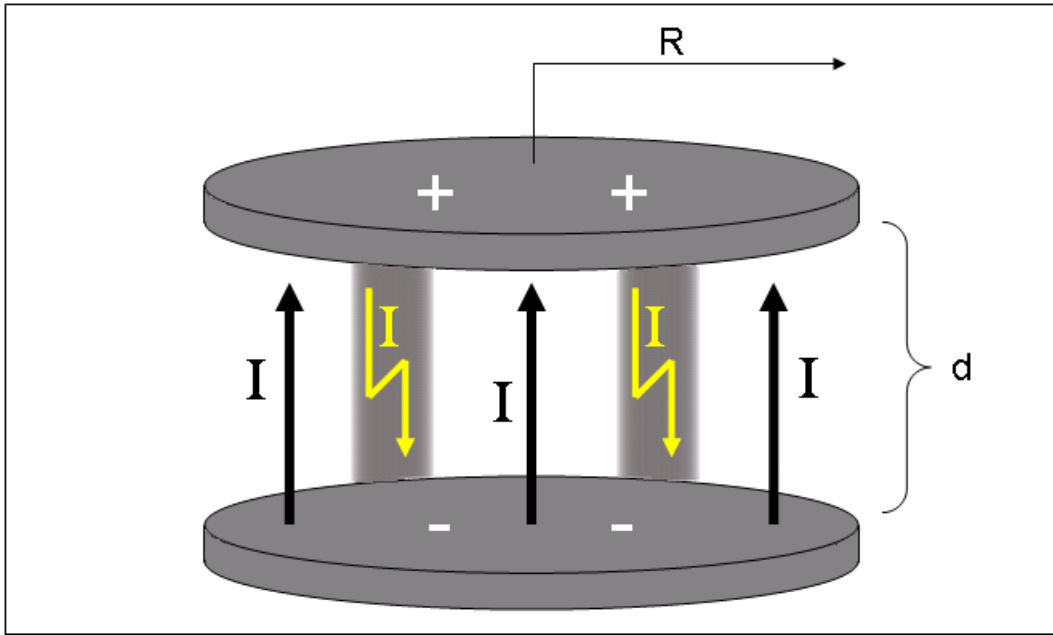
Figure 2.7: Sketch of the capacitor used to model the space-charge regions of a thunderstorm. The geometric parameters, R and d, are shown, as well as the lightning current (yellow, lightning-shaped arrows) and the generator current (black arrows). Plus and minus signs refer to the sign of the plate charge.

charging current and lightning current is consistent with Eq. (2.10), which simplifies to

$$I_c - I_L = 0, \tag{2.12}$$

where the charge, Q was inserted for Ψ. The charging current, I_c, is given by $\partial_t Q$.

This means that if the charging current is known, then the lightning current is known as well. In order to infer the flash rate, only the lightning charge needs to be prescribed (this will be done in the next chapter). Assuming positive charge on the upper capacitor plate and negative charge on the lower capacitor plate, the electric field in the center of the capacitor and in the middle of the plates is given by (see Appendix A.1 for a detailed derivation):

$$E(R, d) = -\frac{\sigma}{\epsilon} + \frac{\sigma}{2\epsilon} \frac{d}{\sqrt{R^2 + (\frac{d}{2})^2}}, \tag{2.13}$$

where σ is the charge per unit area, ϵ is the permittivity of the air, d is the distance between the plates, and R is the radius of the plates. The second term vanishes for large radii, so that the solution reduces to the well-known solution for an infinite sheet of charge. Note that E is negative for the given charge configuration. If the distance, d, becomes large, the two terms eventually cancel, and the field vanishes.

Differentiating Eq. (2.13) with respect to time yields

$$\frac{\partial E}{\partial t} = \frac{j}{2\epsilon}[G(R,d) - 2], \qquad (2.14)$$

where

$$G(R,d) = \frac{d}{\sqrt{R^2 + (\frac{d}{2})^2}} \qquad (2.15)$$

is the geometric term, which depends on the radius of the plates and their separation distance. This expression is valid only in the center of the capacitor between the plates where lightning initiation usually occurs (see Stolzenburg and Marshall, 2009, and also Appendix A.1). Upon inserting Eq. (2.14) into the flash-rate equation,

$$f = \frac{1}{\Delta E} \frac{\partial E}{\partial t}, \qquad (2.16)$$

one obtains for the lightning frequency

$$f = \frac{1}{2\epsilon} \frac{j}{\Delta E} \left(G(R,d) - 2 \right). \qquad (2.17)$$

2.4.3   Assumptions and their limitations

Two charge regions

An obvious simplification is that the model features only two charge regions. However, it is generally agreed upon that the main positive dipole represents the gross charge structure of thunderstorms (MacGorman and Rust, 2008, p. 50), with additional charge regions having smaller magnitudes. Though these may be crucial for the details of the electric activity of thunderstorms, it is suggested in this study that the gross electric behavior is described already if only two charge regions are assumed. This simple assumption is not expected to hold if large thunderstorm systems (rather than isolated cells) are considered, because such systems exhibit substantially more complicated charge distributions (Stolzenburg et al., 1998).

Equal size of charged regions

This assumption was introduced for simplicity. One might argue that since the anvil cloud extends beyond the core of the thunderstorm, the upper charge region needs to have a larger horizontal extent than the lower charge region. However, to this author's knowledge, there exists no universal relation between the space-charge density in the anvil cloud and the distance from the horizontal cell centroid. This means that *any* generalizing assumption about the decay of space-charge density towards the anvil edge is not supported by observations. Numerical simulations

indicate a rather complicated charge structure in the anvil (e.g., Mansell, 2000). The degree of inaccuracy resulting from the choice of equal plate size is thus not larger than assuming a radially-symmetric charge-density decay. In this implementation, the choice was made in favor of the easier solution.

Qualitatively, this choice has two effects: The total critical charge is reduced compared to the case where the upper plate is bigger than the lower plate. This effect implies an increased lightning rate, because the relative reduction of space charge decreases with increasing plate geometry (Fig. 2.8(b)). The other effect is that an increased size of the space-charge region increases the lightning charge, which contributes to a reduced flash rate. Though these two effects may cancel one another, this cannot be quantified based on the current state of knowledge.

Circular plates

The assumption that the horizontal cross-section through a deep convective cloud is circular, is a first-order approximation. One may consider the actual (usually, non-circular) charge distribution as being composed of a circular contribution and a departure thereof. The main effect of this perturbation from the circular base-state configuration is that boundary effects gain dominance (these contributions increase as the perturbation increases). To quantify these effects, the numerical solution of Gauss' law for arbitrary plate shapes may be compared to the analytical circular-plate solution. In general, the deviation from the circular-plate solution will vary from storm to storm, depending on the departure from a circular charge distribution. The fact that an analytical solution exists for the electrostatic potential around circular plates (Appendix A.1) was the main reason for assuming this charge geometry. Moreover, convective updrafts are often successfully modeled as horizontally circular objects (e.g., Davies-Jones, 2002).

The radius of the circular area equivalent is given by

$$R = \sqrt{\frac{A}{\pi}}, \tag{2.18}$$

where A is the horizontal cross-sectional area of the graupel region through its vertical centroid location.

Though not required to determine the flash rate, the vertical separation distance of the plates is also determined as part of the model output (see p. 58 for more details). The separation distance is given by the distance between the centroid positions of the two space-charge regions.

Although the depth of the plates does not explicitly appear in the flash-rate equation, it is required for determining the space-charge volume which is needed to specify the lightning charge. The thickness of the plates is the average of the depth

of the space-charge regions. This thickness, multiplied with the plate area is the assumed charge-region volume.

2.4.4   Interpretation of the flash-rate equation

Equation (2.17) is the key to understanding the general behavior of lightning activity as a function of the storm's geometry. Fig. 2.8(a) shows the dependence of the charge required to create an electrostatic field of 100 kV m^{-1} on the geometry of the capacitor. On the x-axis, the plate radius is shown, and on the y-axis, the plate separation distance. The contours represent the critical charge in Coulomb. The larger the radius of the plates, the more charge is required to achieve critical field strength. This is because the field strength depends on the charge per unit area, σ. The vertical distance between the plates has only little impact on the required charge. Consequently, the response of the electrostatic field to a certain amount of charge that is removed from the capacitor plates, will decrease as the radius increases (Fig. 2.8(b)). The explanation is that the charge per area, σ, is less affected by a given change of the total charge if the plates are large than when they are small. Based on the foregoing, the larger the plates' geometry, the smaller the field-neutralization efficiency. This effect is proposed as explanation why the flash rate so strongly depends on storm size (e.g., Williams, 2001). Apart from
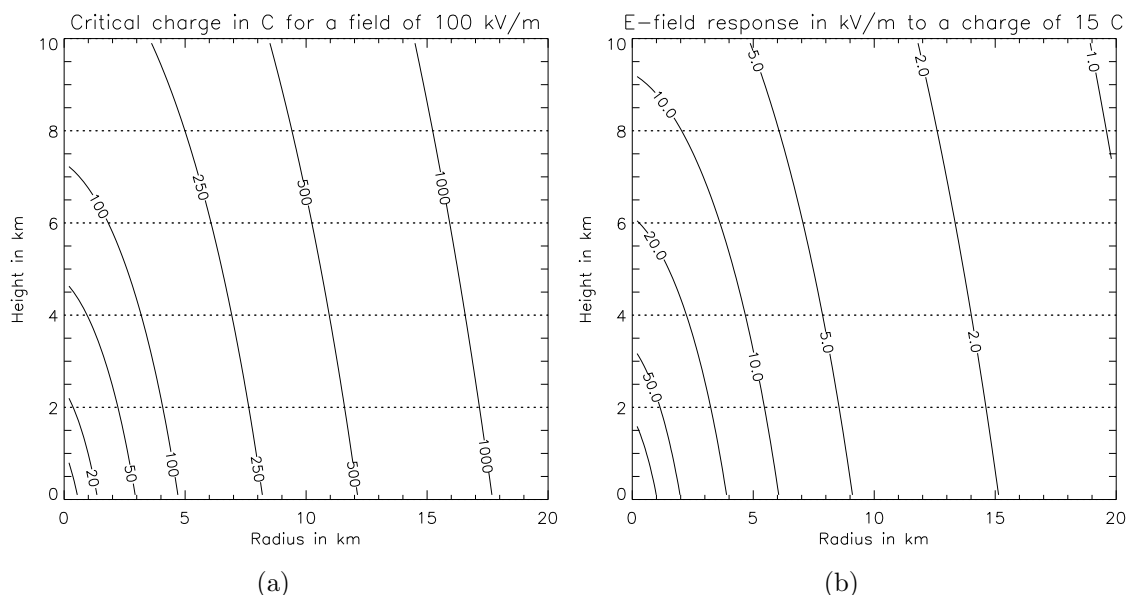
Figure 2.8: The abscissa shows the plate radius and the ordinate the plate distance. (a) Charge in C required to create an electric field strength of 100 kV m^{-1}. (b) Response of the electric field to a charge of 15 C for variable capacitor geometries.

the field-removal efficiency, the charging rate determines the flash frequency. The
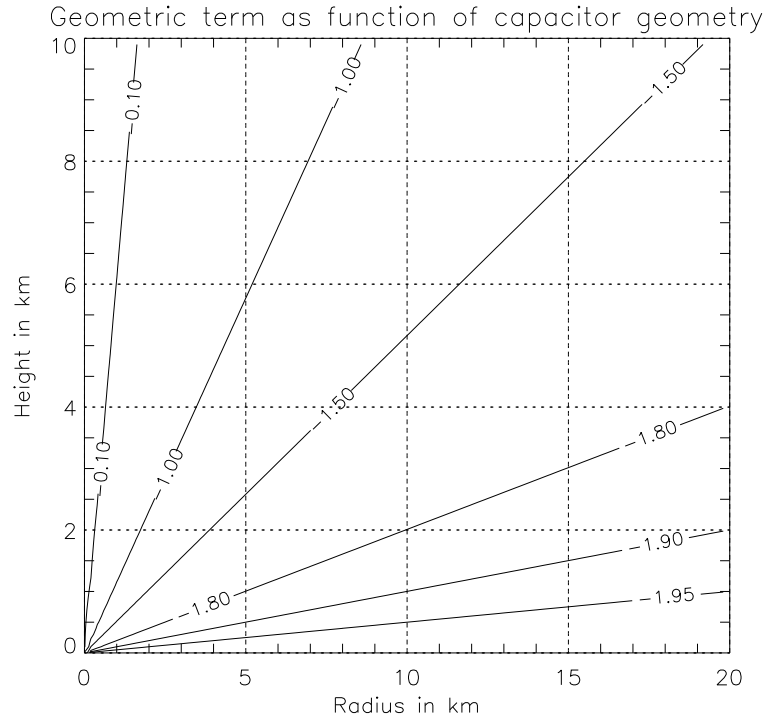
Figure 2.9: The geometric term as a function of the plates' radius and their separation distance. The constant offset of -2 has been added in the plot.

charging rate is given by (Appendix A.2)

$$\frac{\partial E}{\partial t} \propto j \left(G(R,d) - 2 \right). \tag{2.19}$$

The geometric term, G, does not vary substantially for most storm geometries and accounts for departures from the infinite-width solution. The geometric term is plotted for a wide range of storm geometries in Fig. 2.9 and can be seen to assume values between minus one and minus two for most geometries.

Thus far, it has been assumed that the only way to discharge the capacitor is lightning. This is not necessarily realistic, since corona discharges and precipitation charge also contribute (MacGorman and Rust, 1998). This fact is accounted for by an additional factor, γ, which is defined by the fraction

$$\gamma = \frac{j_l}{j_d}, \tag{2.20}$$

where j_l is the current-charge density due to lightning and j_d is the total discharging current density. γ will be referred to as lightning efficiency (γ will be specified in the next chapter). Then, the flash-rate equation is given by

$$f = \frac{\gamma}{2\epsilon} \frac{j}{\Delta E} \left[\frac{d}{\sqrt{R^2 + (\frac{d}{2})^2}} - 2 \right]. \tag{2.21}$$

This equation is somewhat redundant, as the dissipated electric field, ΔE in the denominator also depends on the geometric term. Specifically,

$$\Delta E = \frac{\Delta \sigma}{2\epsilon} \left[\frac{d}{\sqrt{R^2 + (\frac{d}{2})^2}} - 2 \right]. \tag{2.22}$$

Inserting this expression in Eq. (2.21) results in

$$f = \gamma j \frac{A}{\Delta Q}, \tag{2.23}$$

where A is the area of the capacitor plates and use of the fact that $\sigma = Q/A$ has been made. The dependence of the vertical separation distance has dropped out in Eq. (2.23). The strong dependence of the flash rate on the horizontal area of the charge region was also observed by Larsen and Stansbury (1974).

2.5   Single-parameter approaches

Apart from the new parameterization developed in this work, additional parameterizations that were created by Price and Rind (1992, henceforth PR92), Yoshida et al. (2009, henceforth YMUK09), and Grewe et al. (2001, henceforth GR01) will be investigated. The motivation is a comparison of the new parameterization with previous work. In this section, these existing parameterizations will be derived and discussed from a theoretical perspective. The purpose is to demonstrate the underlying assumptions that are usually made in this context (Vonnegut, 1963; Williams, 1985; Price and Rind, 1992; Boccippio, 2001; Yoshida et al., 2009). The reader only interested in the new parameterization developed in this study, may skip this section.

2.5.1   Popular single-parameter approaches and their limitations

Williams (1985) related the flash rate linearly to a single quantity, and these univariate approaches have remained popular in lightning research. Usually, the flash rate has been linearly related with the charging current (e.g., Blyth et al., 2001; Deierling et al., 2008) or with the generator power (e.g., Williams, 1985; Price and Rind, 1992; Yoshida et al., 2009).

Only the charging rate is prescribed in these approaches. The charging rate may be expressed by any quantity that is represents a breakdown criterion (like critical electrostatic field strength, critical field energy, critical charge density, etc.). As in section 2.4, this quantity is symbolized by Ψ. Then a linear proportionality

of discharge rate to the rate at which Ψ changes with time, is stipulated in these approaches:

$$f_\Psi \propto \frac{\partial \Psi}{\partial t}. \tag{2.24}$$

As the discharge rate has the unit s^{-1}, the factor of proportionality is required to have the inverse unit of Ψ, so that

$$f_\Psi = \frac{1}{\Delta \Psi} \frac{\partial \Psi}{\partial t} \tag{2.25}$$

where consequently $\Delta \Psi$ is a constant for each and every discharge. In terms of the Ψ-neutralization efficiency (analogous to Eq. (2.7)), η_Ψ, this means that

$$\eta_\Psi \Psi_c = \text{const}, \tag{2.26}$$

where Ψ_c is the critical value of Ψ. One of the most popular choices of Ψ is the electrostatic energy,

$$W = UQ, \tag{2.27}$$

where U is the voltage between the charge regions. Then, $\Psi = W$ (e.g., Williams, 1985; Price and Rind, 1992; Yoshida et al., 2009). Since the time rate of change of W is just the electric power of the storm, P, the flash rate, f_W, is given by

$$f_W = \frac{1}{\Delta W} P, \tag{2.28}$$

where consequently the discharge energy, ΔW, is universally constant.

Another popular choice for Ψ is the charge, Q (e.g., Blyth et al., 2001; Deierling et al. 2008). Then,

$$f_Q = \frac{1}{\Delta Q} I, \tag{2.29}$$

where I is the charging current, and ΔQ is the universally-constant charge that is removed during a flash. Yoshida et al. (2009) have discussed both relationships, $f \propto I$ and $f \propto P$, though they used electrostatic energy rather than electric power[3]. Another possible choice for Ψ is the charge per unit area, σ, so that

$$f_\sigma = \frac{1}{\Delta \sigma} j, \tag{2.30}$$

where j is the generator current density.

Although all of these parameters arguably do have relevance in determining the flash rate, all of them yield different predictions.

---

[3]Their reasoning suggests that they erroneously used energy instead of power, as did Price and Rind (1992). Setting $f \propto W$, while lightning energy, ΔW, is constant, is inconsistent. Stipulating an f-W-proportionality implies a global constant that has the unit of action (Js).

For a given storm, any of the approaches predicts the same flash rate, if the constant, $\Delta\Psi$ is selected accordingly, i.e., to fit the observation. However, as soon as the storm parameters (e.g., its size) change, $\Delta\Psi$ would need to be adjusted accordingly. However, $\Delta\Psi$ is *not* allowed to vary in these univariate approaches. It follows that all of the parameterizations are generally inconsistent among each other.

To gain insight into the different predictions, assume a simple dipole, and in addition that the storm's width covaries with the storm's depth. I.e., a variable, l, which is proportional to both the diameter and the depth is introduced. Then it can be shown that the voltage, U, between the charge centers is proportional to l (see Appendix A.4 and section 2.5.2). Now assume that the flash energy is stipulated to be constant, then

$$\Delta W = U \Delta Q = \text{const}, \tag{2.31}$$

and hence,

$$\Delta Q \propto l^{-1}. \tag{2.32}$$

In other words, the charge per flash decreases as the size of the storm increases if ΔW is to remain constant. In a similar vein, the behavior of lightning charge can be derived for other choices of Ψ, as summarized in Tab. 2.1. For a given storm geometry (in this example described by l), $\Delta\Psi$ can be adjusted to yield identical flash rates for the different choices for Ψ. However, the predicted charge that is removed by a flash strongly diverges as the geometry (in this case, l) changes. So does the response of Ψ to the discharge; both contributes to $\Delta\Psi$, and this results in different field-neutralization efficiencies and hence, in different flash rates.

The predictions of all the univariate parameterizations could be reproduced by Eq. (2.8), if the field-neutralization efficiencies based on the predicted charge transfer from Tab. 2.1 were inserted. This implies that all the univariate approaches are included in the more general approach which resulted in Eq. (2.8). Consequently, there is no single parameter that describes the flash rate best – all of them are inappropriate to describe the entire spectrum of storms.

Based on the foregoing, the main problem with the approaches that assume a linear relationship between flash rate and a single parameter, $\partial\Psi/\partial t$, is that the amount of neutralized Ψ is not allowed to vary. This means that non of the single-parameter approaches are correct from a physical perspective. Besides, the choice of Ψ seems to be quite arbitrary, with some authors preferring the energy, and others preferring the charge. As alluded to on p. 27, and demonstrated at the end of this section, the approach developed in this work is independent of the choice of Ψ.

Another problem is that it has not been observed that any of these quantities is globally constant for every discharge (e.g., Maggio et al., 2009; Cooray, 1997). Also,

some predictions are unphysical. For example, a discharge may remove more charge than is actually present in the storm. This leads to an underestimation of the flash rate, and defies basic physics. Moreover, there does not seem to be any reason why the flash rate should be uniquely and linearly associated with any of the parameters introduced above. As has been demonstrated, the linear relations enforce a certain degree of neutralization of Ψ: If $\Psi = E$, then the field neutralization is constant; if $\Psi = W$, then the dissipated energy is constant, and so forth. Moreover, the charge that is transferred in a lightning flash is merely a "by-product" of the choice of Ψ (Tab. 2.1) and hence would only coincidentally predict the correct lightning charge.

Ψ	f_ψ	$\Delta\Psi$	ΔQ
Q	$f_Q = \frac{1}{\Delta Q}\frac{\partial Q}{\partial t} \propto I$	ΔQ	$\Delta Q = const$
W	$f_w = \frac{1}{\Delta W}\frac{\partial W}{\partial t} \propto P$	ΔW	$\Delta Q \propto l^{-1}$
σ	$f_\sigma = \frac{1}{\Delta\sigma}\frac{\partial\sigma}{\partial t} \propto j$	$\Delta\sigma$	$\Delta Q \propto l^2$
E	$f_E = \frac{1}{\Delta E}\frac{\partial E}{\partial t}$	ΔE	$\Delta Q \propto l^2$

Table 2.1: Expressions for the flash rate for different choices of Ψ. The implied universal constant and the implied charge transfer per flash are also shown. l is a length scale that linearly varies with both, height and diameter of the storm.

The "single-parameter" approaches are a limiting case of the general formulation of the flash-rate relation, Eq. (2.9), in the limit of constant $\Delta\Psi$. The general flash-rate equation, Eq. (2.9), is independent of the choice of Ψ. This equation may be written as

$$f = \frac{1}{\Delta E}\frac{\partial E}{\partial t} = \frac{j}{\Delta\sigma} = \frac{I}{\Delta Q} = \frac{P}{\Delta W} \cdots \tag{2.33}$$

Now

$$
\begin{aligned}
[\Delta E] &= Vm^{-1}, & \left[\tfrac{\partial E}{\partial t}\right] &= Vm^{-1}s^{-1}\\
[\Delta\sigma] &= Cm^{-2}, & [j] &= Cm^{-2}s^{-1}\\
[\Delta Q] &= C, & [I] &= Cs^{-1}\\
[\Delta W] &= J, & [P] &= Js^{-1},
\end{aligned}
$$

where $[Q] = 1\ As = 1$ C. Eq. (2.33) is thus dimensionally consistent and

$$[f] = s^{-1}. \tag{2.34}$$

This shows that the result does not depend on whether the charging current (and the charge neutralization), or any other choice for Ψ (and $\Delta\Psi$) is considered. The validity of Eq. (2.33) was demonstrated when expressing the flash-rate equation in terms of the charge per area, σ, on p. 26.

2.5.2   Flash rate and generator power

PR92, YMUK09, and indirectly GR01, all assumed a linear proportionality between the flash rate and the storm-generator power[4],

$$f \propto P. \tag{2.35}$$

GR01 modified the PR92 approach by expressing the flash rate in terms of the upward motion, rather than cloud-top height.

Setting the flash rate proportional to the electric power has a long tradition. Vonnegut (1963) suggested that in order to determine the storm's electric power, the flash rate as well as flash energy need to be known. He also derived an expression for the storm's electric power, and found that under certain assumptions, the electric power varies with the 5th power of the storm's height. Williams (1985) suggested that the flash rate linearly varies with the storm's electric power.

In the following, an expression for the flash rate is derived, based on the linear relationship between power and flash rate.

As derived in Appendix A.4, the storm power, P, is given by

$$P = IU, \tag{2.36}$$

where U is the potential difference between the plates. As also shown in Appendix A.4, the voltage is given by

$$U = \frac{\sigma}{\epsilon}(\sqrt{R^2 + d^2} - R - d). \tag{2.37}$$

The electric current, I, is determined by

$$I = A\rho_c v_s, \tag{2.38}$$

where ρ_c is the charge density in the current and v_s is the velocity of the charge. Then, the power is given by

$$P = IU = A\rho_c v_s \frac{\sigma}{\epsilon}(\sqrt{R^2 + d^2} - R - d). \tag{2.39}$$

---

[4]YMUK09 suggest that under several assumptions, their parameterization is consistent also with $f \propto I$, i.e., a proportionality between flash rate and charging current. Their exposition is somewhat unclear, however. They stipulate a proportionality of the charging rate, $\partial Q/\partial t \propto n_g n_i v_g v_i$, where n_g and n_i are the numbers of graupel and ice particles, respectively, and v_g and v_i are their terminal fall velocities. This equation is supposed to express that the charging rate is proportional to the number of collisions between upward moving ice particles and downward moving graupel pellets. While this statement may generally be true (though incomplete, because the velocity of the charge transport is neglected), the number of collisions is not given by $n_g n_i$ but by complicated spectral integrals. The charge-separation velocity, which has been included in the above formula, is given by *difference*, $\|v_g - v_i\|$, rather than by the product, $v_g v_i$. While a 5th-power law may be constructed from the above equation, it is not describing the charging rate.

Setting the flash rate proportional to power, implies

$$f_W = \frac{P}{\Delta W}, \tag{2.40}$$

so that

$$f_W = \frac{\sigma}{\epsilon \Delta W} A \rho_c v_s (\sqrt{R^2 + d^2} - R - d). \tag{2.41}$$

If a finite depth, h, of the plates is admitted, then this equation may be written as

$$f_W = \frac{1}{\epsilon \Delta W} A \rho \rho_c v_s h (\sqrt{R^2 + (d+h)^2} - R - d - h), \tag{2.42}$$

where now d is the distance between the plate surfaces and ρ is the charge density on the plates. This equation shows how many parameters are involved when setting lightning rate proportional to power:

$$f_W = f(\rho, \rho_c, v_s, R, d, h). \tag{2.43}$$

In order to arrive at the 5th power law, many assumptions need to be made, which are detailed in the next paragraphs.

The Price and Rind (PR92) and Yoshida et al. (YMUK09) parameterizations

A famous "law" which may be derived from the assumption that

$$f \propto P \tag{2.44}$$

predicts that the flash rate is proportional to the 5th-power of the storm depth (e.g., Vonnegut, 1963; Williams, 1985; Price and Rind, 1992; Yoshida et al., 2009). In these approaches, it is assumed that the aspect ratio of all thunderstorms is the same, i.e., that

$$R \propto d \propto h. \tag{2.45}$$

Then, the geometric term in Eq. (2.42) is of order h, and Eq. (2.42) may be written as

$$f_W \propto \frac{1}{\epsilon \Delta W} \rho \rho_c v_s h^4. \tag{2.46}$$

In order to arrive at the 5th-power relationship, the additional assumption needs to be made that the charge velocity *also* varies linearly with the cloud depth, h, as in Vonnegut (1963)[5]. Then,

$$f_W \propto \frac{1}{\epsilon \Delta W} \rho \rho_c h^5. \tag{2.47}$$

---

[5]This assumption has been omitted by Price and Rind (1992) and Yoshida (2009), as they apparently confused energy with power.

In a last step, the product of the rest of the variables is assumed to be constant, i.e.,

$$C = \frac{1}{\epsilon \Delta W} \rho \rho_c = \text{const.} \tag{2.48}$$

This yields the desired relation:

$$f_W = C h^5. \tag{2.49}$$

Based on measurements of individual thunderstorm clouds, Price and Rind (1992) found that

$$f_{pr} = 3.44 \cdot 10^{-5} H^{4.9}, \tag{2.50}$$

where f_{pr} is the flash rate in min^{-1} and H is the height of the storm top in km. This is the "continental" parameterization; a different formula was found for oceanic storms. In this study, only the continental parameterization of PR92 is considered. Similarly, Yoshida et al. (2009) parameterized the flash rate by

$$f_{ymuk} = 10^{-6.1} \bar{H}^{4.9}, \tag{2.51}$$

where f_{ymuk} is the flash rate in s^{-1} and $\bar{H}$ is the cold cloud depth in km (Yoshida et al. 2009). This parameterization is valid for the entire domain covered by the TRMM satellite (see section 7.3).

This demonstrates which assumptions these parameterizations are based upon. These are

- the flash rate varies linearly with storm power

- the aspect ratio of all storms is the same

- the charge velocity is linearly proportional to storm size.

2.5.3 The Grewe et al. (GR01) parameterization

The GR01 parameterization (Grewe et al., 2001) is a formulation of the flash frequency depending on the mean convective mass flux divided by the density as an indicator for the updraft velocity. The intention was to reproduce the PR92 results, but using the mean updraft speeds rather than the cloud-top heights, which allowed them to avoid using different parameterizations over land and ocean as in PR92. This was possible since the global circulation model they used, ECHAM4, produces different mass fluxes over land and ocean with the same cloud top heights.

In the GR01 approach, the cloud-top height, H, in Eq. (2.50) is replaced by

$$H = 10^{-3} a \left(w \sqrt{d} \right)^b, \tag{2.52}$$

where w is the mean updraft velocity in ms^{-1} and d is the cloud depth in m. Several simulations were performed with COSMO-DE to obtain the relation described by Eq. (2.52). The parameters, a and b, were determined by a least-square fit: In Fig. 2.10, the cloud-top height, H, in meters is plotted against $w\sqrt{d}$ in m$^{3/2}$ s^{-1} in log-log (a) and linear (b) coordinates. The regression lines are plotted over the data. The y-intercept determines a in Eq. (2.52) where the slope, b appears as power of $w\sqrt{d}$. The magnitude of the mean absolute error (`Mean` in the inset of Fig. 2.10(a)) as well as the RMSE of substantially less than one suggest a very good fit, but this is owed to the logarithmic nature of the variables. As suggested by the data points, the scattering comprises nearly an order of magnitude of cloud height. The slope of the linear fit is given by $b = 0.54$ and the linear correlation coefficient was determined as $r = 0.68$. Several COSMO-DE simulations in different synoptic regimes were used to obtain the N = 1,010 data points. Based on this analyses, Eq. (2.52) may be written as

$$H = 10^{-3} \cdot 10^{2.63} \left(w\sqrt{d} \right)^{0.54}. \tag{2.53}$$

Inserting this expression in Eq. 2.50, one obtains

$$f_{gr} = 3.44 \cdot 10^{-5} \left[10^{-3} \cdot 10^{2.63} \left(w\sqrt{d} \right)^{0.54} \right]^{4.9} \tag{2.54}$$

$$= 3.44 \cdot 10^{-5} \cdot 10^{-1.84} \left(w\sqrt{d} \right)^{2.64}, \tag{2.55}$$

so that

$$f_{gr} = 5.01 \cdot 10^{-7} \left(w\sqrt{d} \right)^{2.64}, \tag{2.56}$$

where f_{gr} is the GR01 flash rate in min^{-1}. The original GR01 flash rate, f_{gr}^{or}, (using global-model data; this original parameterization is *not* used in this study) is given by

$$f_{gr}^{or} = 1.54 \cdot 10^{-5} \left(w\sqrt{d} \right)^{4.9}. \tag{2.57}$$

This equation is more sensitive to the updraft speed and updraft depth than Eq. (2.56). Also, the constant factor is about two order of magnitudes larger than in Eq. (2.56). These differences result from the stronger updrafts in COSMO-DE clouds compared to parameterized ECHAM4 clouds.

In the original GR01 implementation, the vertical velocity, w, was calculated via the convective mass flux, which is supplied by the Tiedtke convective scheme:

$$w_k = \frac{\Phi_k}{\rho_k}, \tag{2.58}$$

where w is the vertical velocity, Φ is the convective mass flux provided by the Tiedtke scheme, and ρ is the air density. The index, k, refers to the kth model
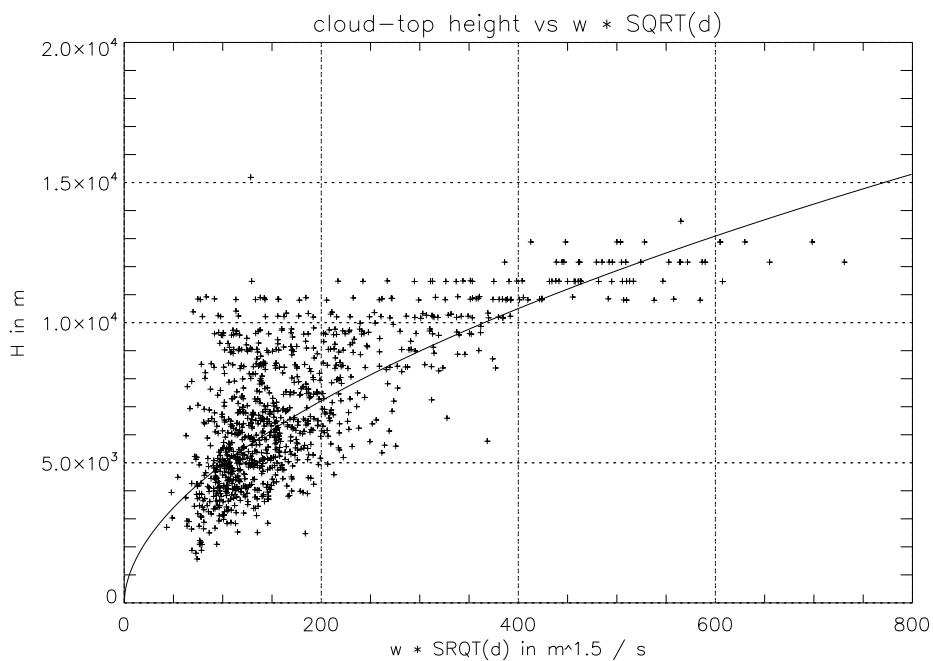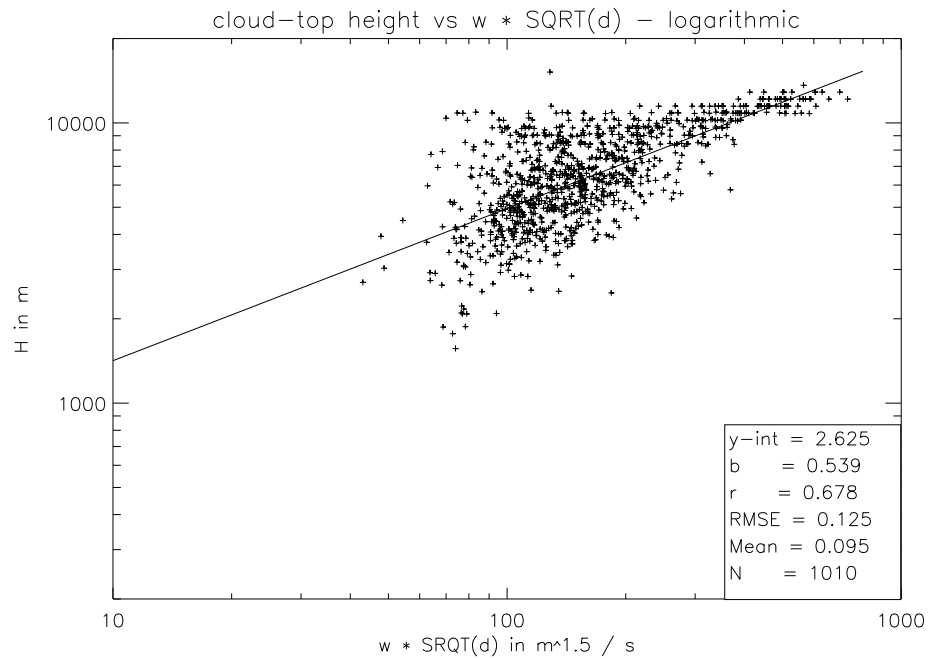
Figure 2.10: Relationship between cloud top height, H, in meters and $w\sqrt{d}$ in m$^{3/2}$s^{-1} in log-log (a) and linear (b) coordinates. The inset in (a) pertains to the logarithm of the displayed variables. $y-int$ is the logarithmic value of the y-intercept of the regression line and b is its slope. r is the correlation coefficient, $RMSE$ is the root mean square error, $Mean$ is the average magnitude of the residuals, and N is the number of data points. Solid lines are least-square fits.

level. For the implementation in the COSMO-DE model with explicit convection, the mean vertical velocity could be used directly (without resorting to the mass flux) by calculating the average updraft speed per thunderstorm cell. Section 3.2 deals with the definition of a cell in these approaches).

Chapter 3

The New Lightning-Frequency Parameterization

In this chapter, the new lightning parameterization is specified. Henceforth, it will be abbreviated D10. This parameterization will be applicable to real-world thunderclouds and is not specific to COSMO-DE.

3.1 Parameterizations

In the previous chapter, the general theoretical framework has been established, and the geometry of the space-charge regions has been specified. As none of the variables appearing in the flash-rate equation,

$$f = \gamma j \frac{A}{\Delta Q},$$ (3.1)

is simulated by the model directly, the next step is parameterize these variables with the aid of available model fields. In Eq. (3.1) there are four variables that need to be determined in order to calculate the flash frequency, i.e.,

$$f = f(A, \gamma, \Delta Q, j).$$ (3.2)

The parameterized variables are the size of the space-charge regions (area and volume), the lightning charge, and the generator current density (including space-charge density in the current as well as the motion speed of the charge). Tab. 3.1 introduces the variables and their parameters. This chapter mainly deals with the justification for choosing properties of the graupel field as parameter, and the origin of the specific constants.

Variable	Parameterization
Space-charge area, A	graupel-mass field
Space-charge volume, V	graupel- and ice-mass fields
Generator charge density, ρ_c	graupel-mass field
Generator charge velocity, v_g	graupel-mass field (terminal graupel fall velocity)
Lightning charge, ΔQ	graupel- and ice-mass fields (space-charge volume)
Lightning efficiency, γ	Set to constant value

Table 3.1: Introduction of parameterized variables and their parameters.

3.1.1   Area of the capacitor plates

The lower (negative) space-charge region is parameterized by the graupel-mass field and the upper (positive) charge region is parameterized by the ice-mass field. To obtain the area of the plates, a horizontal cross section through the graupel-containing region of the thunderstorm is taken. This section is made at the altitude of this region's centroid position. The area of the plates is determined by the equivalent circular area of this cross section (see also section 2.4.3).

The contiguous region where the graupel mass exceeds 0.1 gm^{-3} and where the temperature is lower than 263 K will be referred to as "graupel region". The temperature threshold is based on the charge-reversal temperature of the non-inductive charging mechanism (see section 2.2). The reasons that 0.1 gm^{-3} is used to define the area boundaries are manifold. First of all, the cloud boundaries in the model are somewhat diffuse, with the hydrometeor-mass fields becoming increasingly noisy with masses of less than about 0.1 gm^{-3}. On the other hand, using a higher threshold has proven to filter out weakly electrified convective clouds in some cases, which is not desired. Thus, 0.1 gm^{-3} is proposed as reasonable compromise. Moreover, a hydrometeor mass of 0.1 gm^{-3} roughly seems to correspond to visually-observed cloud boundaries (see Fig. 4.2 and also Fehr, 2000, p. 55, for a similar definition of cloudy regions). For later reference, the "ice region" is defined as contiguous area where the sum of the snow and cloud-ice masses[1] exceed 0.1 gm^{-3}. If other thresholds than 0.1 gm^{-3} are chosen, the cross-sectional area will be changed accordingly. Assuming a circular region, decreasing the threshold effectively increases the radius of the plate, where

$$\Delta A \propto \Delta(R^2) \approx R\Delta R. \tag{3.3}$$

In most general terms, the larger the area, the stronger it is affected by a change

---

[1]In the bulk-microphysics scheme used in COSMO-DE, an artificial distinction is made between non-sedimenting cloud ice and sedimenting snow.

of the threshold. How strong this effect is in quantitative terms depends on how quickly the graupel mass decreases away from the center of the graupel-mass region. Since the flash rate varies linearly with the area, the choice of the threshold directly affects the flash-rate predictions.

3.1.2 The lightning efficiency, γ

This parameter describes the contribution from lightning to the total discharging of the capacitor. Aside from lightning, corona currents, and precipitation currents contribute. No well-established quantitative estimates exist with respect to the magnitude of these contributions (see, however, MacGorman and Rust, 1998, p. 53 ff. for an overview). A simple solution would have been to set this parameter to one (i.e., to neglect it). However, in order to obtain a realistic framework of the model, this parameter was included, and it is set to

$$\gamma = 0.9. \tag{3.4}$$

Once more measurements become available, this parameter may be adjusted accordingly. The flash rate is linearly proportional to this parameter.

3.1.3 Lightning charge and generator-current density

For the remaining two variables, j and ΔQ, an iterative approach was adopted, using COSMO-DE data, rather than measurements of real-world thunderclouds. This way, a larger number of thunderstorm types could be investigated, and the required graupel-field properties could be retrieved comfortably. The details of the implementation of the lightning scheme in COSMO-DE are presented in chapter 4. Although the calibration of the parameterization was realized with the aid of model data, the resultant parameterization is directly applicable to observed storms (see section 5.1). I.e., no model-specific assumptions are involved. This was possible because before the calibration of the parameterization, it was ascertained that the storms' graupel regions are simulated realistically (see section 4.3). The independence of the parameterization on the model is addressed also in section 7.2.

The calibration procedure was as follows. First, a "best guess" formulation of the parameterizations, involving simple (i.e., linear) relationships between variables and parameters was implemented in COSMO-DE. Subsequently, the relationships between the variables (j, ΔQ) and their parameters (graupel mass and volume of the graupel plus ice regions) were refined iteratively, based on repeated simulations. The parameterization was tuned until horizontally extensive cells with much graupel content were producing more flashes than horizontally less extensive clouds with comparatively little graupel content while demanding consistency with the physical

reasoning detailed in the next sections. Isolated cells were considered and the constants were adjusted to yield about 60 flashes per minute with large (diameter of several tens of kilometers) and intense (graupel concentration greater than 6 g kg^{-1}) cells. The lower bound was about 1 flash every 15 minutes with polar-air graupel showers, which featured graupel mass fractions of less than 1 g kg^{-1} and diameters of less than 10 km in the COSMO-DE simulations. I.e., the extreme ends of the isolated-thunderstorm spectrum were sought and the calibration was continued until the desired flash rates were simulated. The freedom inherent to this tuning (essentially, a "trial and error" method) was confined by the required consistency with the basic physical model, the known qualitative relations between variables and parameters, as well as order-of-magnitude estimates, as will be detailed in the next paragraphs.

Lightning charge

Given a finite space-charge region, an important question is how much charge is depleted during breakdown. This question led to laboratory experiments (Williams et al., 1985; Cooke et al., 1982) and theoretical considerations (Phelps, 1974). The basic result is that as long as a critical streamer propagation field is maintained, the channel system will continue to propagate into the space-charge region and deposit charge along the channel. The more extensive the channel system, the more charge is depleted. The channel-propagation depth was determined by the space-charge density in the laboratory experiments. These have been confirmed with numerical simulations (Mansell, 2000). If the space-charge density is held constant, then the size of the space-charge region determines the channel-propagation depth (Cooke et al., 1982), consistent with the notion of critical propagation field strength. As implied by Fig. 3.1, the critical charge density does is nearly constant (between 0.2 and 0.3 nC m^{-3}) for typical storm geometries, so that lightning charge (and lightning-channel length) primarily depends on the volume of the charge region. The dependence of channel length on storm size was also suggested by Huntrieser et al. (2008). A quantitative estimate of the discharge amplitudes is taken from Maggio et al. (2009), who measured typical charge amplitudes between 5 and 25 C. Hence, the overall structure of the lightning-charge parameterization is proposed to involve an increase of lightning charge between about 5 and 25 C as the volume increases. The following relationship is consistent with this requirement. The involved constants were found by employing the procedure described at the beginning of this section.

$$\Delta Q = 25 \cdot (1 - \exp(-0.013 - 0.027V)), \qquad (3.5)$$

where the lightning charge, ΔQ, is given in C and the space-charge volume, V, is given in km^3.
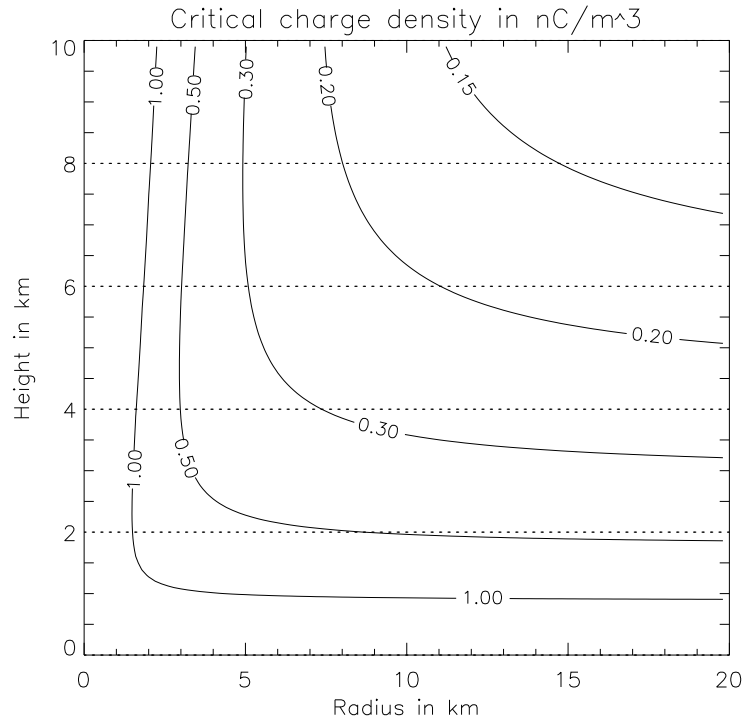
Figure 3.1: Charge density in nC m^{-3} required to create an electric field strength of 100 kV m^{-1} as a function of plate radius and plate separation distance.

This implies that the minimum charge transferred in a flash as defined in section 2.3.3 is about 2 C and the maximum charge is 25 C.

If the total charge required to achieve the critical electrostatic field is smaller than what is dictated by the volume-based parameterization, Eq. (3.5), it is possible that Eq. (3.5) demands that more charge be removed than was present before the discharge. This may happen with small geometries (bottom left regime in Fig. 2.8). I.e., less than two Coulomb may suffice to achieve critical field strength. In this case, the lightning charge is limited by the total charge. The upper limit of the lightning charge is 25 C.

The flash rate, given by Eq. (2.23), is inversely proportional to the lightning-charge amplitude, ΔQ. In other words, halving the charge amplitude doubles the flash rate.

The graupel-mass threshold that defines the graupel region influences the cross-sectional area of the space-charge region, and thus also its volume (section 2.4.3). Choosing a smaller threshold results in a bigger volume and hence in a faster saturation of the lightning charge at 25 C. The flash rate in cells with less than about 300 km^3 charge-region volume would be reduced by this effect. As before, the specific change of the flash rate as a function of the threshold depends on the size of the graupel region and on the rate of decrease of graupel mass towards the edge of this region.

Fig. 3.2 summarizes the functional relationship between the volume of the grau-pel region and the lightning charge.
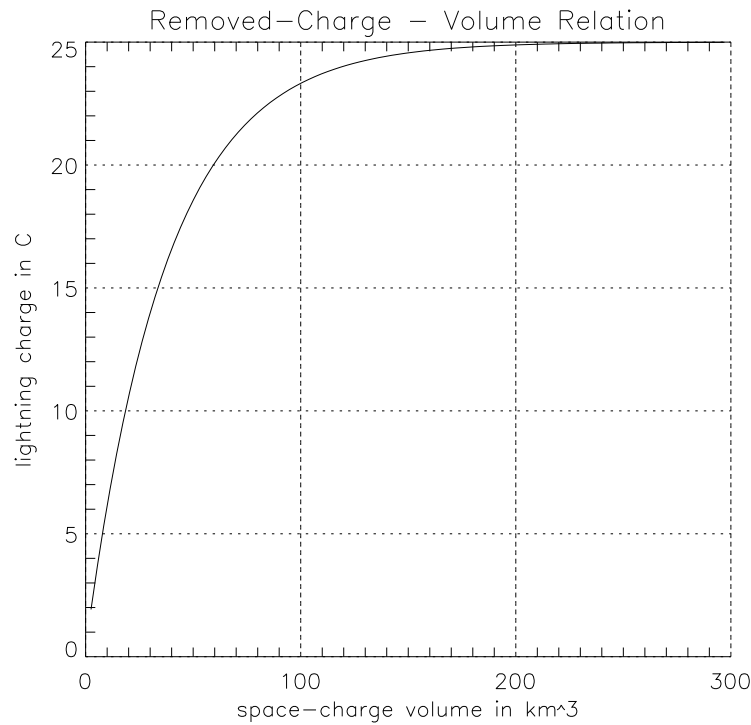
Figure 3.2: Charge in C deposited in a flash as a function of the volume of the space charge region.

The influence of the critical field strength

Although the strength of the critical field does not influence the flash rate in general, it does have an indirect influence when the thunderstorm cell is so small that the lightning charge needs to be limited by the total charge. The stronger the critical field, the more charge is required to achieve breakdown strength. In this case, a higher critical-field threshold would allow more charge to accumulate in the thunderstorm cells, allowing for larger charge transfers during a flash. This reduces the flash rate somewhat in the case of diminutive cells, where little charge is required to achieve breakdown field strength (Fig. 2.8). However, this limitation only affects very small cells, which owing to their generally small lightning rate, do not contribute much to the overall lightning activity (the flash rate is proportional to the storm's horizontal area). Hence, by all practical means, the flash rate does not depend on the value chosen for the critical field. However, to render the electrification model as realistic as possible, the height of the runaway-breakdown threshold is also determined:

$$E_c = -201.736 \cdot \exp\left(-\frac{H}{8400}\right), \tag{3.6}$$

where H is the altitude in m and E_c is the breakeven field strength in Vm^{-1}. This expression (including the constants) is due to Marshall et al. (2005).

The height of lightning initiation is assumed to be in the middle between the capacitor plates (Stolzenburg and Marshall, 2009 and Appendix A.1). The permittivity of air is given by (e.g., Meschede and Vogel, 2006):

$$\epsilon = 8.854 \cdot 10^{-12} \mathrm{As\ V^{-1} m^{-1}}. \tag{3.7}$$

Generator current density

The generator-current density is given by

$$j = \rho v_g, \tag{3.8}$$

where ρ is the space-charge density and v_g is the terminal velocity magnitude of graupel (see Appendix A.3). j includes two contributions, the charge density in the current as well as the velocity of the charged particles. The following assumptions are made:

1. The number of graupel pellets increases as the graupel mass increases; this assumption is justified in the context of the bulk-microphysics parameterization used in the COSMO-DE. In that approach, the slope parameter of the drop-size distribution is determined by the respective hydrometeor mass fraction (e.g., Doms and Schättler, 2004).

2. the number of graupel pellets per unit volume is directly proportional to the space-charge density; this assumption is based on the non-inductive charging mechanism (section 2.2): The more graupel particles exist, the more collisions between graupel and ice particles are possible. This implies that the space-charge density due to charge carried on both, graupel and ice particles, increases as the graupel mass increases.

3. The size of the graupel particles increases as the graupel mass increases; this also follows from the bulk-microphysics approach.

Assumptions 1) and 2) are contained in the following relationship, resulting from the tuning procedure presented at the beginning of this section:

$$\rho = \begin{cases} 4.467 \cdot 10^{-10} + 3.067 \cdot 10^{-9} m_g & \text{if } m_g \leq\ 3\ \mathrm{gm}^{-3} \\ 9.8 \cdot 10^{-9} & \text{if } m_g >\ 3\ \mathrm{gm}^{-3} \end{cases} \tag{3.9}$$

where ρ is the space-charge density in the generator current, given in Cm^{-3}, and m_g is the graupel mass in gm^{-3}. The upper bound of $9.8 \cdot 10^{-9}$ Cm^{-3} was introduced because otherwise the flash rates would become excessively large with intense storms.

In the central regions of the graupel-mass interval, charge density attains values of about 1 nC m^{-3}, which is the order of magnitude found for capacitors with the size of natural thunderclouds (Fig. 3.1).

The flash rate linearly depends on the generator current density, j, see Eq. (2.23). Consequently, varying the charge density also results in a linearly proportional variation of the flash rate.

The velocity in the generator current is given by the terminal fall velocity of the graupel pellets (see Appendix A.3). Now assumption 3) is used, which implies an increase of graupel-pellet size with increasing graupel mass. Typical sizes of graupel pellets were considered (e.g., Heymsfield and Kajikawa, 1987; Pruppacher and Klett, 1997, p. 58 ff.), ranging from 2 mm to 12 mm. A linear increase was assumed for simplicity, the slope being a result of the calibration procedure introduced in section 3.1.3:

$$D_g = \begin{cases} 1.833 \cdot 10^{-3} + 3.333 \cdot 10^{-3} m_g & \text{if } m_g \leq 3 \text{ gm}^{-3} \\ 0.012 & \text{if } m_g > 3 \text{ gm}^{-3} \end{cases} \tag{3.10}$$

where D_g is the graupel diameter in m. The terminal graupel fall velocity is adopted from the COSMO-DE source code, where it is given by

$$v_g = 422.0 \cdot D_g^{0.89}, \tag{3.11}$$

where v_g is the magnitude of the terminal graupel fall velocity im ms^{-1}. This formulation is based on work by Heymsfield and Kajikawa (1987). Accordingly, the charge-flux velocity ranges from about 2 ms^{-1} to 8 ms^{-1}.

The choice of numerical values for D_g affects the resultant flash rate in a nearly linear fashion:

$$f \propto D_g^{0.89}. \tag{3.12}$$

The parameterizations are summarized in Fig. 3.3. Tab. 3.2 summarizes all assumptions.

3.2 Definition of a cell in the PR92, YMUK09, and GR01 approaches

While the convective cloud-top height (or depth) can in principle be determined directly, it is impossible to cleanly distinguish between convective and non-convective clouds in a convection-resolving model. Circumventing this restriction by using e.g.,
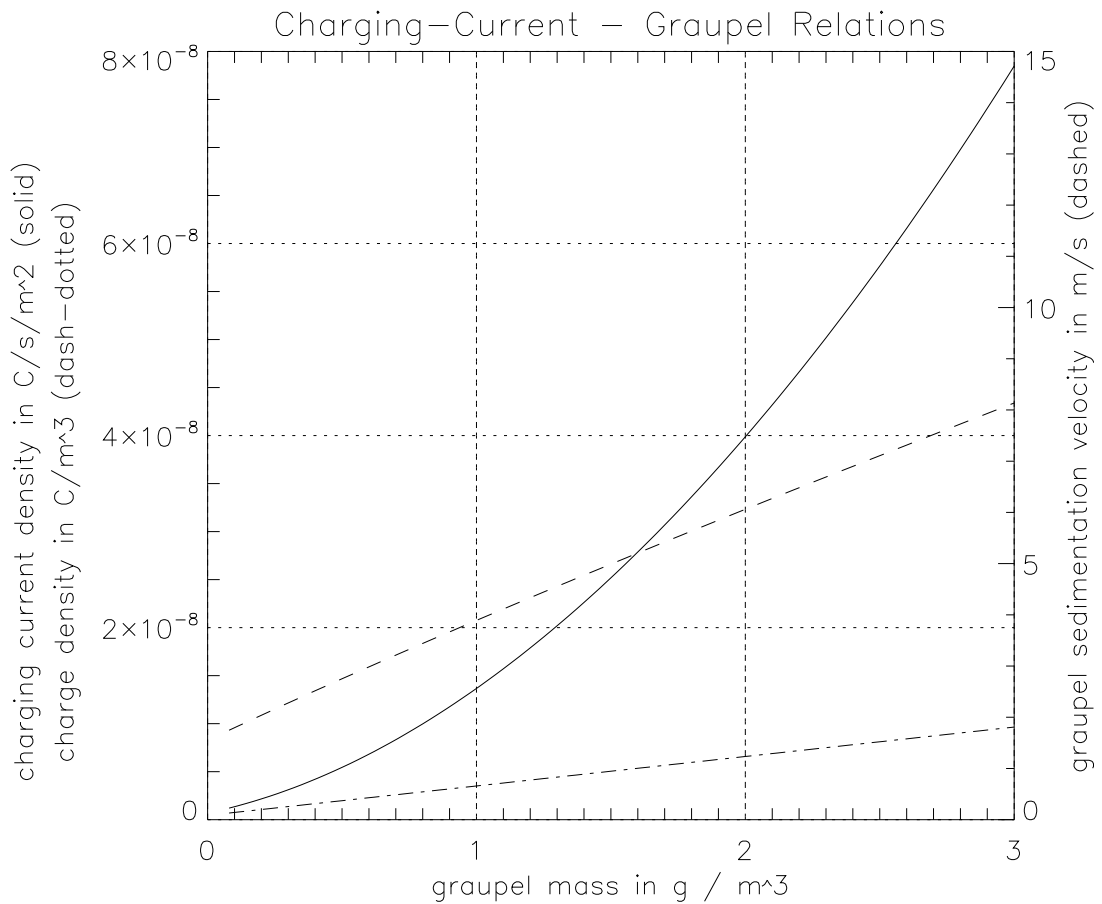
Figure 3.3: Parameterizations based on the graupel mass. The dashed line represents the terminal fall velocity of the graupel in ms^{-1} (right scale), the dash-dotted line represents the charge density in the generator current in Cm^{-3}, and the solid line represents the resulting generator current density.

Variable	Category	Justification
no charge below 263 K isotherm	stipulated	section 3.1.1
A	parameterized (m_g)	section 3.1.1
A threshold	stipulated	section 2.4.3
A equal size	stipulated	section 2.4.3
A circular	stipulated	section 2.4.3
ΔQ	parameterized (V)	section 3.1.3
ρ	parameterized (m_g)	section 3.1.3
D_g	parameterized (m_g)	section 3.1.3
V_g	observed	section 3.1.3 and Appendix A.3
E_c	observed	section 3.1.3
γ	stipulated	section 3.1.2

**Table 3.2:** Summary of assumptions regarding the variables that appear in the flash-rate equation.

the height of upper-level clouds exceeding a certain thickness has proven impractical, as i) stratiform clouds may be included and ii) individual cells cannot be identified if they share a common anvil cloud (which often is the case). This would underestimate the number of thunderstorm cells and also renders the distribution of flashes unrealistic.

The solution was to use the updraft velocity to identify convective clouds. A threshold of two ms^{-1} was chosen because it includes comparatively weak convective cells but excludes vertical-motion regimes associated with heavy stratiform precipitation. To assess the sensitivity of the flash-rate predictions to the choice of the updraft thresholds, two vertical cross sections of modeled convective clouds are shown in Fig. 3.4. The simulations were performed with the COSMO-DE model (see Appendix B). The topmost extent of the thick dashed contours represent the height of the thunderstorm cell for three thresholds of one, two, and four ms^{-1}. The middle contour depicts the threshold of two ms^{-1}, which is used in this study. The figure reveals that other choices (i.e., one and four ms^{-1}) would lead to variations of order $\pm$ 1 km. In this example, the strong updraft (Fig. 3.4(b)) exhibits a stronger vertical gradient of upward motion than its weaker counterpart (Fig. 3.4(a)). This implies that the sensitivity of the cloud-top definition via the upward-motion field varies from storm to storm.

Since COSMO-DE allows for gravity waves, there often is upward motion exceeding 2 ms^{-1} in the upper troposphere. Because the algorithm searches the highest points of regions where $w > 2$ ms^{-1} to find the cloud-top heights, gravity-wave
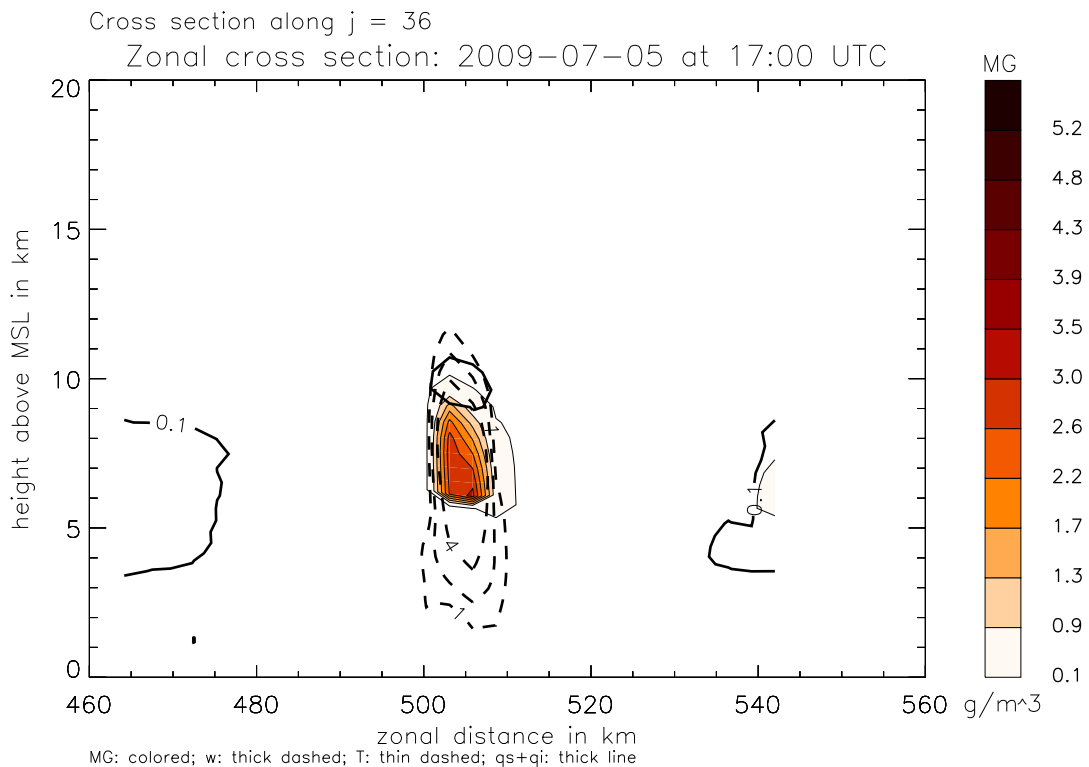
(a)
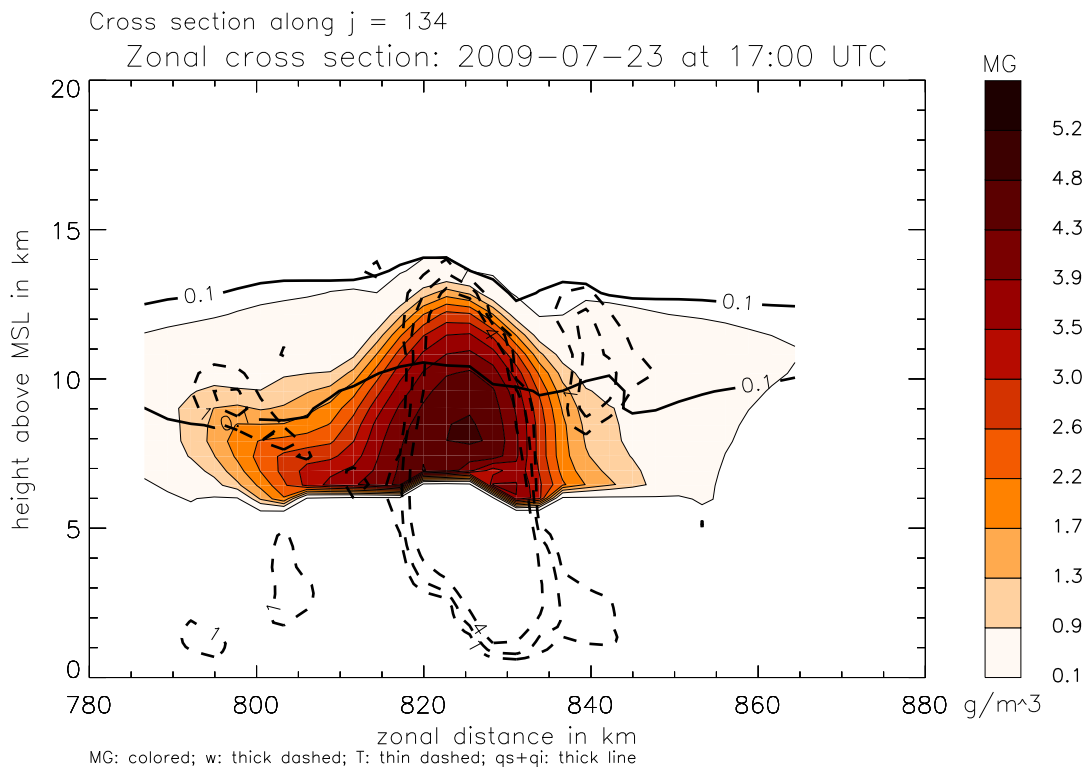
(b)

Figure 3.4: Shown are two cross section through modeled cumulonimbus clouds. Plotted are the updraft-velocity contours of 1 ms^{-1}, 2 ms^{-1}, and 4 ms^{-1} (thick, dashed), the graupel mass ("MG") in gm^{-3} (shaded), and the ice-mass contour of 1 gm^{-3} (thick solid).

related updrafts may erroneously be identified as thunderstorms. This effect has largely been reduced by demanding that the region where 2 ms^{-1} of upward motion are exceeded includes at least 10 gridpoints. These thresholds still allow cells at the weak and small end of the thunderstorm spectrum to be identified.

Chapter 4

Implementation

4.1 Description of the algorithm

To apply the flash-rate equation discussed in the previous chapter, knowledge about the spatial distribution of the graupel mass and of the ice mass is necessary. Also, the temperature field is required in order to determine the height of the 263 K isotherm. See section 3.1.3 for the parameterization of the charge regions in terms of graupel mass.

The variables that need to be determined by the algorithm are:

- The height of the 263 K isotherm,

- The centroid of the graupel region,

- The diameter of the horizontal cross section through the graupel region at the height of the centroid location,

- The storm's maximum graupel mass,

- The thickness of the graupel and ice regions.

If these quantities are known, the flash rate can be determined. Fig. 4.1 schematically shows how the required parameters are found by the algorithm. In the first step, a graupel region is identified. The centroid position of this region is determined. Then, the existence of ice crystals above the graupel region is verified. In the model, ice crystals are contained in the snow and cloud-ice categories. Thus, the sum of both categories is required to have a mass of greater than 0.1 gm^{-3} above the centroid position of the graupel region (section 3.1.3). If this condition is fulfilled, then it is assumed that the identified regions are part of a cumulonimbus cloud and that electrification is occurring. Else, the cloud is not considered to have the potential of producing lightning. The next step involves the determination of
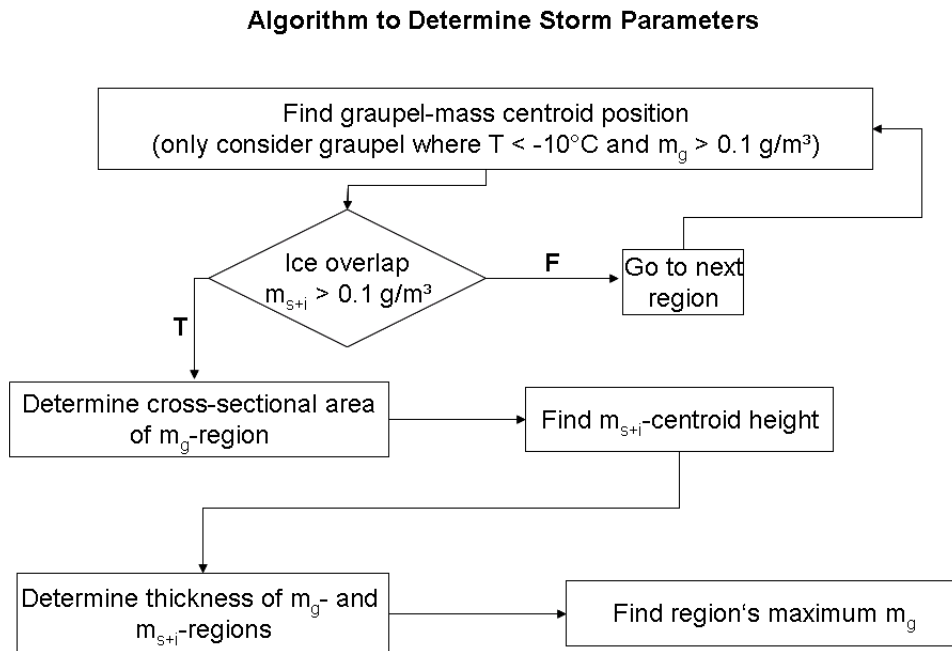
Algorithm to Determine Storm Parameters

Figure 4.1: Pseudo-flowchart of the flash-rate algorithm. See text for discussion.

the cross-sectional area of the graupel region at the height of its centroid. With this information, the equivalent circular radius is calculated. Also, the height of the centroid of the 3D ice region is determined. Now both, the area and the separation distance of the capacitor plates are known[1]. Fig. 4.2 shows the mapping of circular capacitor plates onto the graupel and ice regions for a comparatively small and a comparatively large convective storm, respectively. To parameterize the charge deposited in the lightning channels, the charge-region's volume needs to be known. As the equivalent circular radius is known, only the vertical thickness needs to be determined. The thickness of both, graupel and ice regions, is determined at the graupel region's horizontal centroid position. The arithmetic mean of both depths is taken to represent the charge regions' depths. In case of vertical intersections of graupel and ice regions, this may overestimate the actual thickness of the charge regions. Based on the investigated cross sections during the calibration of the parameterization, substantial overlaps tend to occur mainly with intense and usually horizontally extensive convective clouds which have strong updrafts. In this case, the lightning charge has saturated at 25 C already owing to the large area, independent of the thickness and is thus not affected by a possible overestimation of the thickness of the charge regions.

---

[1]Although the separation distance does not appear in Eq. 2.23, it is required for the detailed ASCII output (Fig. 4.6).
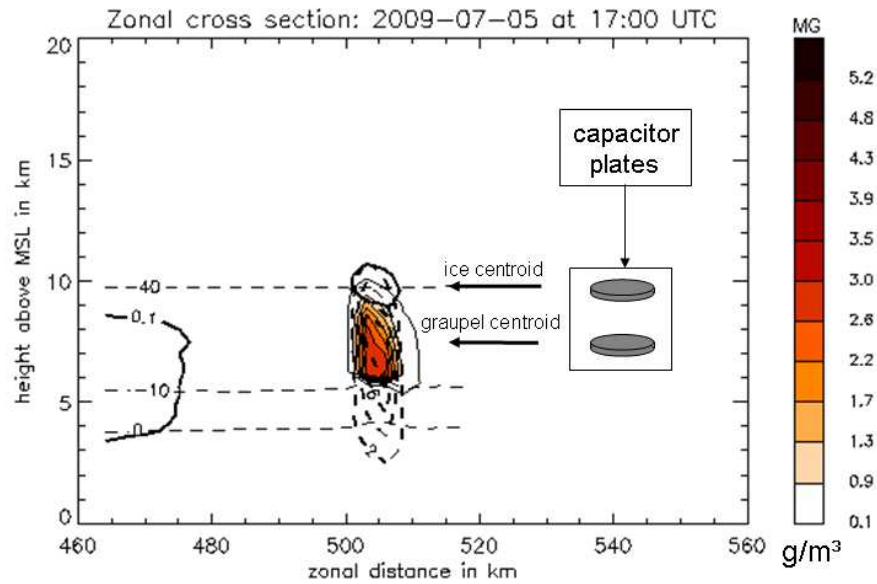
(a)
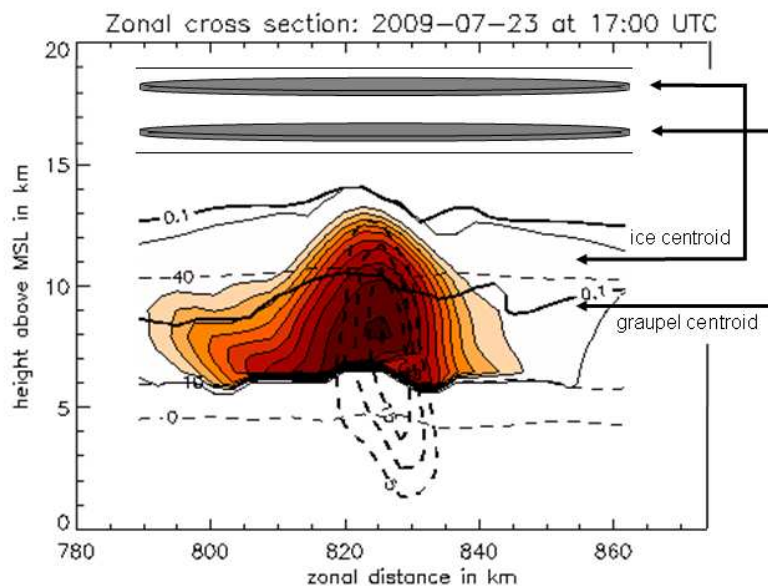
(b)

Figure 4.2: Shown are examples of cross sections of a small (a) and a large (b) convective cloud, as well as the size and the distance of the capacitor plates. The graupel region is colored, the ice is marked with the thick solid line and the updraft velocity is represented by the thick dashed contours. Also shown are isotherms (thin dashed lines). The dark grey ellipses indicate the position and size of the capacitor plates.

4.2   Implementation of the algorithm

Thus far, the procedure of how to determine the variables required to estimate the flash rate has been discussed. The next step is to automatize the algorithm and use modeled hydrometeor distributions. This way, the flash rate of modeled cells may be predicted. With this information, the number of flashes in a given time interval, as well as their location can be simulated.

4.2.1   Source-code organization

The numerical model used in this study is the COSMO-DE weather prediction model (see Appendix B for details). The model version used in this study was version 4.6. COSMO-DE features a 6-category, single-moment microphysics scheme, featuring the solid particles cloud ice, snow, and graupel. Wet growth (hail) is not included in the implementation used in this study. The horizontal resolution is about 2.8 km and the vertical resolution decreases from about 50 m near the ground to 1 km at the top of the domain, which is at 22.5 km MSL.

In order to integrate the algorithm into COSMO-DE, a new module, `src_lightning.f90` was written. In addition a data module, `data_lightning.f90`, was set up. These modules were included in the `Makefile` format file.

In addition, the new namelist parameters `itype_light` and `hinclight` were included, which determine the type of the parameterization and the number of time steps between two calls of the lightning package, respectively. The default setting for `hinclight` is 0.25 h. Tab. 4.1 summarizes the possible choices of the parameter `itype_light`. `itype_light == 3` is not actually used but refers to an experimental routine, which turned out to be inappropriate to simulate lightning realistically. `src_lightning.f90` contains all procedures required to simulate the

`itype_light`	Parameterization
itype_light == 1	D10 (dahl_2010).
itype_light == 2	PR92 (updraft) (pr92_updraft)
itype_light == 3	PR92 (hydrometeor content) (pr92_cwi)
itype_light == 4	YMUK09 (ymuk_2009).
itype_light == 5	GR01 (getal_2001)

Table 4.1: Choices for the namelist parameter `itype_light`. Abbreviations in the brackets refer to the names of the subroutines.

lightning discharges. The main COSMO-DE program, `lmorg.F90` calls the routine that organizes the diagnostic routines, `organize_diagnostics.f90` at the end of a

time step. In this routine, a new section was added where the module procedure `organize_lightning` is called. This procedure checks the namelist parameters that determine which parameterization is selected and calls the respective subroutines.

The software standard adopted in this implementation is the "European Standard for Writing and Documenting Exchangeable Fortran 90 Code" (Andrews et al., 1994) and parallelization was carried out using the message passing interface standard (MPI).

The CD attached to printed version of this work contains the source code of the new modules as well as the parts of the code where adjustments were made. In addition, a post-processing IDL-procedure is included which converts the COSMO-DE ASCII output to the final format (see section 4.2.3).

4.2.2 The module `src_lightning.f90`

A pseudo-flowchart of the steps performed in the module `src_lightning.f90` is shown in Fig. 4.3. First of all, the graupel regions need to be identified and labeled
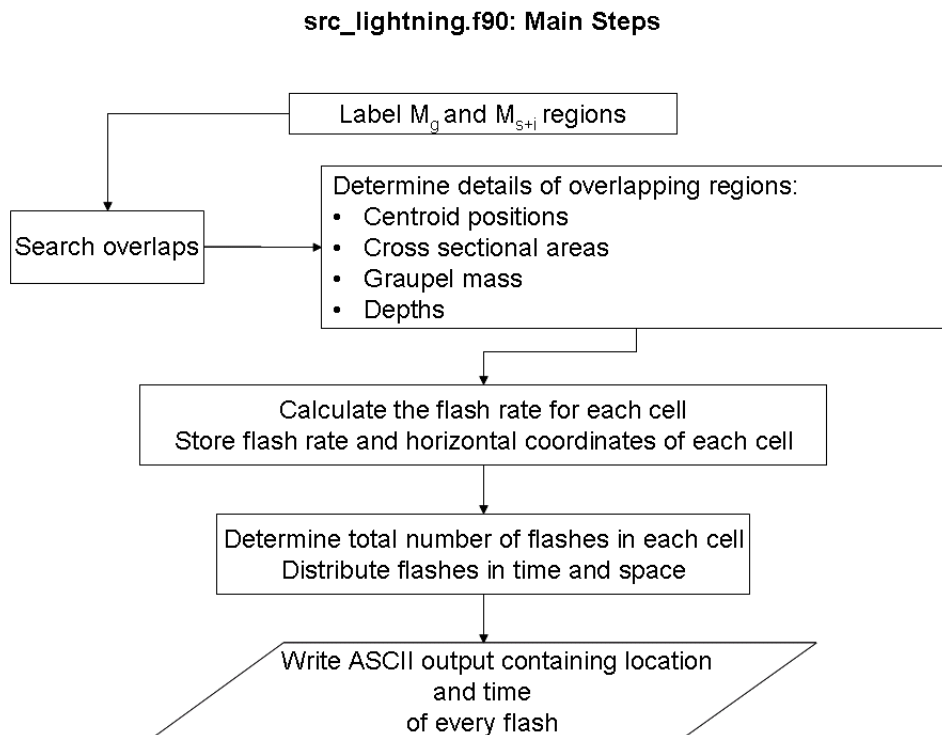

Figure 4.3: Pseudo-flowchart of the module `src_lightning.f90`. See text for detailed descriptions.

in order to assign attributes like size, centroid position, etc. to them. The labeling algorithm is due to Hoshen and Kopelman (1976, in the following HK76) who originally developed it in the context of percolation theory. In order to apply this

algorithm, the gridpoints identified as graupel regions are set to minus one, and all others are set to zero. The program now traverses this binary field and whenever it encounters a value of -1, assigns a positive number to the current site, if the neighbors of the site are zero or minus one[2]. The existence of neighbors is only checked in the directions where previous labeling may have occurred: $(i - 1, j, k)$, $(i, j - 1, k)$, and $(i, j, k - 1)$. If one or more neighbors of the current site have already been assigned a positive number, the site is considered to belong to an already existing cluster and adapts its label.

Now it is possible that there are two previously labeled clusters, and that the current site connects them. In this case, the current site is assigned the minimum of the two neighboring clusters' labels. This would require re-traversing the entire array to re-label the merged cluster with the maximum label, which is very time consuming. For this reason, a separate, one-dimensional array, `csize`, is maintained. The jth element of this array contains the number of gridpoints occupied by the cluster with the label j. If this cluster is merged with another cluster, n, the negative of n is assigned to the jth `csize` element. The absolute value of n is just the label of the merged cluster. At the same time, the nth element of the `csize`-array needs to be updated for the correct number of elements of the two coalesced clusters. A two-dimensional example of how the algorithm works is shown in Fig. 4.4. As nowadays the main application of HK76 is in image processing, the algorithm is usually discussed in two dimensions only. However, cluster merging may occur in three dimensions, which results in multiple combinations of neighbor-site occupations. Moreover, a given neighbor may previously have been coalesced with one or more clusters. See, e.g., Hoshen and Kopelman (1976) or Aldridge (2008) for more details.

COSMO-DE is fully parallelized, employing a domain decomposition. To enable optimum vectorization, the model domain is split into zonal strips, i.e., the domain is decomposed only in the north-south direction. The HK implementation was also parallelized in this work, using the method put forth by Constantin et al. (1997), which was extended to three dimensions. This way, the identification and labeling of contiguous regions can be performed very efficiently[3]. In essence, the result of the HK76 algorithm is that the gridpoint values within each graupel region are replaced by the label number of each region. All gridpoints belonging to a common cluster are assigned the same label. This labeling technique allows one to consider each region as entity whose properties are stored in a derived-type structure. Each element of this structure contains cluster properties (like the label, the number of elements) as

---

[2]The existence of a "neighbor" of site (i, j, k) is assumed if either $(i - 1, j, k)$, $(i + 1, j, k)$, $(i, j - 1, k)$, $(i, j + 1, k)$, $(i, j, k - 1)$, or $(i, j, k + 1)$ have been assigned a positive number.

[3]The run time of the lightning scheme is halved as the number of processors is doubled.

```
Matrix before HK application                    CSIZE
----------------------------                    -----
-1 -1  0  0 -1  0 -1 -1                          1    2
 0  0 -1  0 -1  0 -1 -1                          2   12
 0 -1 -1  0 -1  0 -1 -1                          3   -2
 0 -1  0  0 -1 -1 -1  0                          4    7
 0 -1 -1  0  0  0  0 -1                          5   -4
-1  0 -1  0 -1  0  0 -1                          6    5
-1  0  0  0  0  0 -1 -1                          7    3
-1  0  0  0  0  0 -1  0                          8    1
                                                9   -6

                  CSIZE array during HK application
                  ---------------------------------    Matrix after proper labeling
CSIZE elements: 1 2 3 4 5 6 7 8 9 10             ----------------------------
                  -------------------             1 1 0 0 2 0 2 2
After 1st line    2 1  2 0 0 0 0 0 0 0            0 0 4 0 2 0 2 2
                  2 2  4 1 0 0 0 0 0 0            0 4 4 0 2 0 2 2
        .         2 3  6 3 -4 0 0 0 0 0           0 4 0 0 2 2 2 0
                  2 12 -2 4 -4 0 0 0 0 0          0 4 4 0 0 0 0 6
        .         2 12 -2 6 -4 1 0 0 0 0          7 0 4 0 8 0 0 6
                  2 12 -2 7 -4 2 1 1 0 0          7 0 0 0 0 0 6 6
        .         2 12 -2 7 -4 4 2 1 -6 0         7 0 0 0 0 0 6 0
After 8th line    2 12 -2 7 -4 5 3 1 -6 0

                  Matrix after HK application                 Cluster    number of elements
                  ---------------------------                 ----------------------------
                  1 1 0 0 2 0 3 3                                  -
                  0 0 4 0 2 0 3 3                              1         2
                  0 5 4 0 2 0 3 3                              2         12
                  0 5 0 0 2 2 2 0                              4         7
                  0 5 5 0 0 0 0 6                              6         5
                  7 0 5 0 8 0 0 6                              7         3
                  7 0 0 0 0 0 9 6                              8         1
                  7 0 0 0 0 0 9 0
                                                              Number of clusters: 6
```
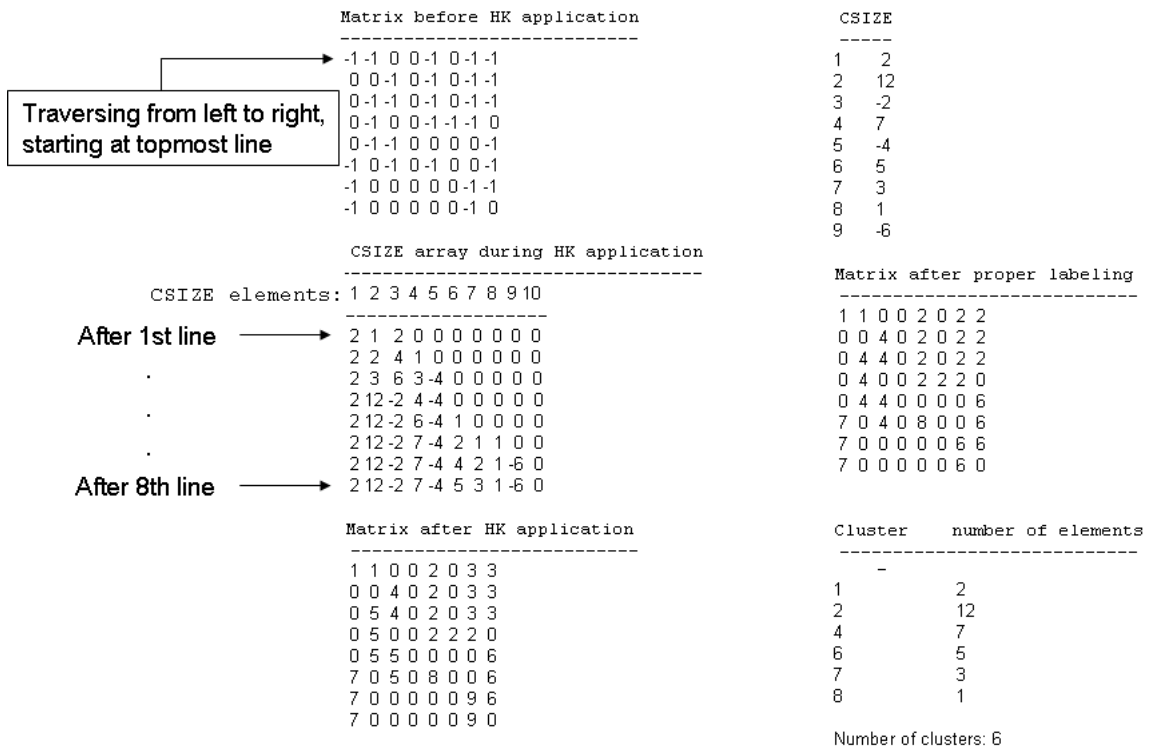
Figure 4.4: This figure summarizes the essence of the HK76 algorithm. The matrix at the top left shows the unprocessed binary matrix that is fed into the HK76 algorithm. The program scans from left to right, starting at the topmost line. Below this matrix, the first 10 elements of `csize` are shown. This array is initialized with zero and is filled with the number of identified elements belonging to a cluster. The `csize` index corresponds to the cluster label. In the 3rd line, cluster merging is occurring for the first time. After the initial traverse, the labels themselves have not been updated (bottom-left matrix). With the aid of `csize`, reproduced at the top right, the array can be updated for the proper labels (center right matrix). The positive `csize` entries contain the cluster statistics, as shown on the bottom right of the figure. Consecutive labeling (not shown) is achieved by another pass through the `csize` array.

components.

A utility routine, called `cluster_analysis`, now determines the centroid position of the graupel regions. Subsequently, the labeling and cluster-analysis algorithms are applied to the ice region, and horizontal overlaps of graupel and ice regions are sought as described in the previous section. All overlapping regions are considered to represent a capacitor. A new structure is set up, containing the capacitor labels and information such as diameter, maximum graupel mass in the graupel region, etc. With this information at hand, the instantaneous flash rate is calculated for each cell. The horizontal coordinates of the cells are given by the respective graupel-region centroid positions. These, as well as the flash rate are stored and handed over to the routine `distribute_flashes`. This routine determines the accumulated flashes of each cell between two calls of the routine. If the lightning package is called every 900 s (15 min), then the accumulated number of flashes of the cell labeled k, is

$$n_k = 900 \cdot f_k, \tag{4.1}$$

where n_k is the total number of flashes of the kth cell and f_k is the flash rate of the kth cell in s^{-1}. As now both the accumulated number of discharges per cell and the cells' positions are known, the individual flashes may be distributed underneath and in the vicinity of the cells. The most realistic-looking reproduction was achieved by simply distributing the flash positions radially around the centroids of the thunderstorm cells.

First of all, the time of occurrence of every flash is determined. For this, the entirety of flashes occurring in the given time interval is randomly distributed within this interval. In the next step, the n_k flashes per cell are spatially distributed around the cell. This distribution is realized in plane polar coordinates. Here the goal was to achieve realistically-looking results when plotting the time and location of each discharge on a map. Many methods were tested, including upstream distribution of flash locations to obtain coherent lightning swaths. The following method was subjectively assessed to yield the most realistic results. The method is tested by comparing simulated and observed lightning-density distributions in the next chapter. Again a pseudo-random number generator is used to spread the flashes within a certain radius, R. This radius is the equivalent circular radius of the graupel area, $R = \sqrt{\frac{A}{\pi}}$. Gauss-weighing is applied to reduce the lightning occurrence towards the edge of the cell:

$$r_i = R_k \cdot \exp(-ai)^2, \qquad \text{where } i = 1,\ldots,n_k; \tag{4.2}$$

r_i is the radial distance of the ith discharge from the cell centroid, assuming that it is located at the origin of the coordinate system. R_k is the plates' radius, $a = 1/(\sigma\sqrt{2})$ with $\sigma = 0.4 \cdot n_k$. The suffix, k, refers to the cell's label and the unit of r_k and R_k

is degrees (these are angular distances) . Fig. 4.5 shows how lightning locations are distributed around a centroid position located at $(\lambda, \phi) = (0,0)$ for $n_k = 50$. This procedure is repeated for every cell. Now that both the times of occurrence and the
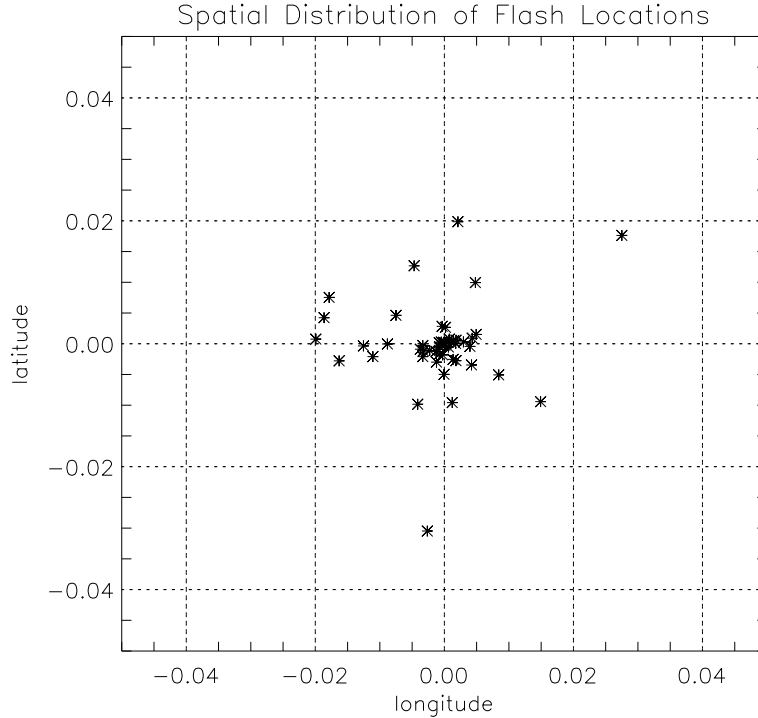

Figure 4.5: Flash locations for $n_k = 50$. The locations are marked by asterisks and the units of the x- and y-axes are degrees. The centroid of the cell is located at (0,0). 0.05° correspond to about 5.6 km.

coordinates of all flashes are known, they are concatenated into a list containing the time and location of all discharges that are simulated within the given time interval. Furthermore, details about the identified cells are accessible. An example of this is shown in Fig. 4.6.

4.2.3 Input and output

COSMO-DE is organized in a way that allows access to all model fields via data modules. These fields include variables pertaining to the model setup, the parallel environment, physical parameters, constants, etc. The lightning module uses quite many of these variables. These are declared at the beginning of the module `src_lightning.f90` (see attached CD). The subroutine that calculates the lightning frequency only uses the solid hydrometeor mass fractions (cloud ice, snow, graupel), temperature, and vertical velocity as input.

Every time the lightning scheme is called (every 15 minutes in this study), ASCII output containing a list with details about every simulated discharge is produced

```
****************************************************
        SRC_LIGHTNING.DAHL_2010: Verbose output
****************************************************

               Max number of cells:   52
                 at time step/hour:    2592  18.00
             Details of storm (label):  28

                  GEOMETRIC PARAMETERS:
                  ---------------------
                     Position (X,Y):   333, 142
          Equivalent circular diameter:  15.5    km
                  Centroid distance:     2.8    km
                  Plate SFC distance:    0.0    km
                       Plate depths:     5.5    km
                   Storm-top height:    11.5    km
                  Total storm depth:    11.0    km
                      Charge volume: 1045.4    km**3
           Max graupel content (MG):     4.1    g/m**3
                      Geometric term:   0.3505

                  ELECTRIC PARAMETERS:
                  ---------------------
                     Critical field: -91.2     kV/m
               Total charge per plate: 185.3     C
                   Charge per volume: 0.177E-09  C/m**3
                      Charge per area: 0.979E-06  C/m**2
                    Graupel diameter: 1.200     cm
                Sedimentation velocity: 8.24     m/s
             Charging current density: 9.800E-09  C/m**3
                      Removed charge: 25.0      C
                      Removed E-field: -12.3     kV/m
              Charge removal efficiency: 0.135
        Field neutralization efficiency: 0.135
                         Flash rate: 33.0151    1/min
```

Figure 4.6: An example of the details of a thunderstorm cell that may be obtained from the lightning scheme.

(apart from the information shown in Fig. 4.6). This list contains

- the time in seconds after initialization of the simulation,

- longitude in rotated coordinates (see Appendix B),

- latitude in rotated coordinates (see Appendix B).

The time is not printed in increasing order. Also, there are altogether 96 output files for a 24 h simulation. Thus, a post-processing routine was written that sorts the entries with respect to time and transforms time to hours, minutes, and seconds. Also, the coordinates are changed into geographical coordinates. The post-processing software also creates a single file out of the original 96 output files, which contains the entire information of all 15-min intervals (or whatever value may be selected for `hinclight`). This way, the results may comfortably be processed for further evaluation.

In addition, details about every thunderstorm cell are written to the log file, Fig. 4.6.

4.3   COSMO-DE-specific additions

So far it has been assumed that real-world convective clouds and modeled convective clouds share identical properties like graupel mass, storm size, etc. However, it is a well-known problem among the COSMO community that the graupel is too "snowy", resulting in low-density graupel pellets and too wide graupel regions[4]. As a consequence, the convective cells tend to be too extensive horizontally in COSMO-DE. Since there exist some principle constraints when attempting to compare individual real-world clouds with modeled ones (see section 6.1), it is not possible to offer sophisticated correction functions for the graupel regions. The following corrections are proposed as "best guess" to account for these known errors:

$$m_{gc} = 1.2 \cdot m_g \tag{4.3}$$

and

$$R_c = \frac{1}{2}R, \tag{4.4}$$

where m_{gc} is the corrected graupel mass and R_c is the corrected equivalent radius. The 20 % increase of graupel mass and halving the radius seem to yield quite realistic pictures for a rather wide spectrum of thunderstorms.

4.4   Other parameterizations

The parameterizations by PR92, YMUK09, and GR01 (see section 2.5.2) have also been implemented. For these parameterizations, the cloud-top cloud-top height (PR92), the cold-cloud depth (YMUK09), and the total cloud depth (GR01) is needed. In addition, GR01 requires the calculation of the mean updraft velocities in the thunderstorm cells. In all of these implementations, the labeling algorithm needs to be called only once, and only some minor cluster analysis is performed. As discussed in section 2.5.2, the PR92 parameterization is given by

$$f_{pr} = 3.44 \cdot 10^{-5} H^{4.9}, \tag{4.5}$$

the YMUK09 parameterization by

$$f_{ymuk} = 10^{-6.1} \bar{H}^{4.9}, \tag{4.6}$$

and the GR01 parameterization by

$$f_{gr} = 5.01 \cdot 10^{-7} \left(w\sqrt{d} \right)^{2.64}. \tag{4.7}$$

---

[4]This topic was addressed during the COSMO user seminar 2009 in Langen, Germany, and on several occasions was confirmed to the author by A. Seifert (DWD; author of the COSMO microphysics scheme).

The geometric cloud properties (cloud-top height, etc.) are determined with the aid of the upward velocity. In the current implementation, regions where the upward velocity exceeds 2 ms^{-1} are considered. For the YMUK09 parameterization, only the depth of the updraft there the temperature is less the 273 K, is analyzed (section 2.5.2).

Since the horizontal area of the cells is not known in these implementations (only the vertical geometric properties are determined), the angular distance representing the maximum radius for the flash distribution, R_k, is determined by the accumulated number of discharges, n_k:

$$R_k = 0.05 + 2.5 \cdot n_k. \tag{4.8}$$

The area dependence of the flash rate was demonstrated in section 2.4.1. R_k is not allowed to be less than 17 °, however. This restriction was included because the cell tracks became unrealistically narrow in some cases when this lower bound was omitted.

Chapter 5

Tests of the New Lightning Parameterization

In this chapter, the parameterization developed in section 2.4 and chapter 3 is tested using observed thunderstorm clouds. For this purpose, radar measurements were used to determine the storm parameters that are required as input for the flash-rate equation. The measurements were obtained from a polarimetric diversity radar, abbreviated POLDIRAD (Schroth et al., 1988). This doppler radar operates in the C-band and is located in southern Germany at DLR in Oberpfaffenhofen, roughly 25 km southwest of Munich. With its polarimetric capabilities the shape of the hydrometeors may be inferred, which in turn may be associated with certain hydrometeor classes. See Höller et al. (1994) for details. The predicted flash rate based on these data was then compared with measured LINET flashes. Three parameterizations are tested, the one developed in this study (D10), as well as the PR92 and YMUK09 parameterizations. Also, alternative ways of predicting the flash rate based on sounding parameters will be presented.

5.1   Individual observed cumulonimbus clouds

As the D10 parameterization (section 3.1) was derived based on theoretical considerations and plausibility, the next step is to test whether the involved assumptions result in meaningful predictions.

To assess the geometry of the graupel regions as well as the graupel mass, constant-altitude plan-position indicator (CAPPI) as well as range-height indicator (RHI) products were used. The software which provided ready access to the required fields is called *Toolkit* (developed by the company GAMIC). Unfortunately, the automated algorithm (section 4.2) cannot directly be applied to the radar data. This is because merely slices through the storm, rather than a coherent three-dimensional

picture, are provided at a given time. This made it necessary to retrieve the required data manually from the analyzed Toolkit fields. Although it was proceeded as discussed in section 4.1, the determination of maximum graupel mass, equivalent circular diameter, etc. was done by eye. While there are inherent inaccuracies associated with this method, it is the only viable procedure in the current context. A mouse-over function enabled the display of the exact distances from the radar, as well as graupel mass and many other parameters, which has increased the accuracy compared to mere "eye-balling". The reading was performed several times (and partly by several persons), and the resulting parameters were sufficiently stable so that this method is used to assess the accuracy of the flash-rate predictions.

An example of how the manual procedure was applied is demonstrated for the case of a severe hailstorm that occurred on 22 August 2008. Fig. 5.1(a) shows the RHI reflectivity field of this storm. The graupel-mass product of the Toolkit software of a supercell on 22 August 2008 is shown in Fig. 5.1(b). The 12 UTC radiosonde ascent from München-Oberschleissheim (not shown) suggests that the 263 K isotherm was located at an altitude near 5.5 km MSL. The centroid position of the graupel region is then estimated to be at an altitude of 8 km. The cross-sectional diameter at this altitude is gauged to be 17 km. Given that attenuation effects may have occurred at the far side of the storm, the value of 17 km diameter may be somewhat inaccurate. Also, cross-sectional area of the graupel region was not completely circular (not shown). In lack of an objective way of assessing attenuation effects, and because of the inaccuracy in determining the cross-sectional area, an error of ± 5 km is assumed for the diameter. To obtain the maximum graupel mass, the hail category has also been considered (Fig. 5.2(a)) because there is no hail category in COSMO-DE. As the graupel mass is not included in the hail-mass display in the Toolkit products, the sum of graupel and hail mass is considered. In the present example of 22 August 2008, this sum is 8 gm^{-3}. The plate thickness is estimated to be roughly 4 km. If these values are inserted into the flash-rate equation for the scans shown above, a flash rate, f_p, of

$$f_p = 40 \text{ min}^{-1} \tag{5.1}$$

is predicted. If the graupel-region's diameter, D, is allowed to vary by ± 5 km owing to reading errors, then the predicted flash rate ranges from 20 to 66 min^{-1}.

The comparison with LINET flashes is done as follows. Since the time of the scan is known, flash-density plots can be produced, including all flashes in certain intervals around the time of the scan. The arithmetic mean of a 5-min interval, a 10-min interval, and a 15-min interval around the time of the radar scans is used for comparison. The reason that three intervals were chosen is that the instantaneous flash rate may tend to fluctuate, and a value that represents the electric activity in
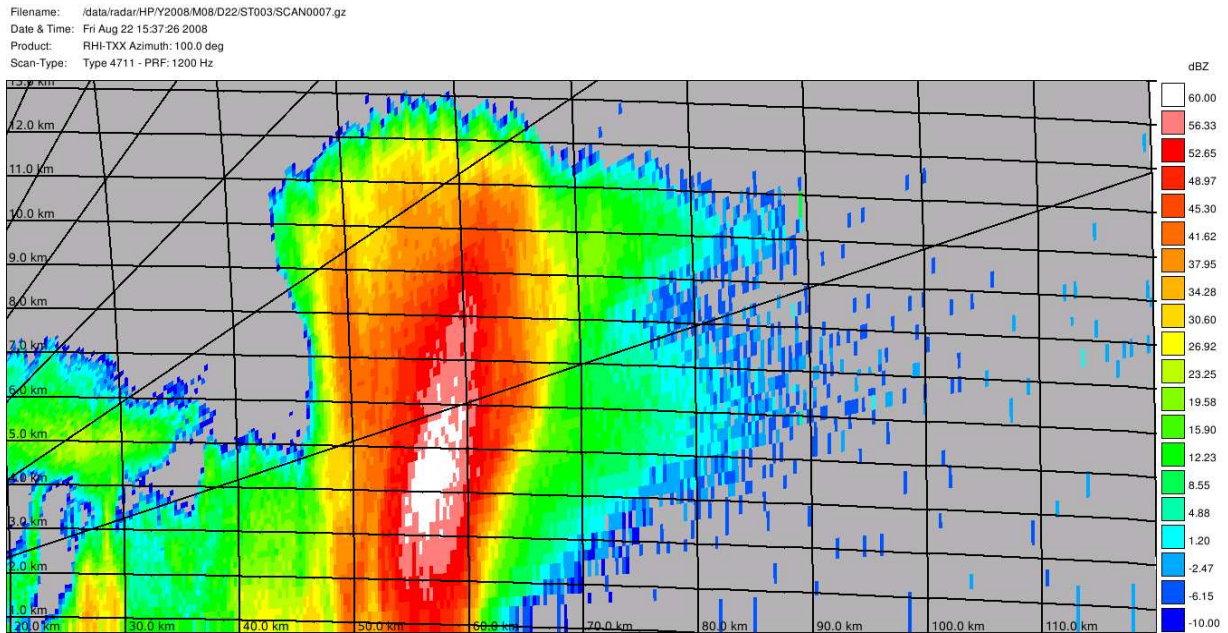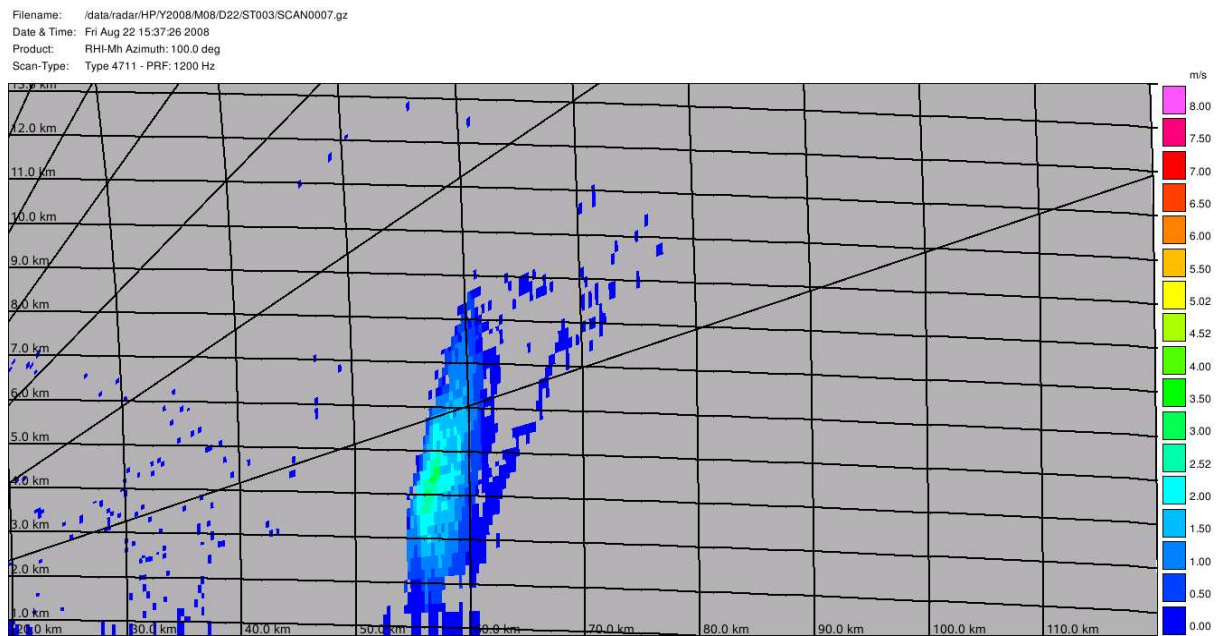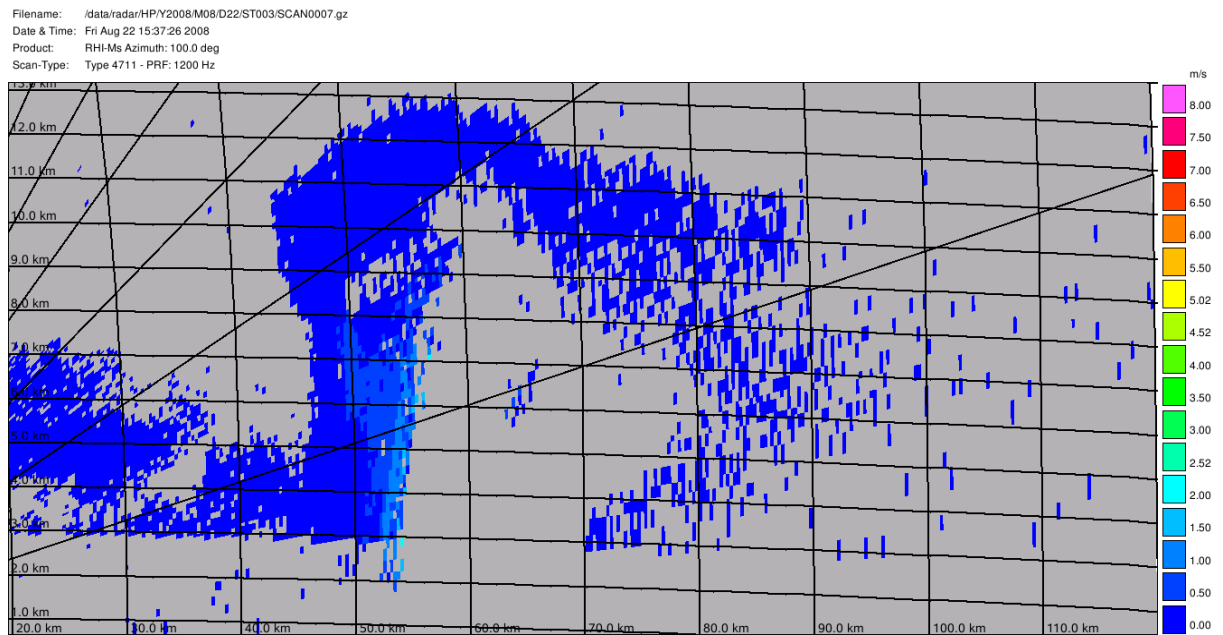
(a)
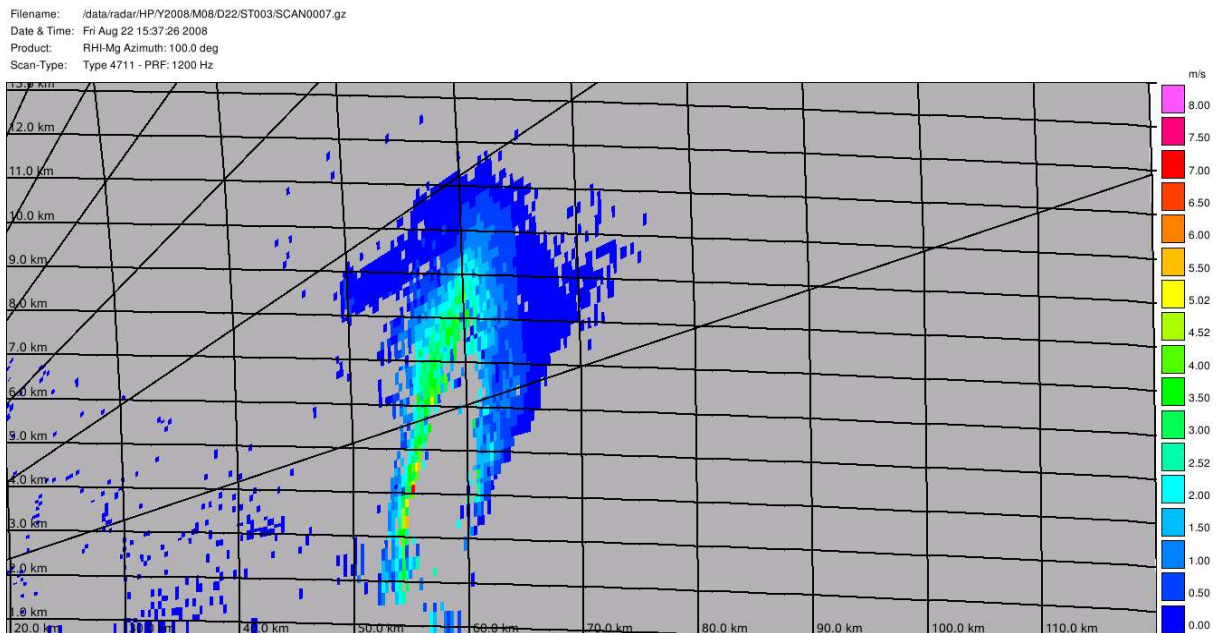
(b)

Figure 5.1: POLDIRAD RHI display of the reflectivity field (a) and the graupel mass in gm^{-3} (b), belonging to a severe hailstorm on 22 August 2008.

(a)

(b)

Figure 5.2: As in Fig. 5.1, but for the hail-mass (a) and the snow-mass (b) fields, both in gm^{-3}.

the current stage of the cell was sought.

The association of a lightning region with the scanned cell was done visually and in most cases was straightforward (see Fig. 5.3). The coherent flash-density regions were identified and labeled, and the total number of flashes contributing to each region was counted. Since the time interval was known, the mean flash rate per "lightning cell" could be determined. In the above example, the averaged measured
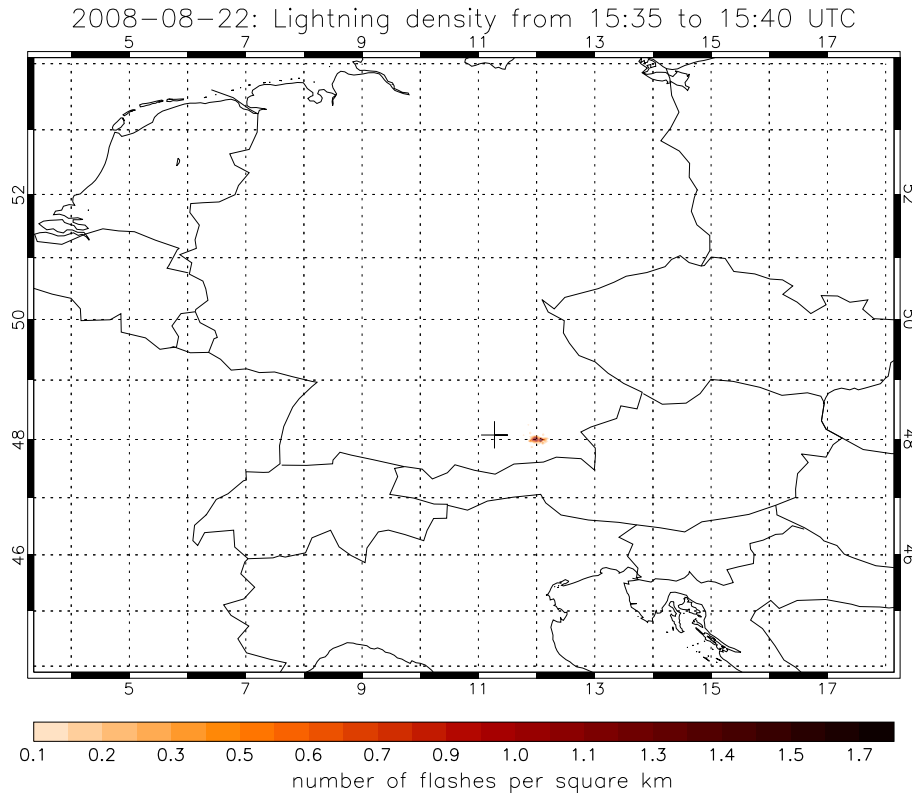
Figure 5.3: Plot of observed flash density in km^{-1} on 22 August 2008 between 1535 and 1540 UTC. Only one flash cell is visible at N48.0 E12.0, which is the supercell storm shown in the radar images above.

flash rate is

$$f_L = 33 \text{ min}^{-1}, \tag{5.2}$$

where f_L is the flash rate based on LINET flashes as defined in section 2.3.3. The flash rates in the three time intervals ranged from 27 to 38 min^{-1}.

The procedure described above was repeated for several cells. The technical criteria used in choosing the cases are:

1. The cells were required to be in reasonably close proximity to the radar, so that the measurement quality was high;

2. The entire cell or the entire segment of a squall line needed to be covered by the scans.

Another criterion was the structure and intensity of the storms. These were supposed to include at least following "types" of convection:

- Shallow, weakly-electrified polar-air convection,

- Isolated, poorly-organized and weak thunderstorms,

- Elevated thunderstorms,

- Isolated, severe supercells,

- Squall lines / bow echoes,

- Well-organized MCS containing supercells.

These scenarios largely comprise the range of convective storms that may occur over central Europe, and it contains rare extremes on both the weak and the strong ends, as well as rather common scenarios.

Unfortunately, POLDIRAD was not operational on 1 March 2008 when a narrow, strongly forced line of convection crossed southern Germany. This line not only produced severe wind gusts and small hail, but also unseasonably frequent lightning. However, this case will briefly be discussed in the next section.

Again, an error of ± 5 km was assumed for the equivalent circular diameters. Only in those cases where i) the cross-sectional area was quite circular and ii) where the graupel region was rather small in extent (say, 5 km in diameter), an error of ± 1 km was considered. Whenever attenuation effects occurred, which could not be accounted for, e.g., by using other scans the case was dismissed.

Tab. 5.1 shows some details about the investigated cases, as well as the observed and predicted flash rates, the predictions being based on the application of the procedure shown in Fig. 4.1. Also, the error is considered that may have resulted from subjectively assessing the diameters of the graupel regions. There is one complete miss on 26 June 2009, where weakly-flashing storms were observed, but no graupel above the 263 K level. As a consequence, application of the algorithm dismissed this cell. A case where precipitating moist convection but no lightning occurred, has also been included (non-electrified graupel shower on 23 Jan 2009), which was correctly dismissed by the algorithm.

A scatter diagram of the results shown in Tab. 5.1 is presented in Fig. 5.4. The error bars indicate the uncertainty involved in determining the cross-sectional diameter of the graupel region. The variation of the flash rate in response to the error is nonlinear and generally increases with increasing flash rate. This plot is dominated by three data points belonging to MCS cases with flash rates in excess of 100 min^{-1}. When omitting these cases and considering only the 11 remaining data

Date	Scenario	f_p	f_L	f_p-range
23 Jun 08	Isolated supercell	26 min^{-1}	21 min^{-1}	[11, 49]
24 Jun 08	WAA-regime, weak, elevated	1.5 min^{-1}	1.5 min^{-1}	[1.1, 1.9]
20 Jul 08	Shallow but sheared	0.17 min^{-1}	0.93 min^{-1}	[0.12, 0.20]
22 Aug 08	Isolated supercell	40 min^{-1}	33 min^{-1}	[20, 66]
23 Jan 09	Shallow snow/graupel showers	0.0 min^{-1}	0.0 min^{-1}	[0.0, 0.0]
26 May 09	Approaching squall line	493 min^{-1}	212 min^{-1}	[414, 579]
26 May 09	Departing squall line	527 min^{-1}	217 min^{-1}	[445, 615]
26 Jun 09	Single cell	0.0 min^{-1}	0.5 min^{-1}	[0.0, 0.0]
30 Jun 09	Single cell	8.5 min^{-1}	2.8 min^{-1}	[6.9, 10.3]
30 Jun 09	Weak multicell	7.5 min^{-1}	5.0 min^{-1}	[6.8, 8.7]
05 Jul 09	Single cell	0.6 min^{-1}	0.5 min^{-1}	[0.5, 0.6]
05 Jul 09	Weak multicell	10 min^{-1}	9.2 min^{-1}	[8.4, 11.7]
23 Jul 09	Isolated supercell	55 min^{-1}	64 min^{-1}	[31, 87]
23 Jul 09	Severe MCS	242 min^{-1}	106 min^{-1}	[188, 303]

Table 5.1: Summary of cases used for testing the flash-rate equation. See text for details. WAA is short for warm-air advection, f_p is the predicted flash rate and f_L is the measured flash rate. f_p-range is the frequency variation based on the diameter errors.

points (non-MCS cases), these are closely aligned along a linear fit, see Fig. 5.5. The slope of this fit is b = 0.91 and the correlation coefficient is 0.98. The RMSE = 4.2 min^{-1}, and the mean absolute error is 3.2 min^{-1}.

For the COSMO-DE implementation, a practical solution was sought to reduce the MCS errors: Between 15 km and about 45 km diameter, the flash rate is artificially reduced to 40 % of the original value. The gradual decrease ensures that e.g., large isolated supercells are not significantly affected by the correction. This ad-hoc correction is given by

$$c = \begin{cases} 1 & \text{if } D \leq 15 \text{ km} \\ 0.4 + 0.6 \cdot \exp[0.085 \cdot (D - 15.0)]^2 & \text{if } D > 15 \text{ km} \end{cases} \tag{5.3}$$

where c is the dimensionless correction factor. Fig. 5.6 shows the correction factor as a function of the diameter. The flash rate is the product of the correction factor and the uncorrected flash rate. This correction is entirely artificial and only serves to render the simulation results more realistic in case of large MCSs. The effect of the MCS correction is shown in Fig. 5.7. This way, the predictions that were excessively large compared to the observations are adjusted to fit the observations. A discussion on this correction is presented in section 7.2.
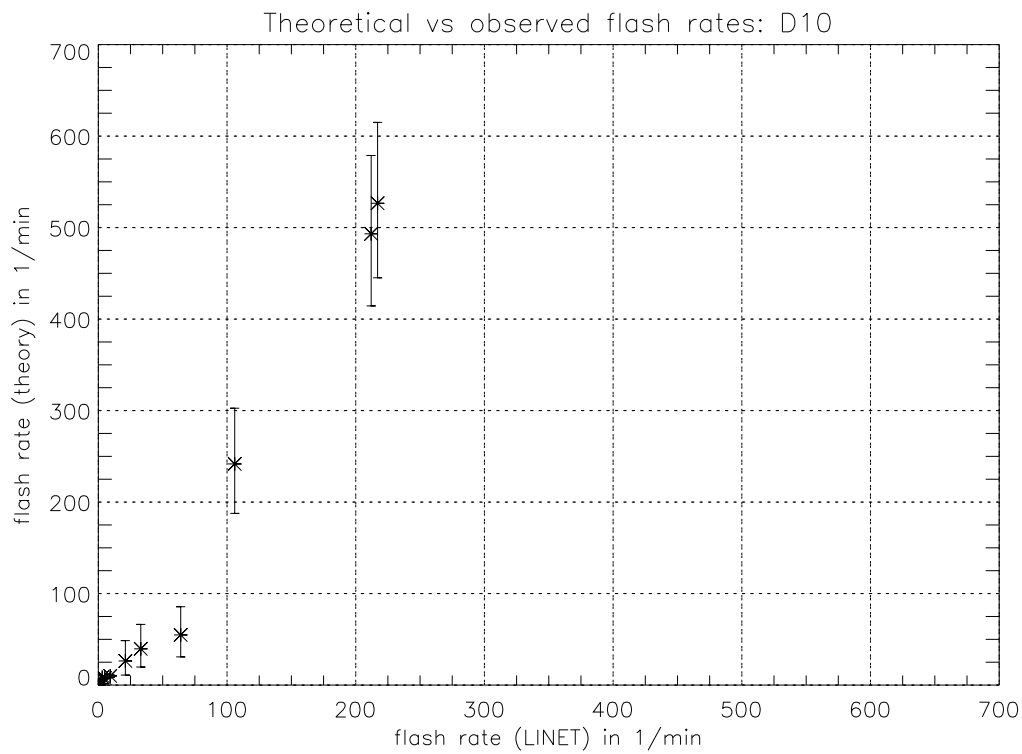
Figure 5.4: Scatterplot showing observed (x-axis) and predicted (y-axis) flash rates. Also shown is a linear-regression line for non-MCS cases.
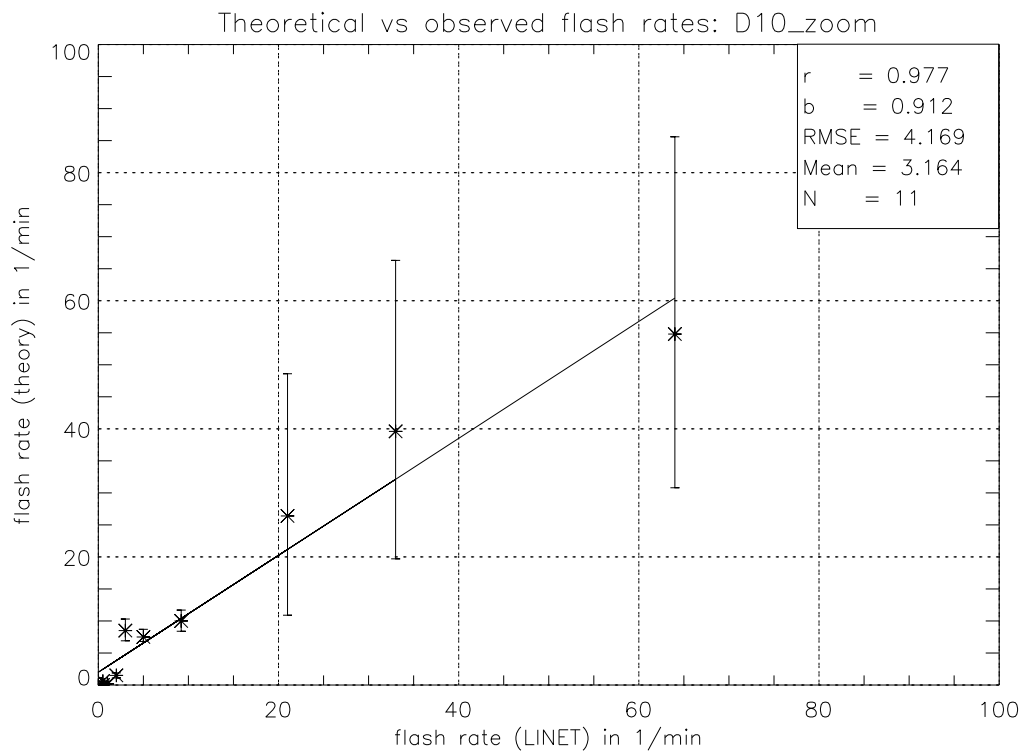

Figure 5.5: As in Fig. 5.4, but omitting the three MCS cases. In the inset, the correlation coefficient, r, the slope of the regression line, b, as well as the RMSE, the mean error, and the number of data points, N, are shown.
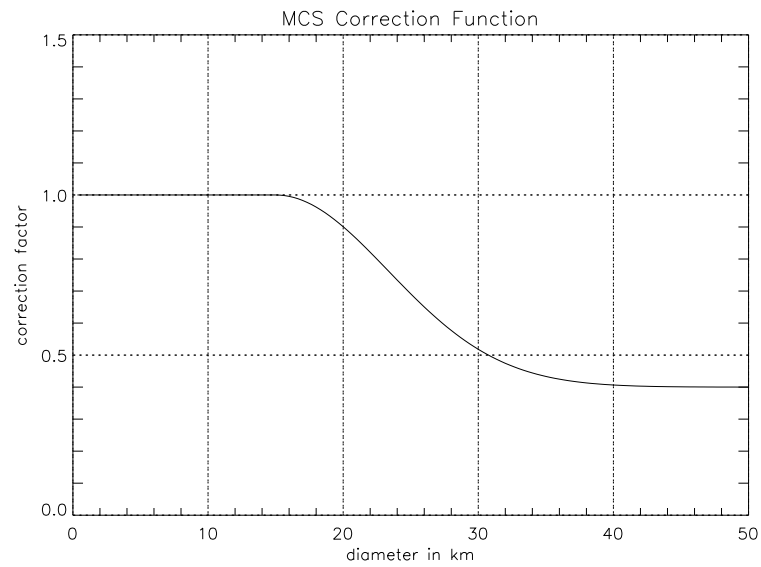
Figure 5.6: Correction factor for the flash rate, depending on the equivalent circular diameter of the graupel region.
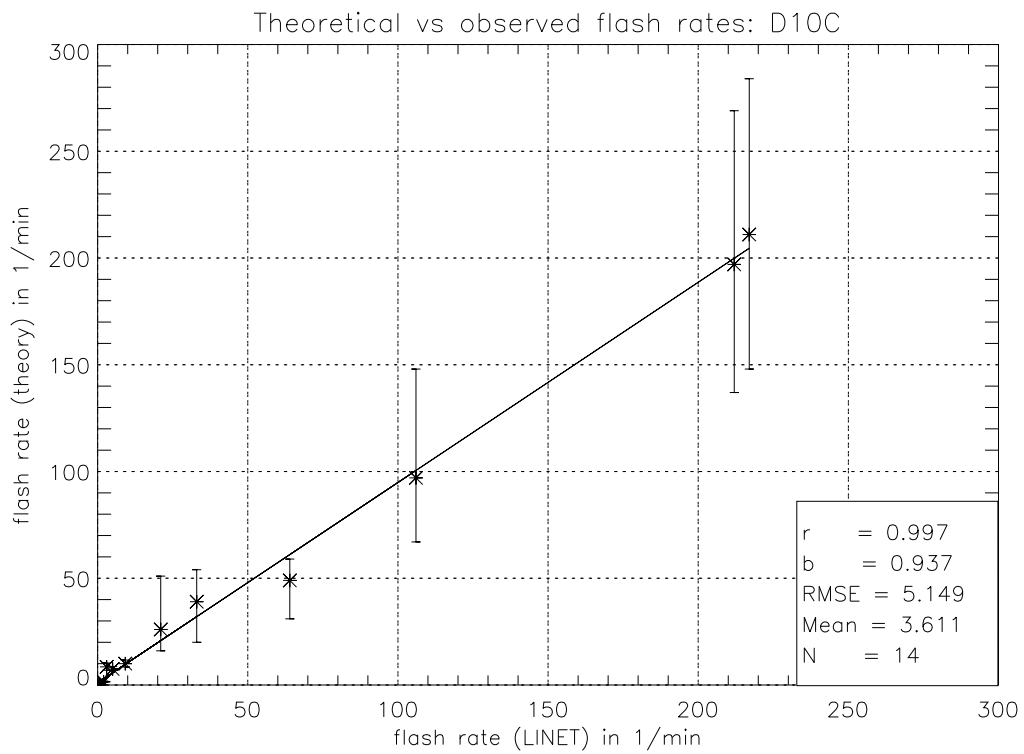
Figure 5.7: As in Fig. 5.4, but with artificial MCS correction.

To compare the new results with existing parameterizations, the PR92 and YMUK09 predictions have been determined as well. For PR92 only the altitude of the cloud top is needed, which has been determined from radar. The highest extent of the available radar echoes has been used and checked against radiosonde data for plausibility. The results are shown in Fig. 5.8. The correlation coefficient is 0.63, and the slope of the regression line is 0.05. The RMSE as well as the mean error are about 5 min^{-1}. Altogether, the flash rate is strongly underestimated, varying between zero and 20 min^{-1}, and being distributed rather randomly across the spectrum of investigated storms. As will be further detailed in chapter 7, the
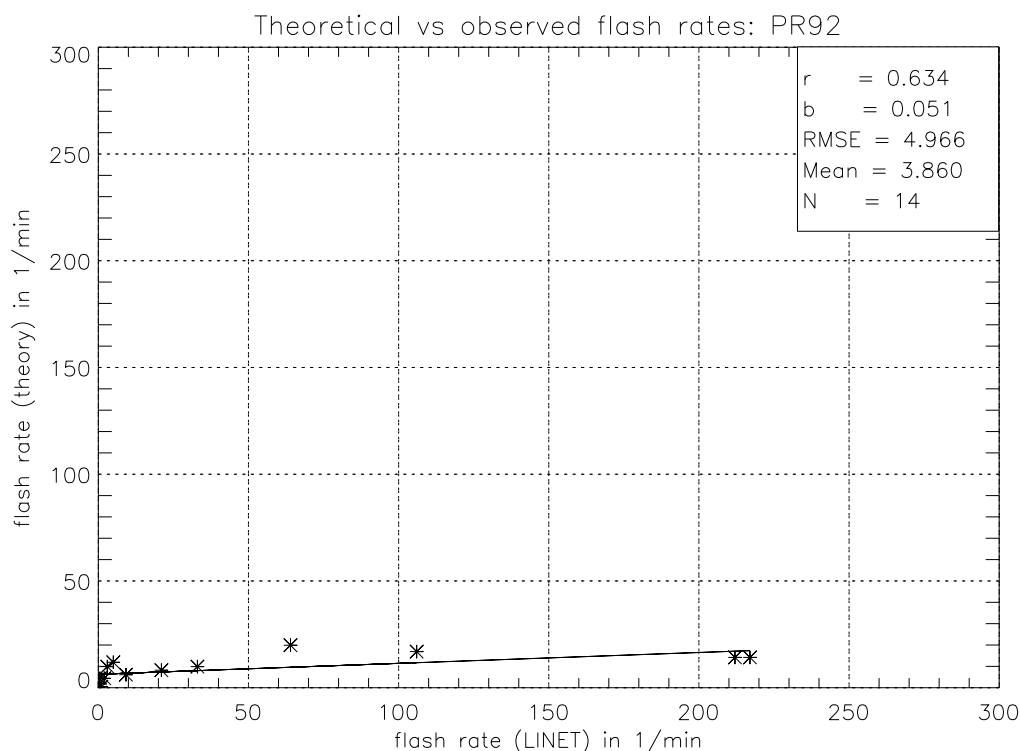

Figure 5.8: As in Fig. 5.4, but for the PR92 parameterization.

underestimation may be a result of different detection efficiencies of the methods used in this study and by PR92. For the present comparison, this may be accounted for by correcting the PR92 predictions: The average lightning rates of the LINET observations and PR92 predictions were calculated, and subsequently the PR92 data were multiplied with a correction factor so that both average values were equal. This was done for all cases (Fig. 5.9(a)) and for the cases including isolated storms only (Fig. 5.9(b)). The slope of the linear fit is 0.28 (r = 0.63) if all cases are considered and 0.43 (r = 0.82) if only isolated storms are considered.

In order to determine the flash rate according to YMUK09, the cold cloud depth was estimated. This was done with the aid of radiosonde data, that were used to assess the altitude of the 263 K level. This altitude was subtracted from the cloud
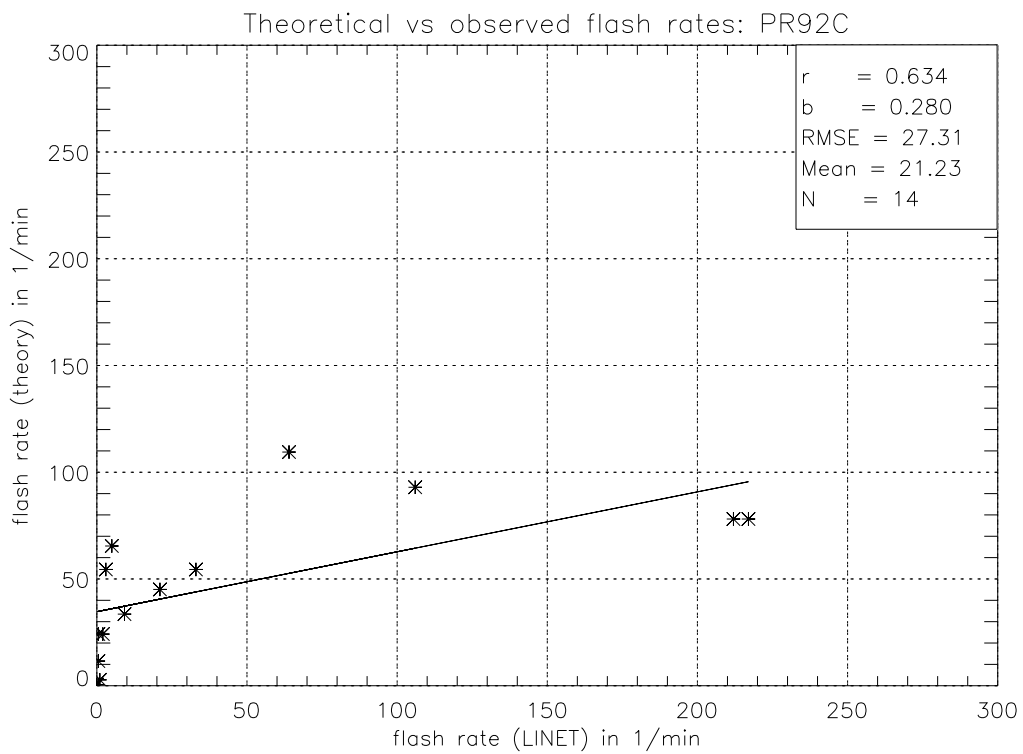
(a)
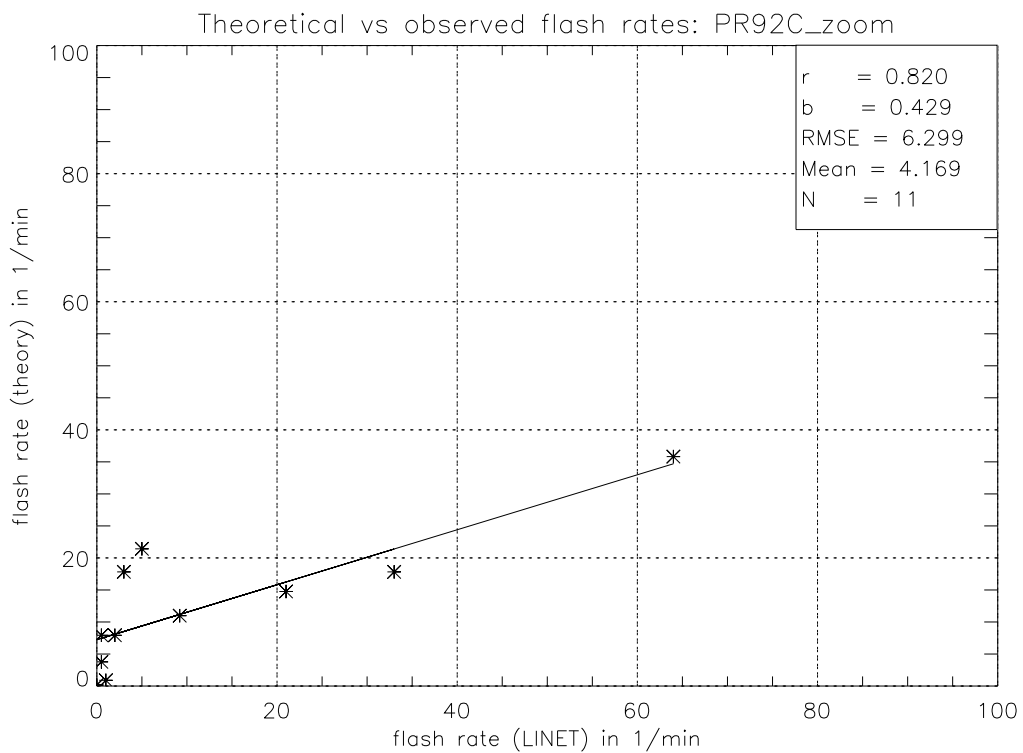
(b)

Figure 5.9: As in Fig. 5.4, but with adjusted PR92 data. In a) all cases are shown, where the correction factor is 5.5 and in b) only those cases where isolated storms occurred, are plotted. In this case, the correction factor was 1.8. Note the different scales of the axes.

top height, which was determined as in the PR92 case. The result is shown in Fig. 5.10. Although the data are aligned very closely to the regression line (RMSE and mean error of about 1 min^{-1}), its slope is only 0.02. Pearson's correlation coefficient is 0.70. The underestimation of the flash rate is more pronounced than in the PR92 parameterization. The predicted flash rate never exceeds 10 min^{-1} within the entire scope of investigated storms. To account for the large difference
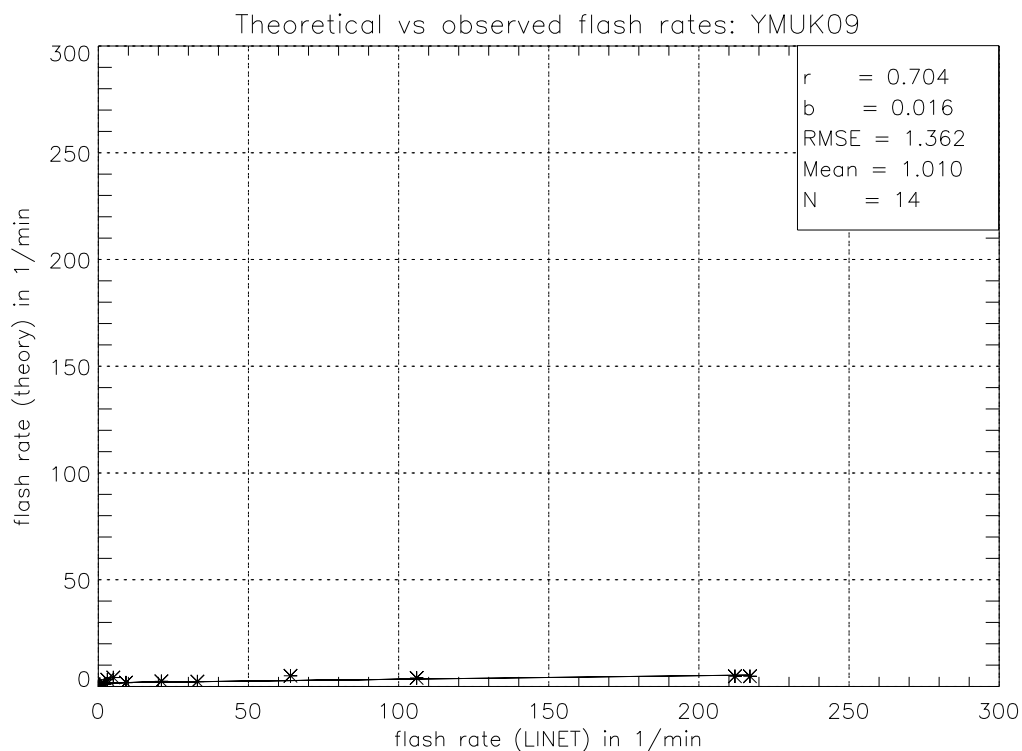

Figure 5.10: Same as Fig. 5.4, but for the YMUK09 parameterization.

between observation and prediction, the YMUK09 predictions are adjusted so that the average flash rate of observation and prediction is equal again. The result of this adjustment is shown in Fig. 5.11. The slope of the fit is 0.33 (all cases) and 0.37 (MCSs omitted), respectively. The correlation coefficient is rather insensitive to whether or not the MCSs are included (0.68 without MCS cases and 0.70 for all cases), but the residuals are reduced if only isolated cells are considered: RMSE = 8.4 for isolated storms and RMSE = 26.3 for all cases.

The GR01 parameterization could not be tested with this method because the vertical velocity distribution in the convective cells is not known (the GR01 parameterization will be applied in the next chapter, though).
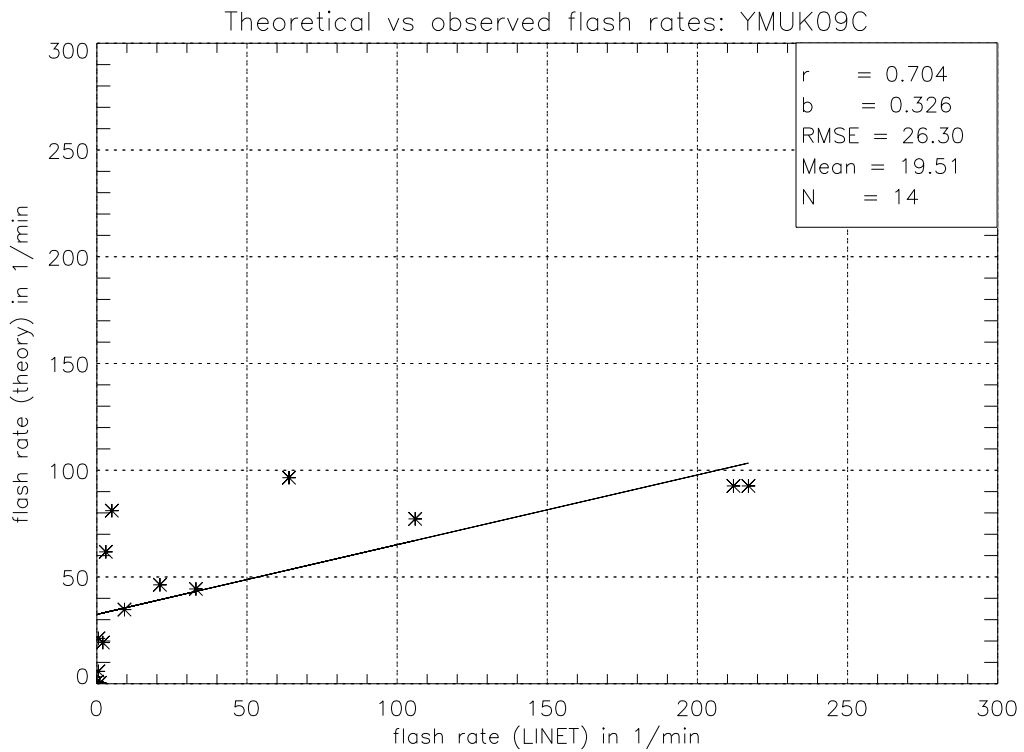
(a)
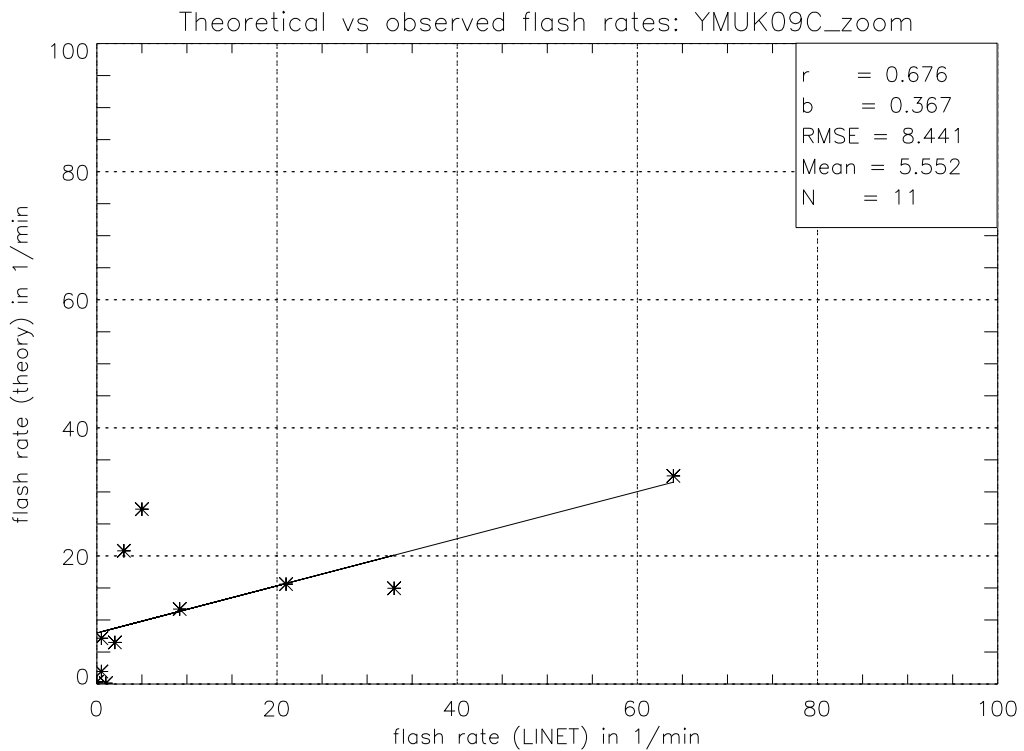
(b)

Figure 5.11: As in Fig. 5.4, but with corrected YMUK09 data. In a) all cases are shown, where the correction factor is 19.3 and in b) only those cases where isolated storms occurred, are plotted. In this case, the correction factor was 6.5. Again, note the different scales of the axes.

5.2   Environmental parameters

An alternative method to predict the flash rate is the evaluation of environmental parameters (e.g., Bright et al., 2005) which may be obtained from rawinsonde ascents. The question is: If deep convection initiates in a given environment, how large will its lightning frequency be? The parameters that will be considered in this section, are:

- most-unstable convective available potential energy (MUCAPE),

- integrated CAPE (ICAPE),

- boundary-layer mixing ratio (Q_MEAN),

- equilibrium-level temperature (T_EL),

- 0-6 km ("deep-layer") shear (DLS),

- 0-3 km storm-relative helicity (SRH).

The most-unstable CAPE (MUCAPE)[1] is calculated rather than surface- or mean-layer CAPE in order to include elevated instability. CAPE was determined with the assumption of a moist reversible process for the parcel ascent curve. The integrated CAPE (ICAPE) is the density-weighted vertical integral of CAPE over all layers that contain parcels with positive CAPE (Mapes, 1993). This measure accounts for the depth of the unstable layer and is a measure of the total energy available to the convective updraft, rather than the mass-specific, parcel-dependent measure CAPE. The mean boundary-layer mixing ratio was calculated using the lowest 5 layers in the soundings. This averaging assures that the impact of surface-based moist layers that are only a few tens of meters deep, is reduced.

Deep-layer shear is the vector difference between the wind in the lowest layer of the sounding and the interpolated wind at an altitude of 6 km MSL. 0-3 km storm-relative helicity is calculated as in Davies-Jones et al. (1990).

It is not useful to compare instantaneous flash rates with the sounding parameters, since the flash rate strongly depends on the stage of evolution of the storm. Thus, an averaged lightning frequency was considered: For this, a box was defined around the München-Oberschleißheim station. The size of this box is about 220 × 220 km². Only storms in this box that occurred within ±4 hours of the ascent (12 UTC) were considered. To identify individual thunderstorm cells, the 8-hour period was split into 15 min intervals. For all intervals, the lightning-density field was calculated, and contiguous regions in this field were identified as lightning (i.e.,

---

[1]This CAPE pertains to the parcel with the highest CAPE value in the sounding.

thunderstorm) cell. An average over all cells per interval was calculated. This procedure was applied in section 6.1.2 already and is repeated for every interval. In a last step, the average over all intervals was taken. The result is a representative flash frequency per thunderstorm cell in the given environment. Cases where the available sounding clearly did not capture the storms' environment were omitted. Tab. 5.2 shows the cases that were investigated, as well as the averaged flash rates.

Date	Scenario	Average Flash Rate in min^{-1}
2 April 08	graupel showers	0.1
23 June 08	supercells	3.3
24 June 08	weak elevated convection	1.3
3 July 08	organized severe	3.8
20 July 08	shallow but sheared	0.9
22 August 08	supercells	11.8
26 May 09	organized severe	14.2
26 June 09	single cells	0.4
30 June 09	single cells	0.6
5 July 09	single cells	1.2
23 July 09	pre-MCS convection	1.0

Table 5.2: Summary of cases used to relate sounding parameters to observed flash rates.

The results are shown in Fig. 5.12. The absolute values of the correlation coefficients are generally about 0.2, except for MUCAPE ($r \approx 0.3$) and T_EL ($r \approx -0.37$). Most of the observed lightning rates are between zero and five flashes per minute. The RMSE of all fits is also about 5 min^{-1}, which is consistent with the strong scattering of the data points around the regression lines. These results will be discussed in section 7.6.
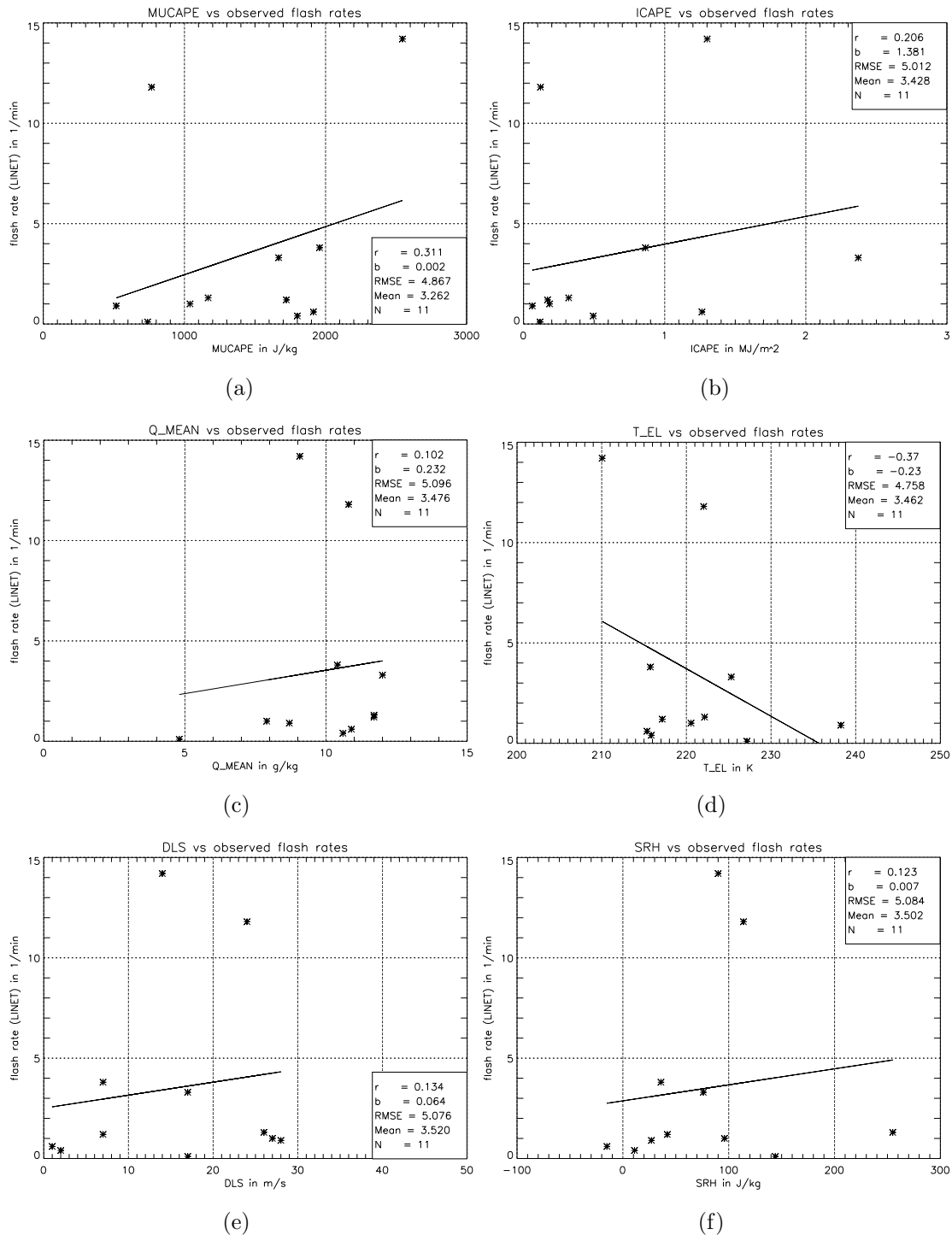
Figure 5.12: Sounding-derived parameters in relation to the average LINET flash rate (see text for details). (a) MUCAPE, (b) ICAPE, (c) mean boundary-layer mixing ratio, (d) equilibrium-level temperature, (e) deep-layer (0-6 km) shear, (f) 0-3 km SRH.

Chapter 6

Application

In this chapter, the results of the implementation of the parameterization into COSMO-DE are presented. Two aspects of the simulations are investigated:

1. The lightning rates of individual COSMO-DE-cells are considered in section 6.1. This is *not* a test of the lightning parameterization, but of the cloud-physical properties of the simulated convective clouds (and of the COSMO-DE-specific graupel-field corrections).

2. The bulk lightning activity on selected days will be presented in section 6.2. This test is aimed at how well COSMO-DE handles the spatial and temporal evolution of deep (i.e., lightning-producing) convection.

For quantitative comparisons between observations and COSMO-DE simulations, the domain highlighted by the red box in Fig. 6.1 will be used. The simulations were initialized at 00 UTC and ran for 24 h. The lightning scheme was called every 15 minutes to keep the run time as short as possible.

6.1 Application to individual simulated cumulonimbus clouds

Because the goal of this study is to simulate lightning in the COSMO-DE model (see Appendix B), the next step is to test if the modeled convective storms produce realistic flash rates. As the flash rate is largely determined by the size of the graupel region, as well as by the graupel mass in this region, this test essentially targets the clouds' microphysics. Naturally, if the COSMO-DE produces convection whose properties are identical to those that were measured, the flash-rate prediction will be identical to the prediction based on the measurements. This would reproduce the results presented in section 5.1. However, the predictions based on the lightning
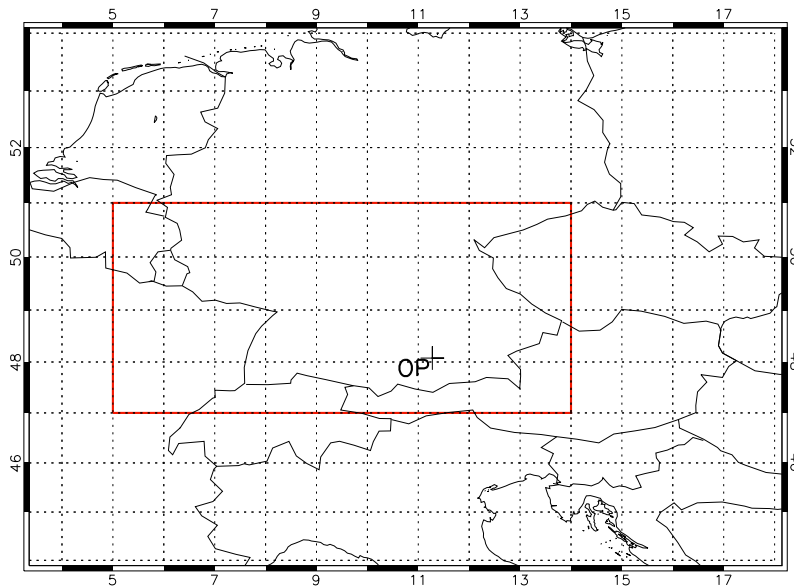
Figure 6.1: The red box highlights the domain used for quantitative comparison between observed and simulated lightning.

parameterization may be used to infer how realistically the graupel regions are modeled.

There are principle difficulties in attempting such a test. First and foremost, the model virtually never generates thunderstorm cells at that time and position at which they were observed in reality. In the model, convective initiation may be delayed or premature, the location may be wrong, or no convection may develop at all. Also, COSMO-DE may develop convective cells where and when none were observed. Moreover, even if the scenario is accurately simulated, there may be, e.g., two MCSs in the model where in reality there was only one. Which of the modeled MCSs should be compared with the observed one?

The strategy pursued to remedy some of these problems is the following. Cases have been identified, where the modeled cells have developed in the correct synoptic regime, (nearly) at the correct time, and which exhibited a largely realistic structural evolution. This assessment is somewhat subjective, but only those cases were considered where the association between modeled and real-world convection was quite clear. POLDIRAD imagery was available for three cases, so that graupel masses and the cross-sectional areas of the graupel-regions could be compared. It was attempted to include as large a range of storm intensity as possible, so that this evaluation is not confined to certain weather regimes or certain types of convection.

In the following analysis, results of the D10 scheme are shown where the MCS-correction (section 5.1) is included.

6.1.1   22 August 2008

The first case involved an isolated supercell, which developed over southeastern Germany in the afternoon of 22 August 2008. This case covers the high-intensity end of the spectrum of isolated thunderstorms, both in terms of storm organization, as well as flash production. On its eastward track, the cell evolved into a severe hailstorm, as reported by eye witnesses and supported by radar data (Fig. 5.2(a)). COSMO-DE failed to develop this convection at the correct time, but towards early evening, a long-lived, isolated cell eventually formed. While this development was somewhat delayed and farther east, the synoptic- and mesoscale environment of the simulated and the observed storms were similar, so that a direct comparison is justified.

The determination of the flash rates of observed and simulated storms was done as described in section 5.1, except that the procedure was repeated for modeled lightning. Several time intervals were compared. At the time when the comparisons were performed, there were two cells apparent in the flash-density fields of observed and modeled lightning. Though the relative position of the cells as well as their distance to each other were not exactly reproduced by the model, a comparison has been attempted. The results for two time intervals are summarized in Tab. 6.1. Between 1930 and 1945 UTC, the observed cells were sufficiently close to each other, so that only one flash-density region was identified. If the flash rate belonging to this region is compared with the sum of the flash rates of the two modeled storms, an agreement to within about 3 % is achieved.

Source	Time Interval	Flash Rate (cell 1)	Flash Rate (cell 2)
LINET	1900-1930 UTC	12 $\min^{-1}$	38 $\min^{-1}$
COSMO	1900-1930 UTC	10 $\min^{-1}$	33 $\min^{-1}$
LINET	1915-1945 UTC	64 $\min^{-1}$	-
COSMO	1915-1945 UTC	17 $\min^{-1}$	45 $\min^{-1}$
LINET	1930-1945 UTC	22 $\min^{-1}$	58 $\min^{-1}$
COSMO	1930-1945 UTC	23 $\min^{-1}$	54 $\min^{-1}$

Table 6.1: Comparison of the flash rates of the simulated (COSMO) and observed (LINET) supercells on 22 August 2008.

6.1.2   2 April 2008

On 2 April 2008, rather shallow polar-air cumulonimbi spread across southern Germany and produced short but intense snow and graupel showers, along with strong

wind gusts. Occasionally, this convection would support a lightning discharge, usually as little as one flash during the entire lifetime of the cell.

In this case, it was impossible to single out a certain cell and compare it with its model analog. The reason is that multiple cells were observed, all individually being short-lived, so that no unique one-to-one mapping between the real world and the model world could be established. In order to circumvent these difficulties, all cells in the domain (Fig. 6.1) were considered. The flash rate of the individual cells was determined as in section 5.1. Once each cell's flash rate was known, the average flash rate per cell was calculated. This calculation was performed for both, observed and simulated cells. The overall temporal evolution of the convection in the model was rather realistic, so that the flash rates were compared at the same time. The results are shown in Tab. 6.2. In this case, a strong dependence of the flash rate on the selected time interval is observed. This is because most flash-density regions contain only one or two flashes, that were produced by short-lived cells (i.e., lifetimes of less than 15 min). This implies that longer averaging time intervals reduce the flash rate. The modeled flash rates are as weak as the observed ones, and the fact that the cells produced only one or two flashes during their lifetime was correctly modeled. The total number of flashing cells is overestimated by the COSMO-DE.

Source	Time Interval	Mean Flash Rate	n
LINET	1330-1400 UTC	0.06 min^{-1}	37
COSMO	1330-1400 UTC	0.07 min^{-1}	79
LINET	1400-1415 UTC	0.15 min^{-1}	8
COSMO	1400-1415 UTC	0.13 min^{-1}	50
LINET	1400-1430 UTC	0.07 min^{-1}	14
COSMO	1400-1430 UTC	0.06 min^{-1}	76

Table 6.2: Comparison between averaged observed (LINET) and averaged modeled (COSMO) flash rates on 02 April 2008. Also shown are the numbers of cells (n) over which the flash-rate average was taken.

6.1.3   5 July 2009

This day was characterized by weak CAPE as well as weak shear and minimal large-scale forcing for upward vertical motion. As only minimal capping was present, scattered short-lived convective cells developed over southern Germany with diurnal heating. COSMO-DE failed to capture this development. However, in COSMO-DE diurnally-driven convection developed over northern Italy, where the thermodynamic environment was very similar to the southern German environment. This is owed

to the fact that there was no air-mass boundary present over central and southern Europe, resulting in rather homogeneous conditions. Because of the general problem of COSMO-DE to develop thunderstorms in synoptically-quiescent conditions[1], it is very difficult to find cases where this scenario is faithfully simulated. For this reason, and with the knowledge that the thermodynamic profiles, the wind profiles, as well as the synoptic regime were practically identical over both regions, the observed south-German cells were compared with modeled cells over northern Italy.

The procedure to determine the flash rates was identical to the previous case: A mean of the flash rates of all cells was determined for observed and modeled convection. The reason is again the numerosity of cells, making individual comparisons impossible. Also, the short-lived nature of the cells would make it very difficult to compare two cells at the identical stage. Tab. 6.3 summarizes the results. The flash rates of modeled and observed convection over 30 min and 15 min averages do not vary more than 0.1 min^{-1}, and the overall weak electric activity is correctly modeled by COSMO-DE.

Source	Time Interval	Mean Flash Rate	n
LINET	1400-1430 UTC	0.2 min^{-1}	67
COSMO	1400-1430 UTC	0.4 min^{-1}	422
LINET	1400-1415 UTC	0.3 min^{-1}	46
COSMO	1400-1415 UTC	0.4 min^{-1}	329

Table 6.3: Comparison between averaged observed (LINET) and averaged modeled (COSMO) flash rates on 05 July 2009. Also shown are the numbers of cells (n) over which the flash-rate average was taken.

6.1.4 1 March 2008

During the morning hours of 1 March 2008, a vigorous cold front, belonging to an intense extratropical cyclone (named "EMMA"), was crossing southern Germany. A narrow and strongly-forced line of thunderstorms developed along the cold front and produced damaging wind gusts and small hail[2]. Also, this convection produced copious amounts of lightning. Aside from the previous case, this is the main scenario in which lightning occurs in the cold season. Hence, this is a nice test for the new lightning scheme.

Although COSMO-DE correctly simulated the development of a strongly-forced convective line, it broke up into more segments than were observed in reality (not

---

[1]This was discussed at the COSMO user seminar, 2009, in Langen, Germany.
[2]Source: http://www.essl.org/ESWD/

shown). For this reason, again the mean over all flash-density regions was taken.
The results are summarized in Tab. 6.4. Comparing the flash rates at the same
times results in an underestimation of the flash rate by the model by a factor of
about six. However, using a later time (0930-1000 UTC), after the modeled convec-
tion had gained some intensity, the modeled flash rate lies within 0.1 min^{-1} of the
observation. Given that the modeled and observed convective lines did not evolve
in a fully identical manner, the flash rates will necessarily vary. Unfortunately, no
POLDIRAD data are available from that day, so that the skill of the flash-rate
equation, based on observations, cannot be ascertained in this case.

Source	Time Interval	Mean Flash Rate
LINET	0830-0845 UTC	0.6 min^{-1}
COSMO	0830-0845 UTC	0.1 min^{-1}
LINET	0830-0900 UTC	0.34 min^{-1}
COSMO	0830-0900 UTC	0.06 min^{-1}
LINET	0930-1000 UTC	0.14 min^{-1}
COSMO	0930-1000 UTC	0.23 min^{-1}

Table 6.4: Comparison between averaged observed (LINET) and modeled (COSMO)
flash rates on 01 March 2008.

6.1.5   26 May 2009

This case represents the well-organized end of the MCS spectrum. A vigorous squall
line with imbedded bow echoes swept across southern Germany in the afternoon
and evening hours, producing widespread severe wind gusts[3]. COSMO-DE devel-
oped widespread and intense convection in the afternoon hours that quickly became
organized into several large MCSs. However, in reality only one large MCS was
observed. In such a case, the comparison between modeled convection and reality is
necessarily arbitrary and shall not be attempted here. Rather, some parameters of
modeled convection will be presented, as well as its flash rate. Tab. 6.5 shows data
pertaining to three of the MCSs that COSMO-DE created. The observed MCSs
maintained a flash rate of about 200 min^{-1} (see Tab. 5.1).

   If an MCS is selected that has the identical diameter (62 km) and a similar
graupel content, the result of the observed MCS is trivially reproduced. Larger
MCSs exhibit substantially higher flash rates. Since no MCS with such dimensions
is contained in the observed cases, it is now known if these predictions are realistic.

---

[3]See http://www.essl.org/ESWD/.

Diameter	Graupel Mass	Flash Rate
87 km	4.3 g kg^{-1}	409 min^{-1}
79 km	4.8 g kg^{-1}	377 min^{-1}
62 km	3.7 g kg^{-1}	209 min^{-1}

Table 6.5: Shown are the cross-sectional equivalent circular diameters of the graupel regions, the maximum graupel mass, and the flash rate of three simulated MCSs on 26 May 2009.

6.2 Observed and simulated lightning over southern Germany

While the former section essentially was devoted towards the cloud-physical properties of the modeled convection, in this section mostly convective initiation in the model is assessed. As such, this section does not directly address the quality of the lightning parameterization, but rather whether COSMO-DE creates the correct amount of cells at the correct time. I.e., the lightning activity is taken as proxy for deep, moist convective activity. Two cases have been selected. The performance of the COSMO-DE in terms of developing convection at the right time and location differs between these two cases. Results of all four parameterizations implemented in the model (D10, PR92, YMUK09, and GR01) are presented. The original PR92, YMUK09, and GR01 parameterizations were used, without the correction accounting for the large underestimation of the PR92 and YMUK09 approaches. This is justified in section 7.3.
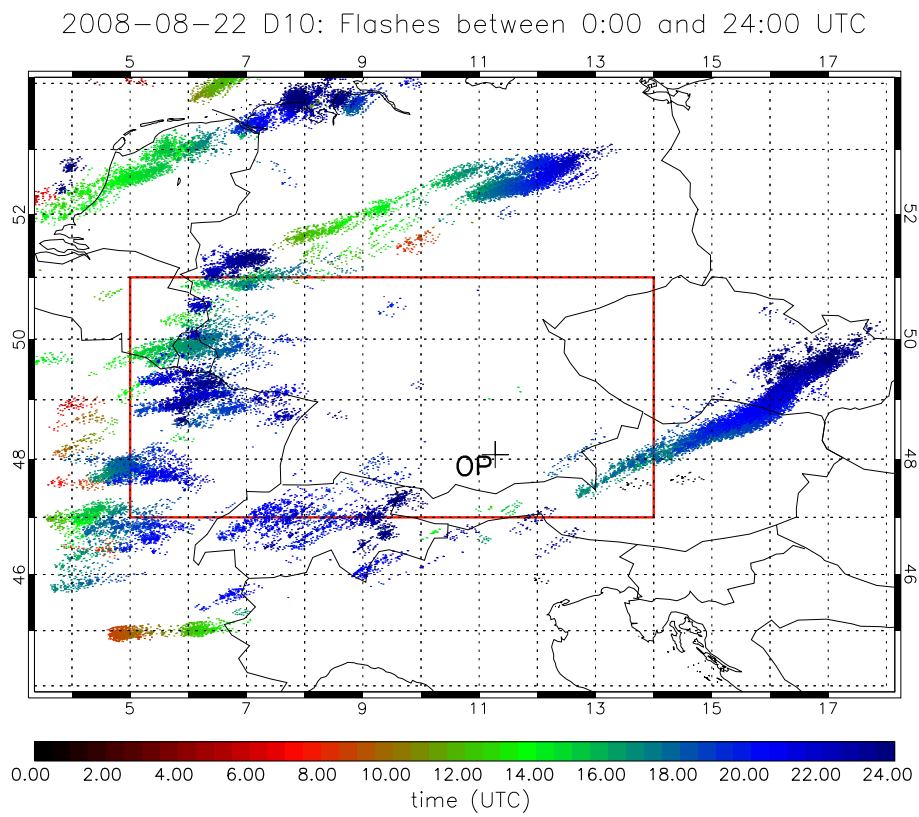
6.2.1 22 August 2008

Some details about the convective evolution on 22 August 2008 were mentioned in section 6.1. The evolution of lightning activity based on LINET measurements is depicted in Fig. 6.2(a). Fig. 6.2(b) shows the same for lightning simulated with the D10 parameterization. Displayed are the times and locations of the discharges. The flash locations are shown as small dots and the time is color-coded, according to the color bar underneath the graphic. In Fig. 6.2(a) a broad "lightning track" is seen to stretch across southern Germany into Austria. This track is present also in the simulation, but it is displaced to the east. Moreover, the associated thunderstorms developed several hours too late in the model. In addition, the model initiated scattered convection with much lightning over eastern France and western Germany, where only minimal lightning activity was observed in reality.

In order to quantify this overestimation, as well as spatial shifts in the modeled
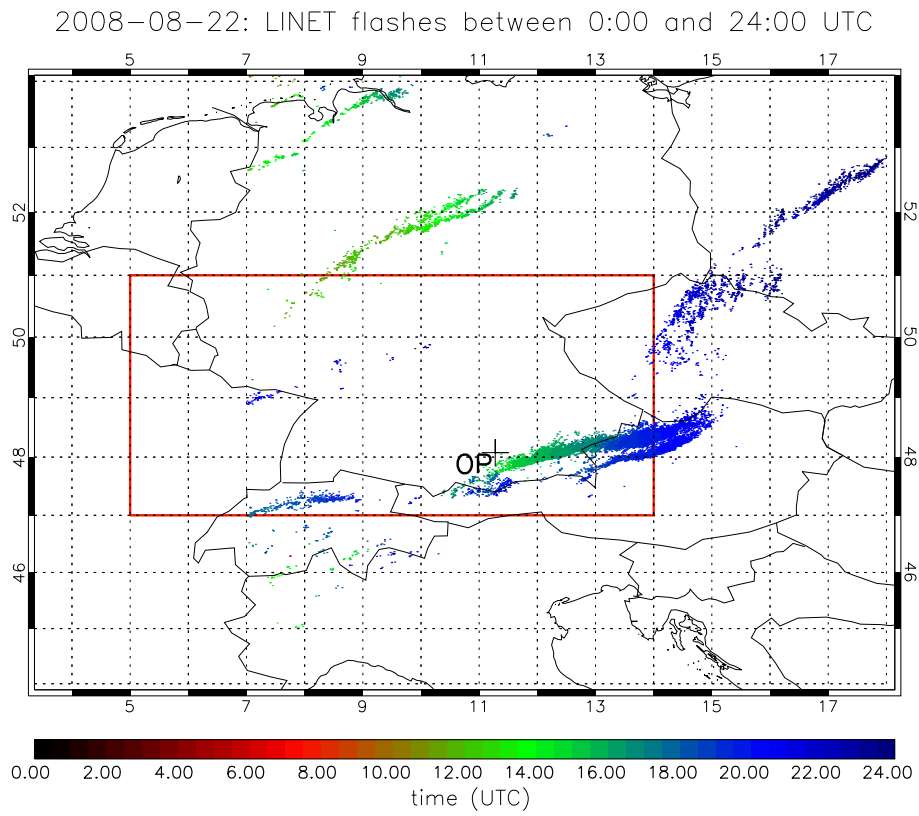
(a)

(b)

Figure 6.2: LINET flashes (a) and COSMO-DE flashes based on D10 (b) on 22 August 2008. Dots represent discharge locations; time is color-coded.

convection, so-called displacement and amplitude error scores were determined. For this, the observed and modeled flash-density fields (accumulated over 24 h) were compared. The quantitative comparisons are based on convection occurring in the domain shown in Fig. 6.1.
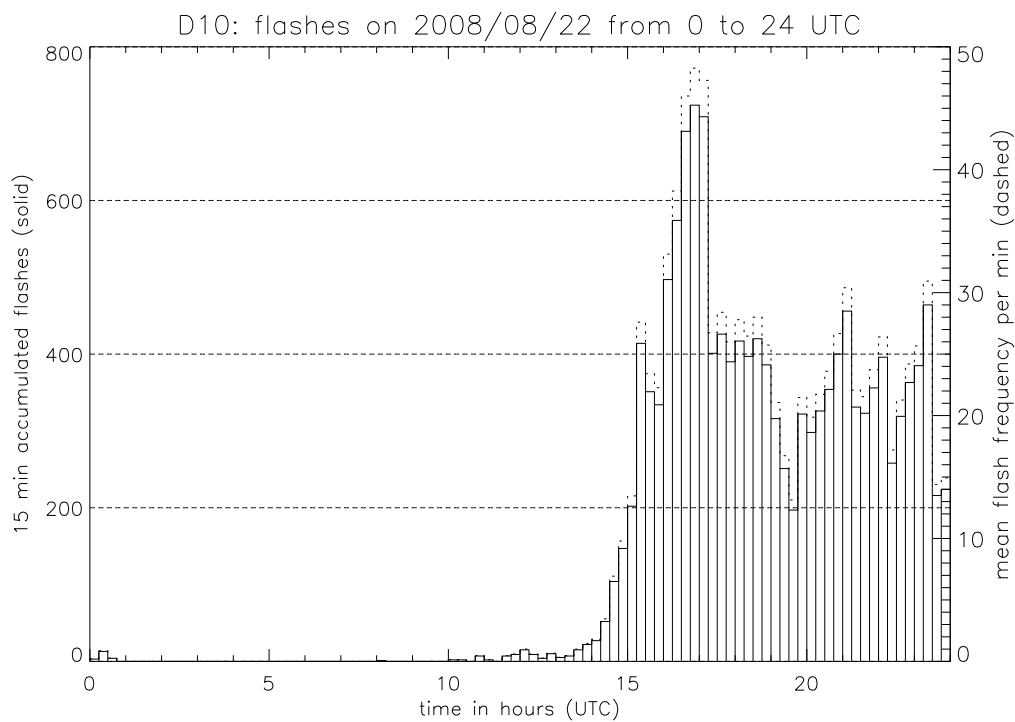
The essence of these measures is that modeled structures are morphed into observed structures using an optical-flow technique. Likewise, the observations are matched with the modeled fields. In the matching algorithm, the optical-flow technique is applied to successively smaller scales in order to achieve an accurate mapping of one image onto the other. This procedure is called pyramidal image matching. See Keil and Craig (2007), Zinner et al. (2008), and Keil and Craig (2009) for details. The algorithm only matches regions within a pre-defined search radius (90 km). Regions outside this search domain are not morphed. This residual is called the amplitude error. The average magnitude of the displacement vectors is the displacement error. These errors are calculated for the observation and forecast spaces and are combined into one error measure, the *displacement and amplitude score* (DAS). The minimum value DAS may attain is zero (perfect forecast), while an upper bound does not exist. Usually, DAS assumes values around one (Keil and Craig, 2009). The amplitude and displacement errors are normalized by the search radius and the climatological flash-density value (estimated to be 6 km^{-2}), respectively. The threshold value for considering flash-density regions is set to 0.0, because otherwise only the tracks of the most intense cells are recognized. The main value of using these scores compared to traditional, grid-point related ones, is that e.g., a slight displacement of lightning tracks is not penalized as much. False-alarm ratio and probability of detection scores suffer from the double-penalty problem that results in poor scores although the scenario may have been correctly simulated. The displacement errors, the amplitude errors, and the DAS scores for all parameterizations are summarized in Tab. 6.6. In this application, these error measures consider the integrated lightning activity during the entire day.

Now, the quality of the temporal evolution of the simulated convective activity is considered. For this purpose, histogram plots showing the accumulated number of flashes in 15-min intervals are shown. Fig. 6.3(a) shows the temporal evolution of measured lightning activity on 22 August 2008. The solid line shows the 15-min accumulated flashes (left scale) and the dashed line shows the flash rate in min^{-1} (right scale). In this plot, the dashed and solid lines coincide, so that they are indistinguishable. The same plot, but for modeled lightning, is shown in Fig. 6.3(b). The number of total flashes as well as the mean flash rate are shown beneath the histograms. For 22 August 2008, COSMO-DE produces about twice as many flashes as were observed (14,354 vs 8,489 flashes). Accordingly, the flash rate averaged over the entire day and over the domain is also overestimated (10 vs 6 min^{-1}). However,

LINET: flashes on 2008/08/22 from 0 to 24 UTC
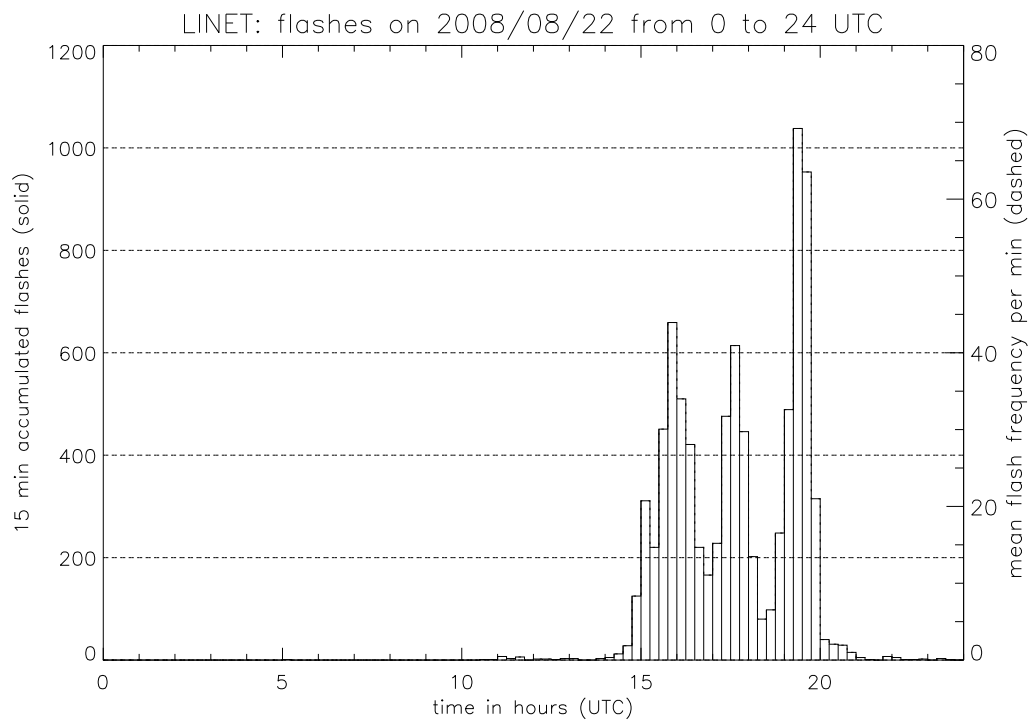
accumulated flashes: 8489   mean flash frequency: 5.9 per minute

(a)

D10: flashes on 2008/08/22 from 0 to 24 UTC

accumulated flashes: 14354   mean flash frequency: 10. per minute

(b)

Figure 6.3: Histogram plots of observed lightning activity (a) and simulated lightning activity using the D10 scheme (b). Solid lines represent the 15-min accumulated flashes, and dashed lines represent the flash rate per minute.

the fact that lightning activity commences in the afternoon hours was correctly predicted. Note the different scales of the histograms, which is due to the fact that the observed intense storms over southern Germany were simulated too far east, outside the domain under consideration. This means that in the simulation the strongly-flashing supercells did not contribute to the flash rate in the domain. Thus the peak flash rates are lower in the simulation compared to the observations. The fact that the modeled *total* number of flashes exceeds the observed one, is owed to the modeled convective activity over western Germany and eastern France, which did not develop as extensively in reality. In order to quantify these differences, a scatterplot is provided in Fig. 6.4. In this plot the modeled and observed 15-min accumulated flashes as a function of time are correlated. The linear correlation coefficient as well as the slope of the regression line are about 0.5. The RMSE of the residuals is 177 flashes per 15 min and the mean-error magnitude is 145 flashes per 15 min.
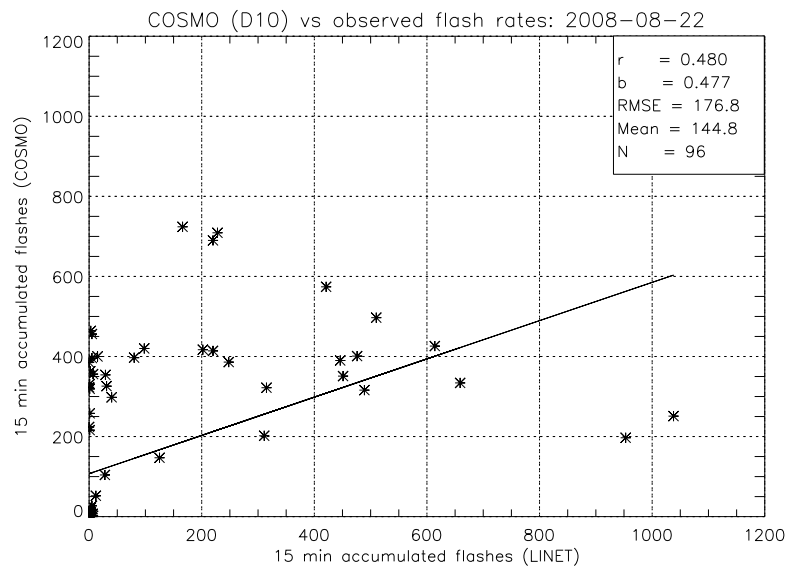

Figure 6.4: Correlation of the temporal evolution of the lightning activity based on LINET flashes and on the simulation using the D10 parameterization.

Fig. 6.5(a) shows the location and time of the discharges for the PR92 parameterization. The result is qualitatively similar to the result shown in Fig. 6.2(b). However, the overall lightning activity is substantially weaker, which is confirmed by the histogram shown in Fig. 6.5(b). The total flash number is 1,980. An interesting feature is the peak of lightning activity during the first minutes after initialization of the simulation. This activity is associated with early-morning convection over the Alps (Fig. 6.5(a)). Since this algorithm (section 3.2) merely identifies the topmost gridpoints of regions where the updraft exceeds 2 ms^{-1}, gravity waves were erroneously identified as convective updrafts. The errors in the temporal evolution
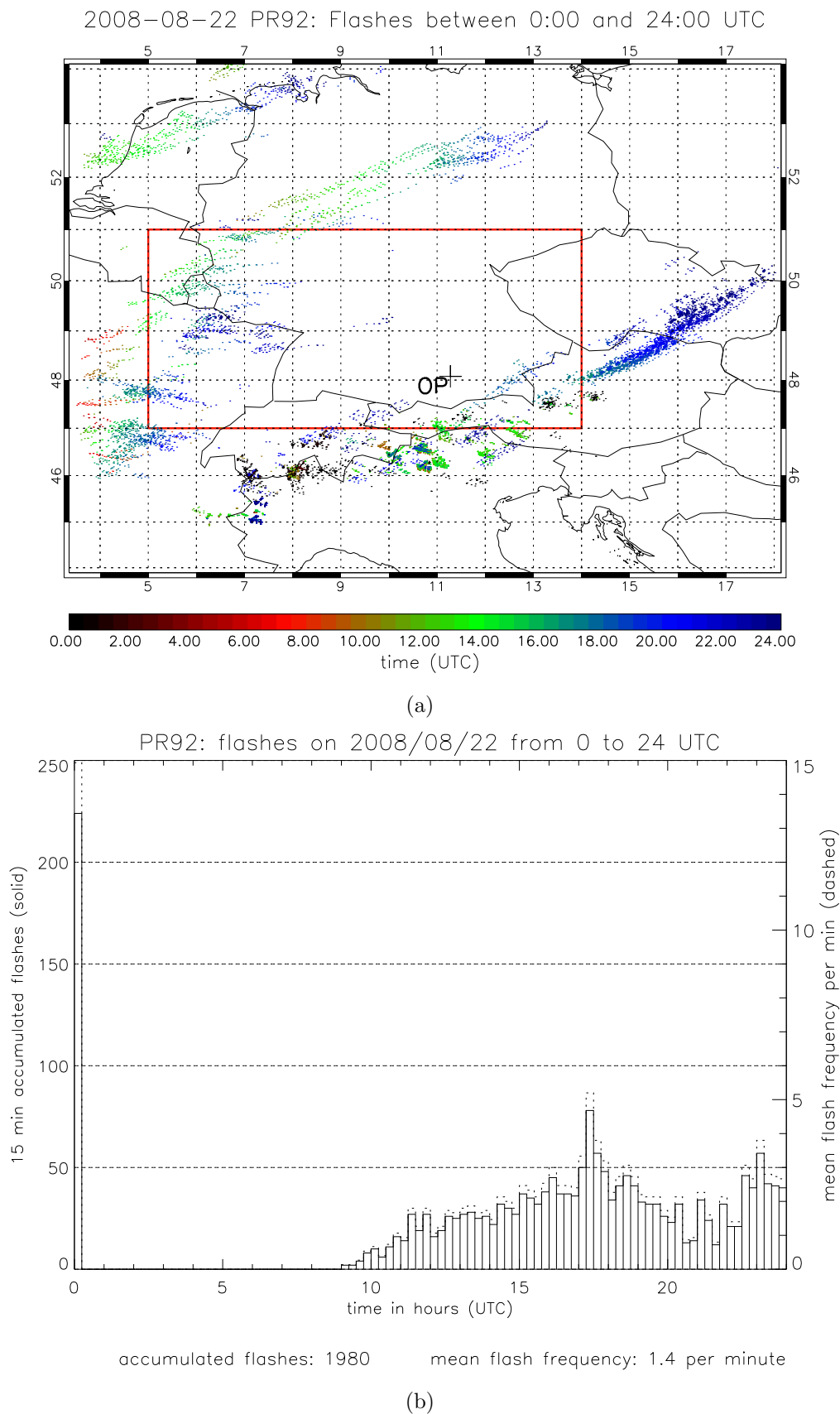
(a)

(b)

Figure 6.5: (a) Overview of the simulated lightning activity based on the PR92 parameterization, as to Fig. 6.2(b). (b) Histogram plot showing the temporal evolution of the lightning activity, based on PR92.

of lightning activity, as well as errors in intensity are summarized in the scatter plot in Fig. 6.6. Although the linear-regression fit represents the data quite well
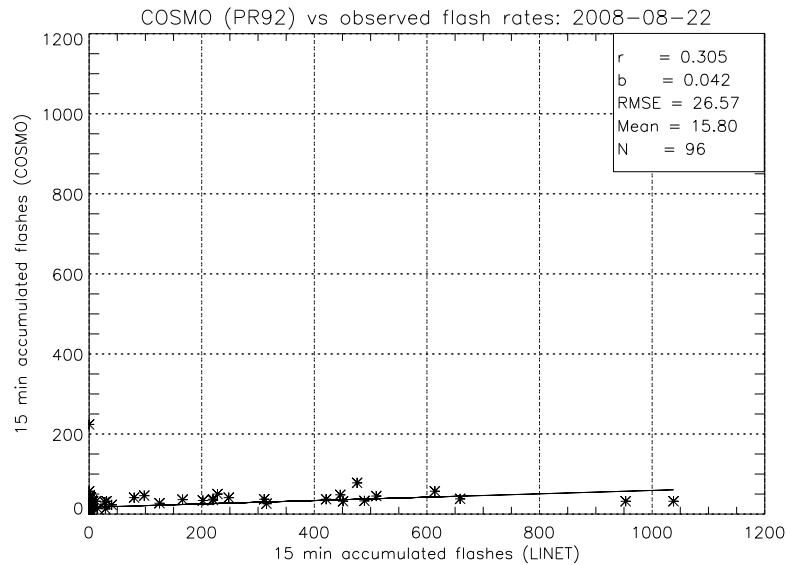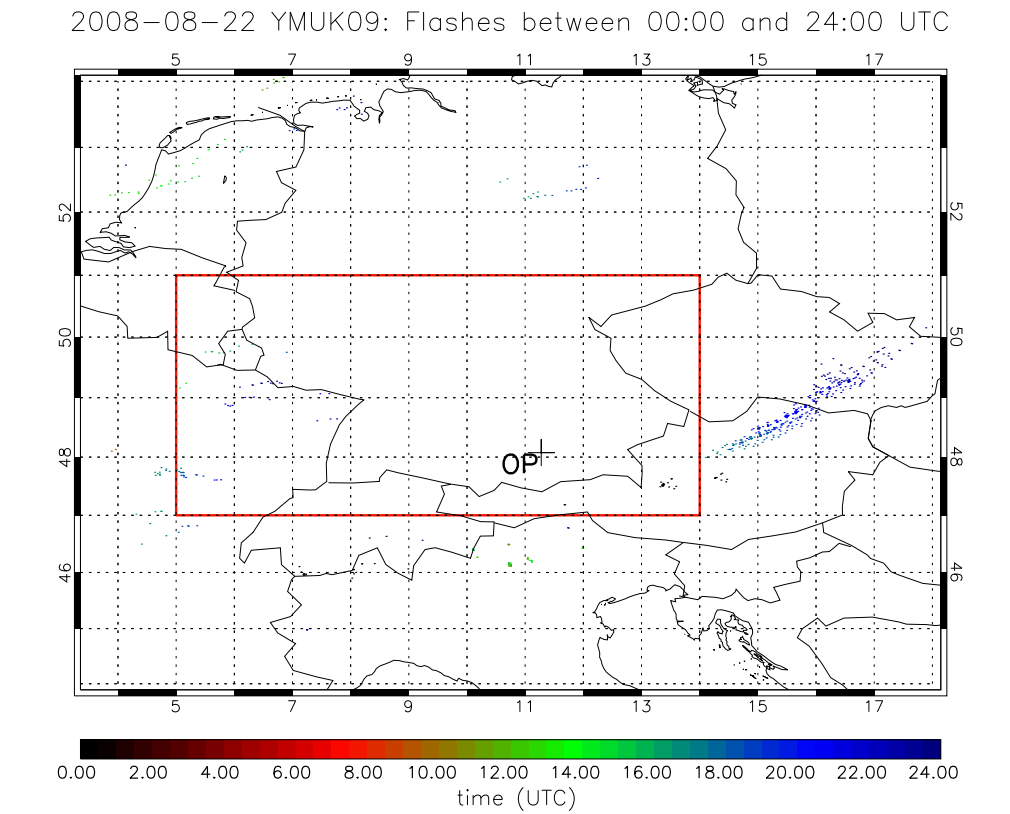

Figure 6.6: Correlation of the temporal evolution of the lightning activity based on LINET flashes and on the simulation using the PR92 parameterization.

(RMSE $\approx$ 27 flashes per 15 min), the correlation is rather weak (r $\approx$ 0.3), and more importantly, the slope of the fit is less than 0.1. This graphic is consistent with the underestimation of the total number of lightning discharges.

The results from the YMUK09 simulations are shown in Fig. 6.7. The coarse structures, like the track of the supercells over Austria and the Czech Republic, are captured, but lightning activity that was evident in the observations and in other parameterizations (like over western Germany) is not present in YMUK09. The total number of flashes amount to 73 min^{-1}. These differences between simulated and observed lightning activity are also evident in Fig. 6.8, which depicts the temporal correlation between measured LINET flashes and the simulated flashes using the YMUK09 parameterization. As shown in Fig. 6.9, the Grewe et al. parameterization is qualitatively identical to PR92, but the overall lightning activity is more intense with 4,678 flashes in GR01 and 1,980 flashes in PR92. However, it is still less than the observation (8,489 flashes in total). Fig. 6.10 shows the temporal correlation between observations and the GR10 parameterization, which is dominated by the strong underestimation of the lightning activity by GR01 compared to LINET data.

Tab. 6.6 summarizes the DAS scores and its contributions for the different parameterizations.

(a)
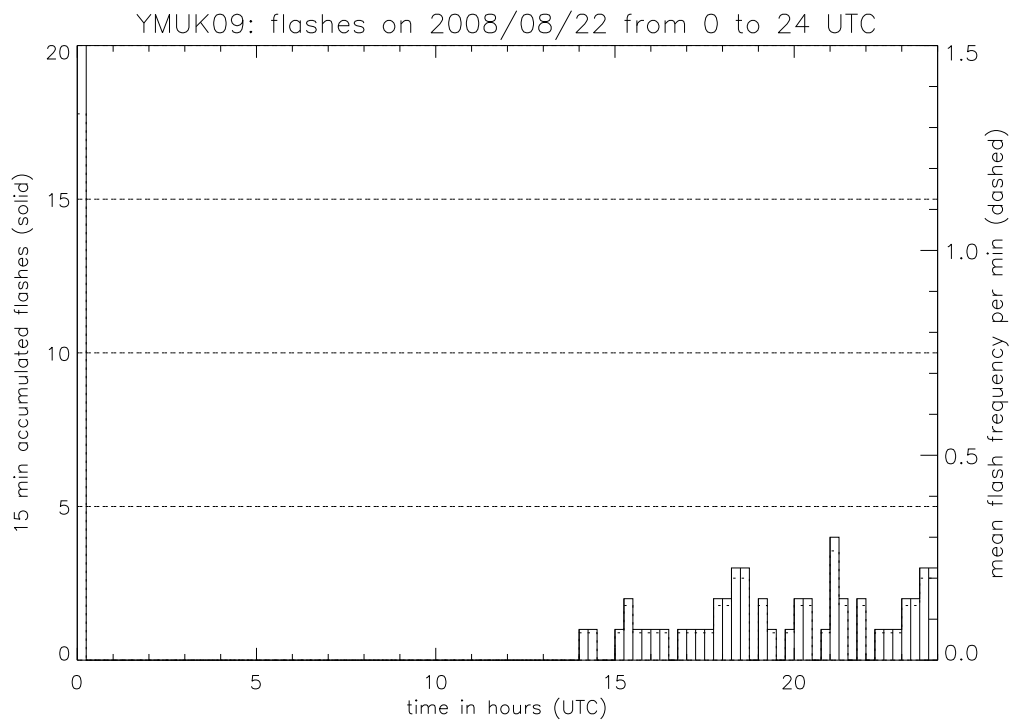
(b)

Figure 6.7: (a) Overview of the simulated lightning activity based on the YMUK09 parameterization, as in Fig. 6.2(b). (b) Histogram plot showing the temporal evolution of the lightning activity, based on YMUK09.
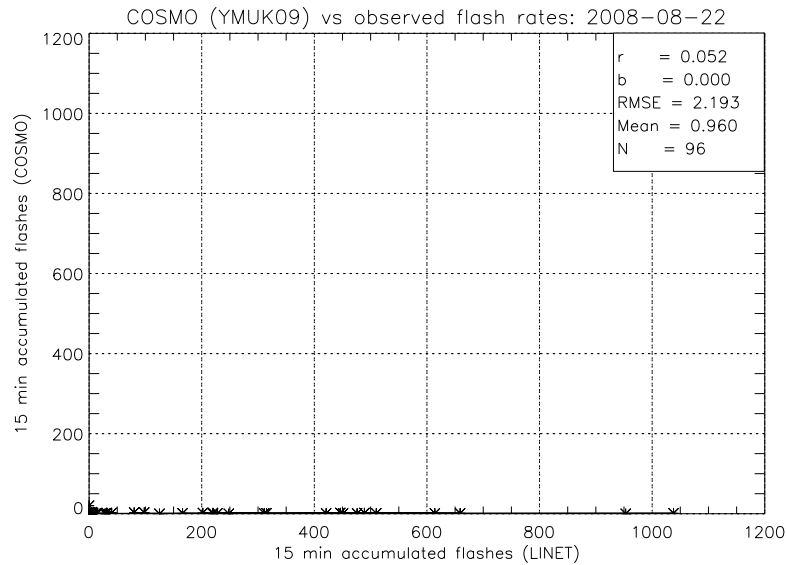
Figure 6.8: Correlation of the temporal evolution of the lightning activity based on LINET flashes and on the simulation using the YMUK09 parameterization.

Scenario	dis	amp	DAS
D10	0.296	0.585	0.881
PR92	0.286	0.357	0.643
YMUK09	0.296	0.900	1.196
GR01	0.285	0.354	0.640

Table 6.6: Summary for 22 August 2008 of displacement errors (dis), amplitude errors (amp), and the displacement-amplitude scores (DAS).

6.2.2 5 July 2009

On 5 July 2009, scattered thunderstorms developed with diurnal heating in a rather quiescent synoptic regime. Fig. 6.11 shows an overview of observed (Fig. 6.11(a)) and modeled flashes based on the D10 parameterization (Fig. 6.11(b)). It is immediately apparent that COSMO-DE generated excessive nocturnal convection over northern Italy, southern Germany, Austria, the Czech Republic, and Poland. In the afternoon, too little convection develops over southeastern Germany. This is confirmed by the histogram plots in Fig. 6.12, which display the temporal evolution of observed and modeled lightning, respectively. Again, only lightning that occurred in the area enclosed by the red box in Fig. 6.1 is considered in the evaluation. The measurements (Fig. 6.12(a)) suggest a rather well-pronounced diurnal cycle. Convective initiation took place in the late morning and early afternoon hours. The activity peaked late in the afternoon, and gradually diminished in the evening hours. Late in the evening, scattered convection formed over western Germany. This activity is responsible for
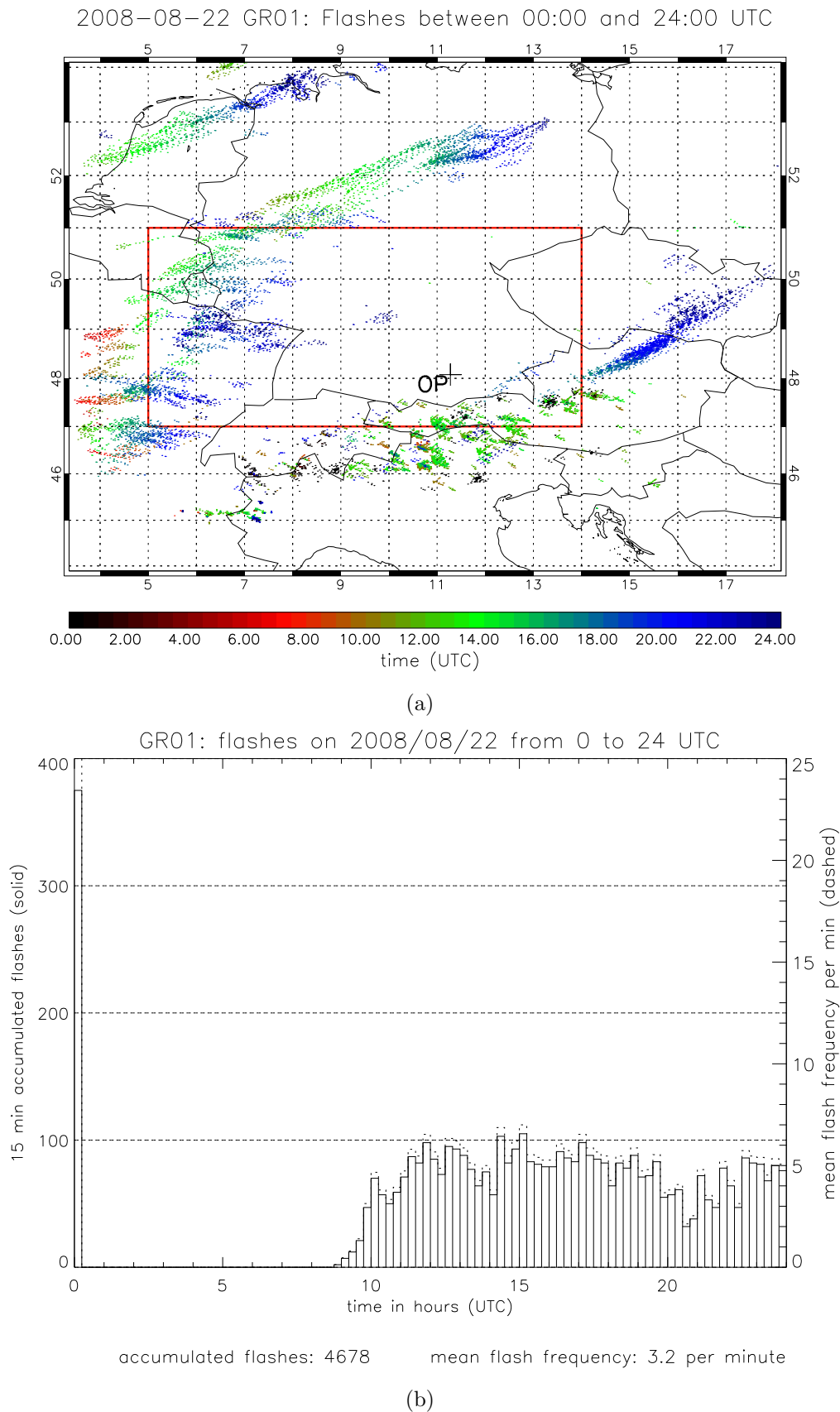
(a)

(b)

Figure 6.9: (a) Overview of the simulated lightning activity based on the GR01 param-
eterization, as in Fig. 6.2(b). (b) Histogram plot showing the temporal evolution of the
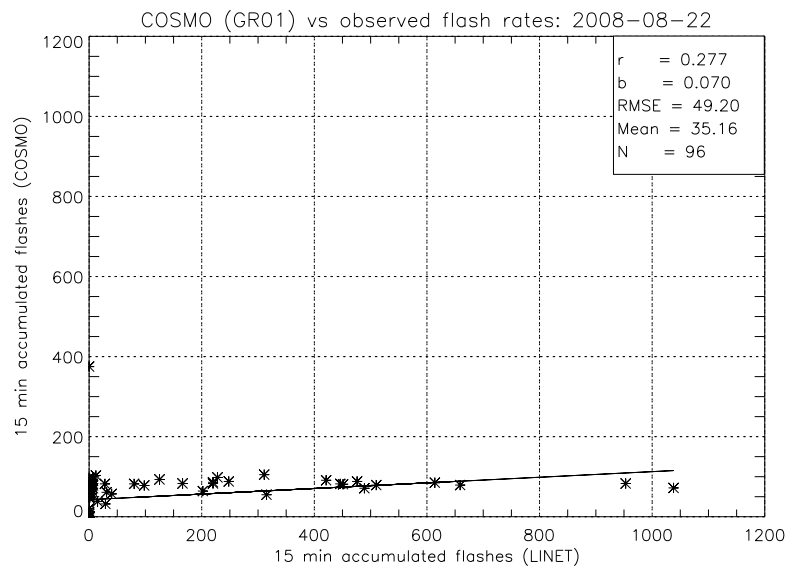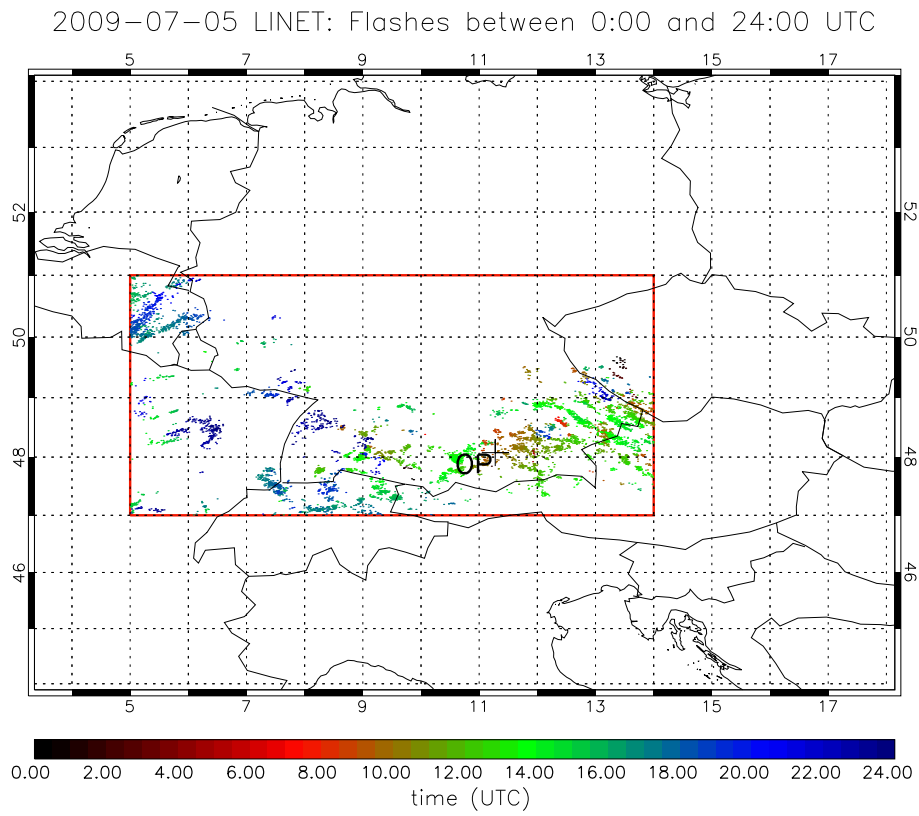lightning activity, based on GR01.

Figure 6.10: Correlation of the temporal evolution of the lightning activity based on LINET flashes and on the simulation using the GR01 parameterization.

the secondary peaks after 2000 UTC. The simulation based on D10 (Fig. 6.12(b)) shows a different evolution. There is quite high lightning activity in the night and early morning (more than 9,000 flashes in 15 min), diminishing towards the late morning hours. The lightning activity in the afternoon is practically missing in the simulation. The total number of flashes is overestimated by the simulation by a factor of about seven (66,300 simulated vs 8,893 observed flashes). In Fig. 6.13, the time correlation between the observed and modeled 15-min accumulated flashes is shown. The correlation coefficient is about -0.3, the regression-line slope is about minus four, and the RMSE is approximately 1,500 min^{-1}, which is the same order of magnitude as the maximum number of flashes occurring in a 15-min interval. This correlation plot is consistent with the inversed diurnal cycle in the simulation.

The simulation results using the PR92 parameterization are shown on Fig. 6.14. The overall qualitative picture is quite similar to the D10 simulation. Especially the strong lightning activity within the first few hours into the simulation is well apparent. The total number of simulated flashes is 11,322, which is closer to the observed total number of flashes (8,893) than the simulation using the D10 parameterization. The temporal correlation between LINET flashes and simulated flashes using the PR92 scheme is shown in Fig. 6.15. The correlation coefficient is about -0.2, with an RMSE of 383. The slope of the linear regression line is roughly -0.75.

The results of the simulation with the YMUK09 parameterization are shown in Fig. 6.16. With 1,219 accumulated flashes over the day, the total number is substantially lower than with either D10 or PR92. However, what lightning activity exists, is also dominated by the early-morning thunderstorm activity, which was not
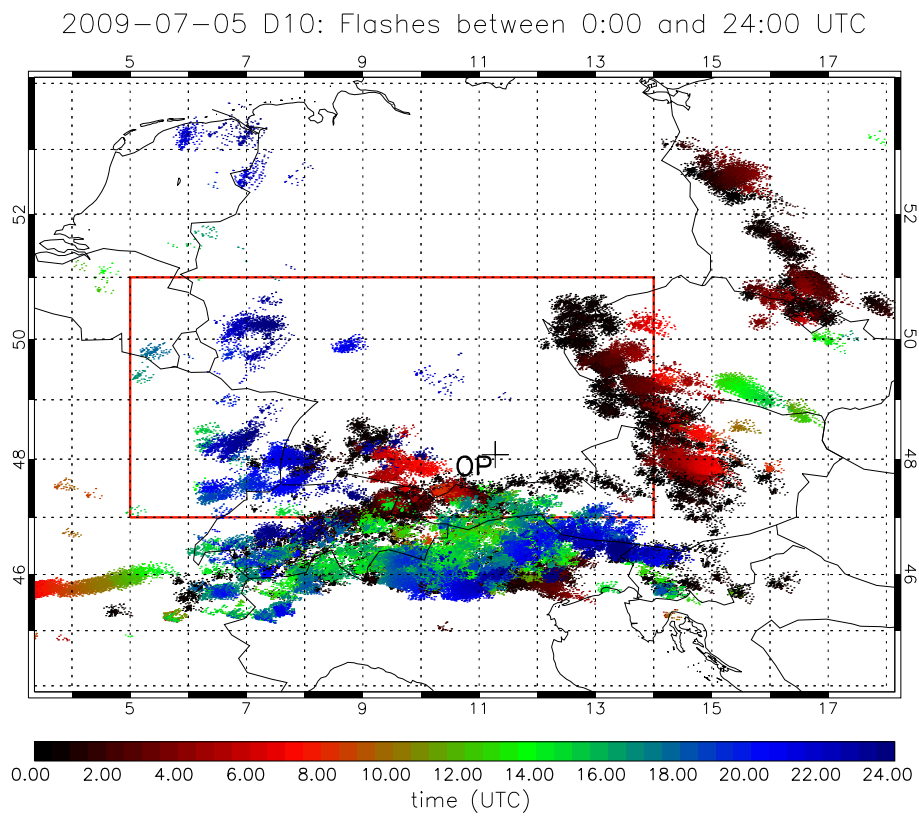
Figure 6.11: LINET flashes (a) and COSMO-DE flashes based on D10 (b) on 05 July 2009. Dots represent discharge locations; time is color-coded.

accumulated flashes: 8893   mean flash frequency: 6.2 per minute

(a)

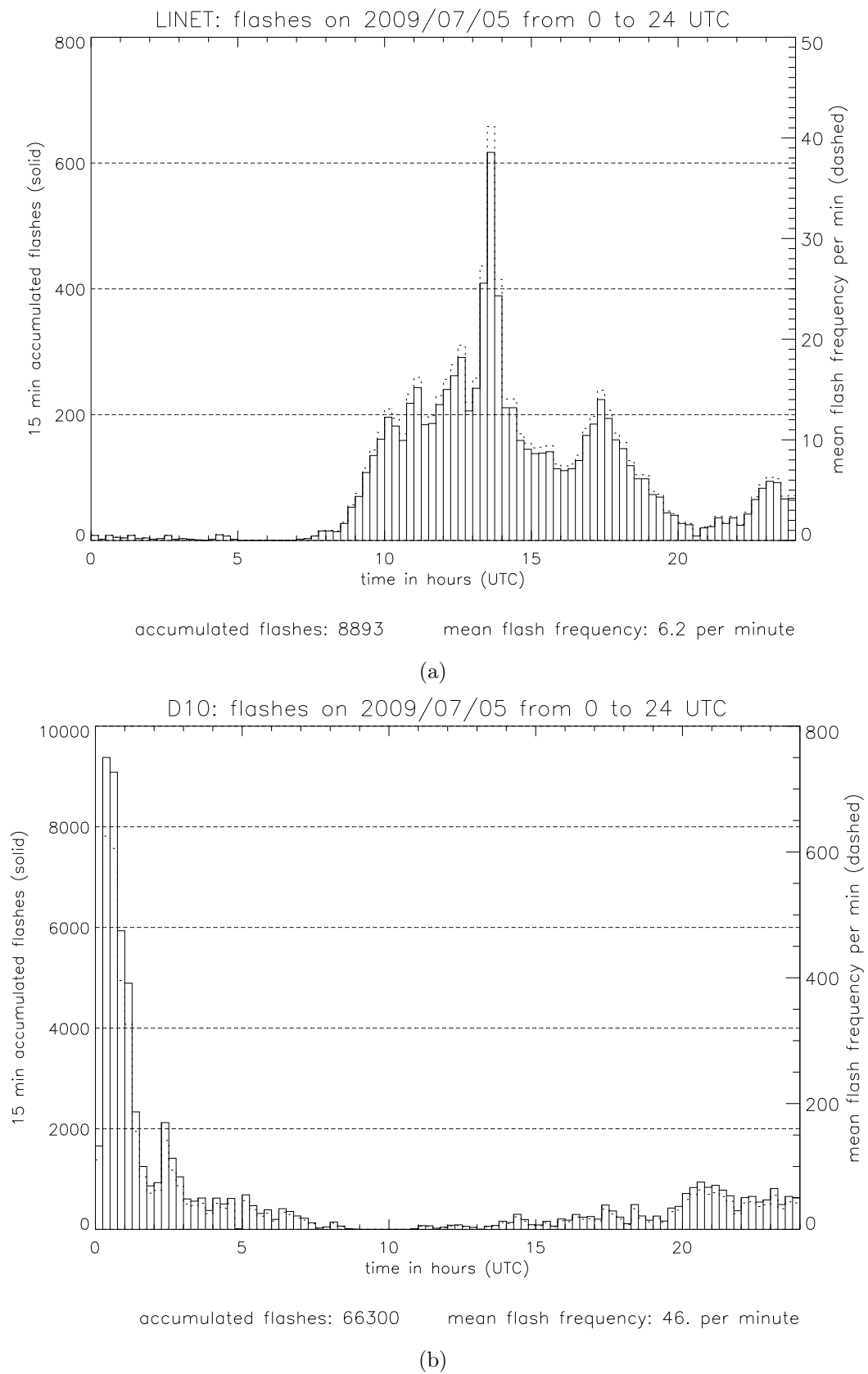accumulated flashes: 66300   mean flash frequency: 46. per minute

(b)

Figure 6.12: Histogram plots of observed lightning activity (a) and simulated lightning activity using the D10 scheme (b). Solid lines represent the 15-min accumulated flashes, and dashed lines represent the flash rate per minute.
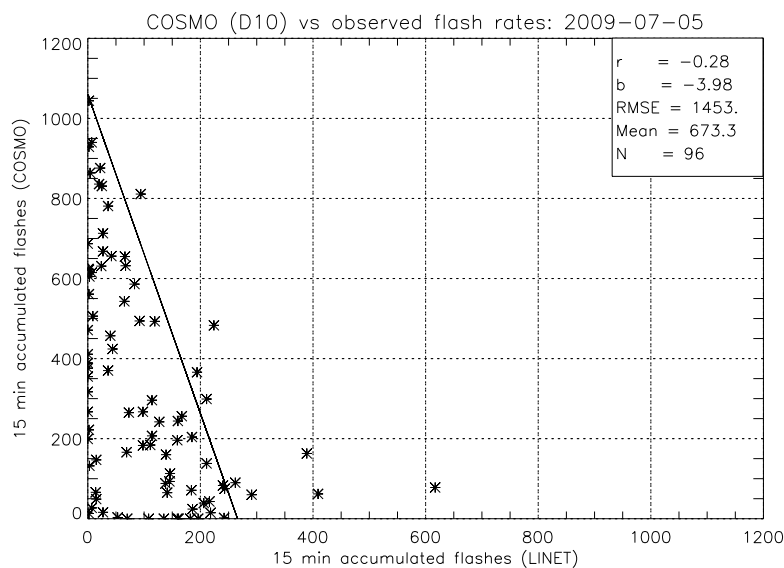
Figure 6.13: Zoomed scatter plot showing the correlation of the temporal evolution of the lightning activity based on LINET flashes and on the simulation using the D10 parameterization. Only 15-min accumulated flashes of less than 1,200 are depicted in this plot for better readability.

observed in reality. Fig. 6.17 displays the time correlation between LINET flashes and flashes simulated with the YMUK09 scheme. The correlation coefficient is -0.17, the slope of the regression line is -0.15, and the RMSE is about 51 flashes per 15 minutes.

The results of the GR01 implementation are shown in Fig. 6.18. Again, the results qualitatively resemble the PR92 parameterization, but the total number of flashes is 17,571 (GR01) vs 11,322 (PR92). Both approaches predict more lightning than detected with LINET (8,893 observed flashes). The temporal evolution is shown in Fig. 6.19. The correlation coefficient is 0.1 with an RMSE of 913.5 min^{-1}.

Tab. 6.7 summarizes the displacement and amplitude error scores for all parameterizations. The D10 approach results in the highest DAS value (DAS = 4.3),

Scenario	dis	amp	DAS
D10	0.358	3.946	4.304
PR92	0.289	0.686	0.975
YMUK09	0.354	0.590	0.944
GR01	0.239	0.937	1.230

Table 6.7: Summary of displacement errors (dis), amplitude errors (amp), and the displacement-amplitude scores (DAS) for 5 July 2009.

(a)

accumulated flashes: 11322   mean flash frequency: 7.9 per minute

(b)
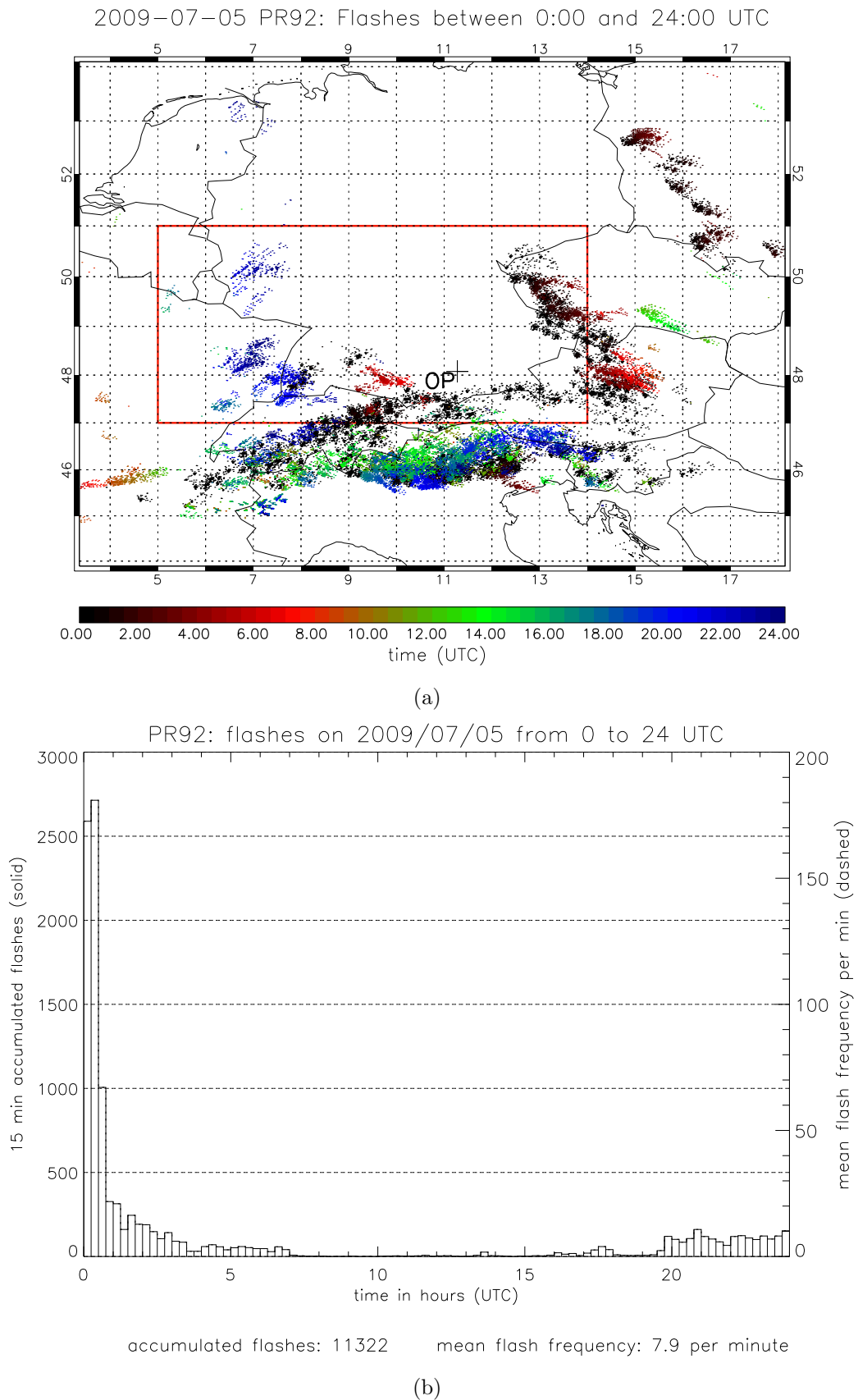
Figure 6.14: (a) As in Fig. 6.11(b), but for the PR92 parameterization. (b) Histogram plot showing the temporal evolution of the lightning activity, based on PR92.

Figure 6.15: Correlation of the temporal evolution of the lightning activity based on LINET flashes and on the simulation using the PR92 parameterization. Two data points of 1,200 flashes per 15 min were omitted in the plot to ensure readability.

(a)

(b)

Figure 6.16: (a) Overview of the simulated lightning activity based on the YMUK09 parameterization, as in Fig. 6.11(b). (b) Histogram plot showing the temporal evolution of the lightning activity, based on YMUK09.

Figure 6.17: Correlation of the temporal evolution of the lightning activity based on LINET flashes and on the simulation using the YMUK09 parameterization.

while YMUK09 with least lightning activity achieves the lowest score of about 0.9.

(a)

(b)
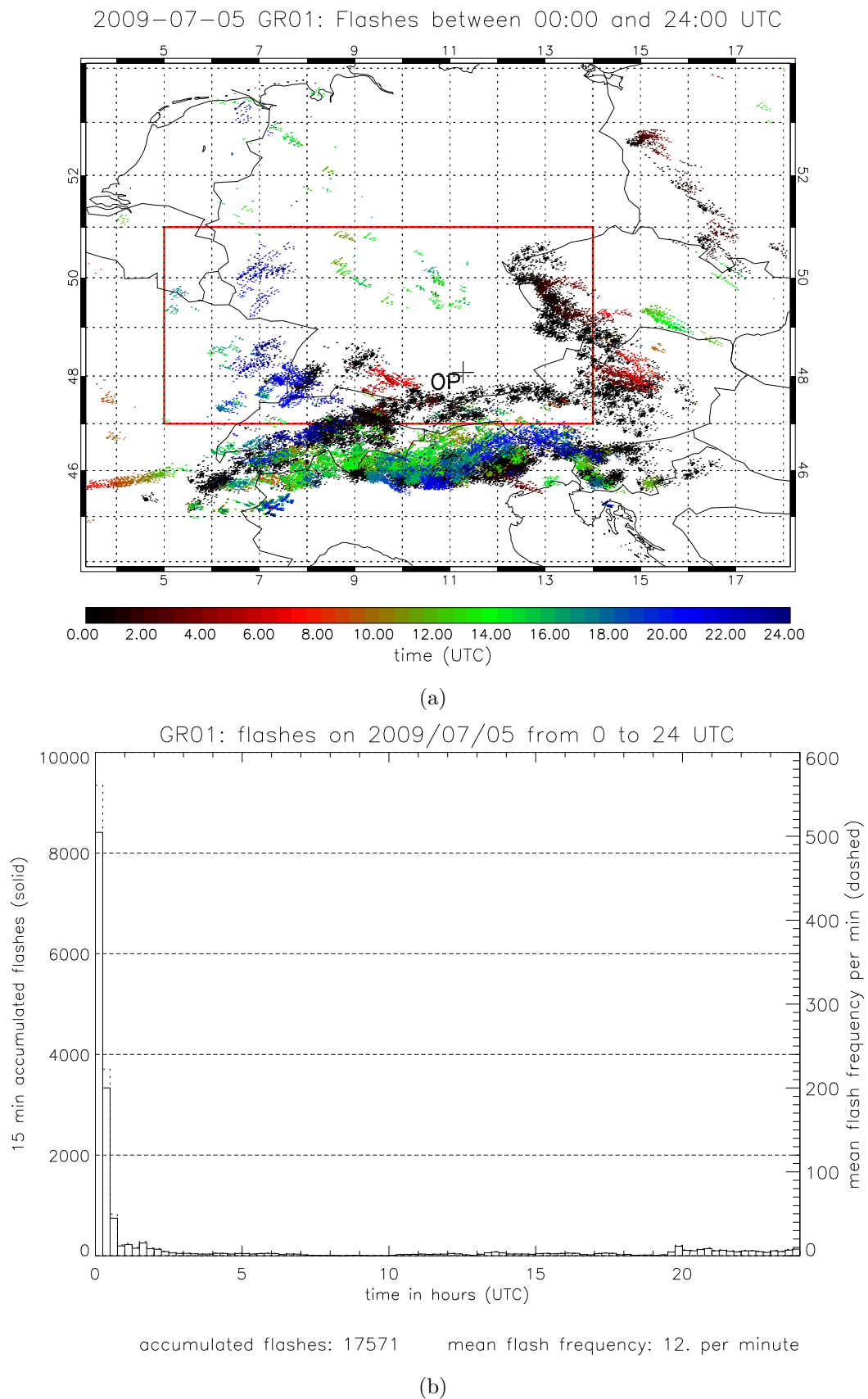
Figure 6.18:   (a) Overview of the simulated lightning activity based on the GR01 parameterization, as in Fig. 6.11(b). (b) Histogram plot showing the temporal evolution of the lightning activity, based on GR01.
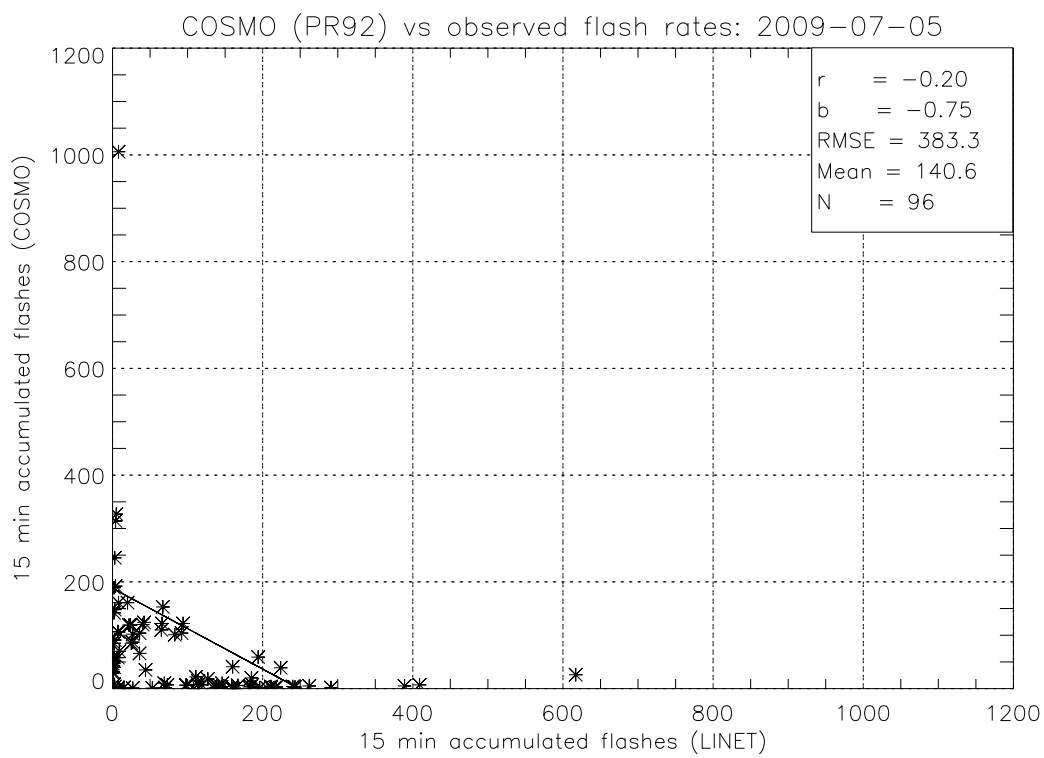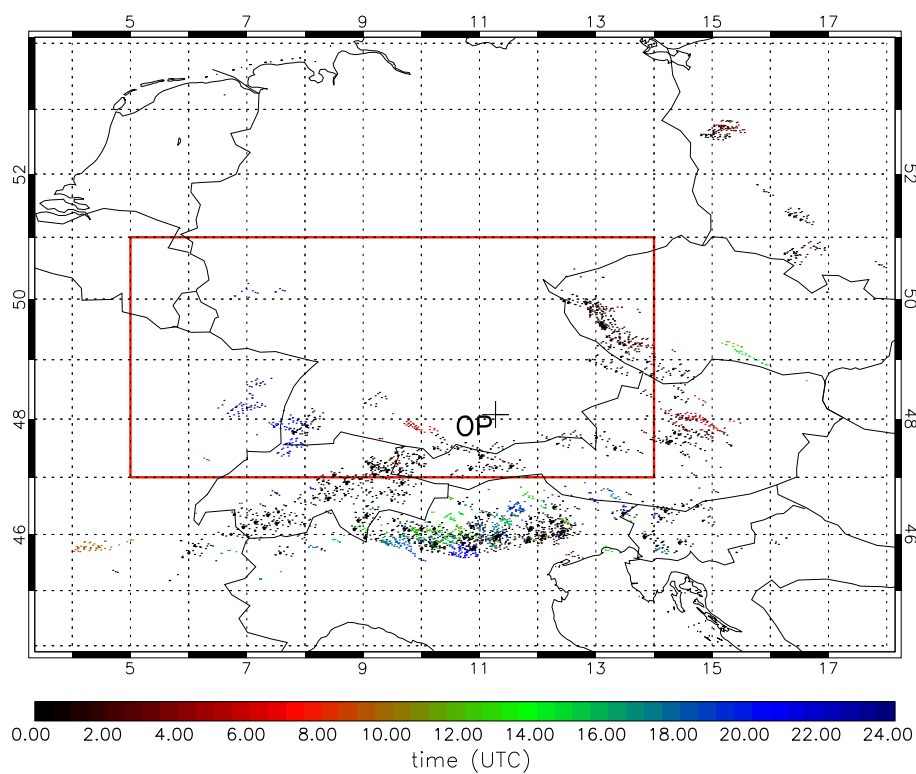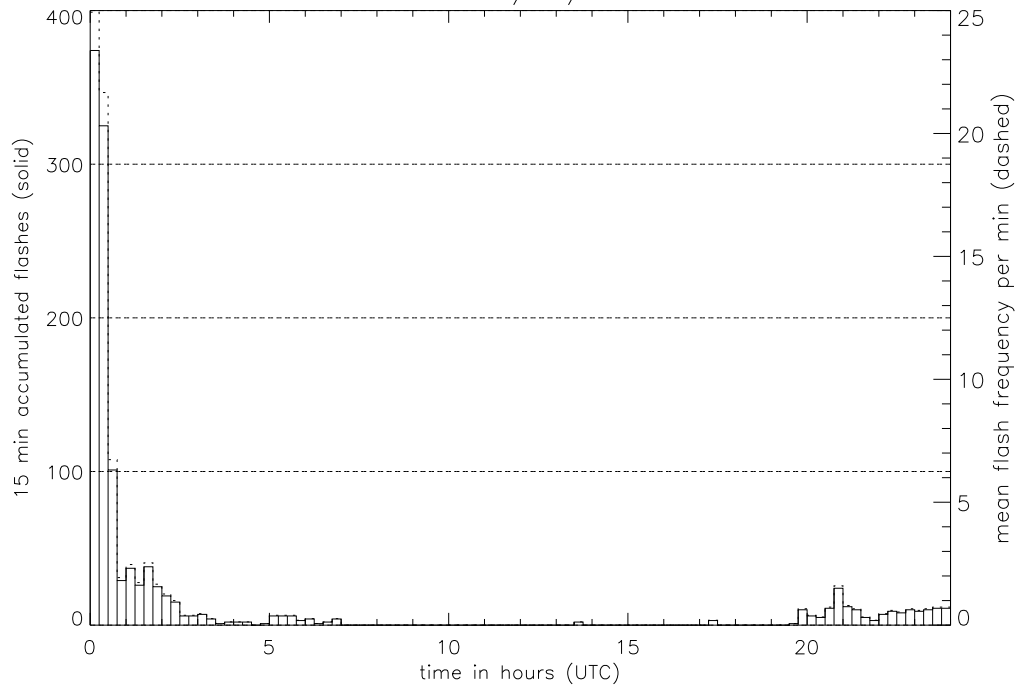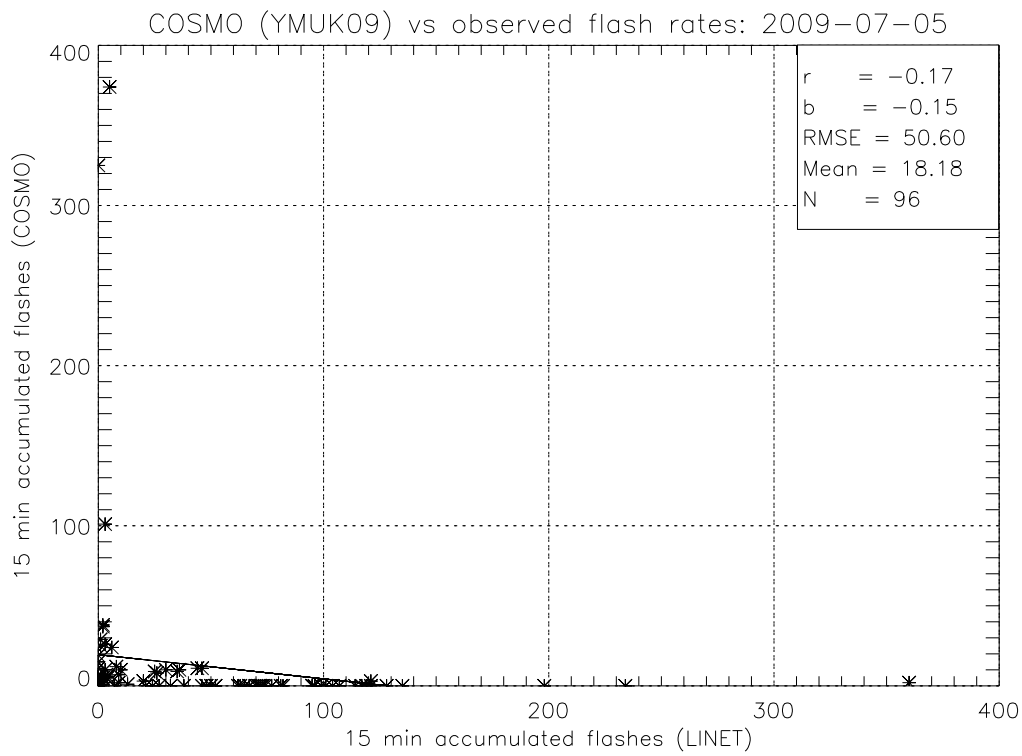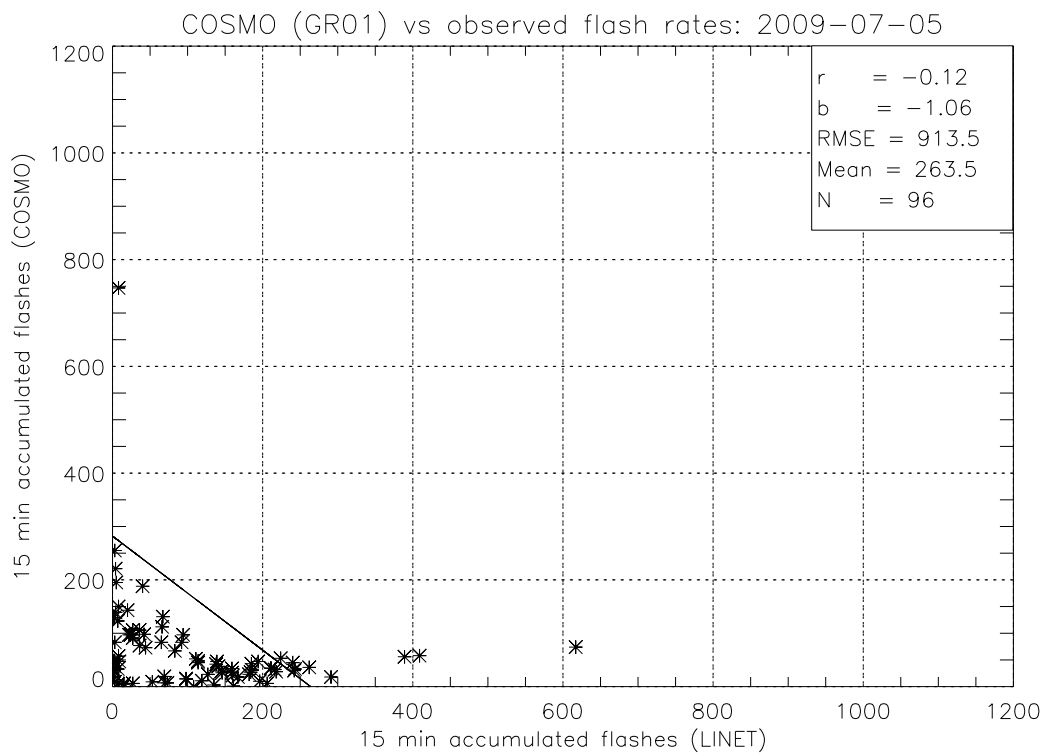
Figure 6.19: Correlation of the temporal evolution of the lightning activity based on LINET flashes and on the simulation using the GR01 parameterization. Two data points in excess of 3,000 flashes in 15 minutes were omitted in the plot to ensure readability.

Chapter 7

Discussion

7.1 Lightning data

Before interpreting the results presented in the previous two sections, a few comments on the objects that are parameterized, i.e., the lightning flashes, are appropriate. The display of flashes as "colored dots" (e.g., Fig. 6.2(a)) suggests a well-defined location where lightning occurred. However, this is an abstraction. Though the location (in space and time) of a CG discharge may be associated with the position where it struck the ground, the localization of an IC discharge requires some abstraction. With these discharges, there is no unique location associated, because the discharge extends over several km in horizontal and vertical directions. LINET reports the location of the strongest radiation source as stroke position. Subsequently, these strokes are grouped into flashes (see section 2.3.3). This implies that a "dot" on the maps showing the lightning activity (again, Fig. 6.2(a)) represent a somewhat abstract picture of the actual discharging process.

The choice of the time and space intervals used in grouping strokes into flashes affects the total number of flashes as well as the flash frequency. The sensitivity of the total number of flashes to the choice of the space-time intervals depends on the spatio-temporal stroke distribution. As shown in Fig. 2.6, the resulting flash number may be half half as large as the number of strokes.

The newly developed parameterization is valid only for the binning of strokes in one second and 10 km intervals. If other intervals were chosen, the parameterization would have to be re-calibrated. The comparatively coarse temporal binning of one second renders the LINET data comparable to data obtained from less sensitive detection techniques.

7.2   The D10 approach

The physical model underlying the lightning parameterization is based on the no-
tion that there is a charging process, represented by the current density, j, and a
discharging process, represented by $A/\Delta Q$, (see section 2.4.2). These processes are
balanced, and if the discharge amount, ΔQ and the space-charge area, A, are known,
then the flash rate may be determined. Up to that point, the only limitation of this
model is its balanced nature. In reality, substantial departures from the critical
electrostatic fields are occurring after a discharge. However, this effect is accounted
for by distributing the flashes randomly in time. The capacitor model in addition
assumes that the plates are circular and of equal size, and that the basic charge
distribution is a dipole.

The dipole assumption is tied to the association of positive charge with ice
crystals and negative charge with graupel. This notion is based on the basic graupel-
ice charging mechanism. Especially with complex storm structures, however, up to
six charge layers have been observed Stolzenburg and Marshall (2009). Even the
gross electric behavior of such storms is very unlikely to be described properly by a
simple dipole model. This may be one reason that the flash-rate forecasts for MCSs
are so poor in the D10 approach. On the other hand, the reduction to a dipole charge
distribution does not seem to have much influence with isolated thunderstorm cells.
Over a wide spectrum of isolated thunderstorms (regarding their size and strength),
the capacitor-based approach yields encouraging results. These results are sensitive
to the capacitor-plate area, and an error of 5 km may double or halve the predicted
flash rate.

The simplifying assumption regarding the charge structure not only limits the
quality of the lightning-rate estimates with large thunderstorm systems, but also
with shallow storms. In order to identify a "charged plate", the graupel region
is required to extend above the 263 K level. Otherwise the convective cloud is
considered to be non-electrified. Although only one case was observed where this
criterion dismissed cells that were observed to produce lightning, it shows that the
simplified picture breaks down in some very marginal situations. This limitation
does not pertain to all shallow and weakly-electrified cells, for in other cases, the
weak flash rates were correctly predicted (namely, on 2 April 2008 where shallow
and weakly electrified graupel showers occurred and on 1 March 2008 where a line
of shallow strongly forced convection was observed).

The error due to the assumed non-circular shape of real thunderstorm cross
sections cannot be established quantitatively. A comparison between the numerical
solution for the non-circularly shaped plates and the analytical solution used herein,
could provide such an estimate for a variety of charge distributions. However, the

basic electric field will always be a dipole field, with higher-order refinements as the charge distribution becomes more amorphous. This would mainly affect the amount of charge necessary to generate the critical field. However, except for very small charge-region geometries (section 3.1.3), where the lightning charge is limited by the total charge, the flash rate does not depend on the actual value of the critical field. The error associated with the assumption of equal plate size is not known, because there does not exist a comprehensive model for the rate of decrease of charge density from a center of a storm to the anvil edge. If the upper charge region is more extensive than the lower charge region, then this would primarily affect the charge volume. Hence, the lightning charge would be slightly bigger than in the symmetric case, yielding slightly lower flash rates.

Even though the charge regions in a real-world storm have finite depths, the electrostatic field between the regions is determined by the charge per unit *area*. This means that mathematically, it is irrelevant whether the plates have finite or infinitesimal depths as long as the field is considered in the exterior of the charge region, which is assured in this model by considering the field in the middle between the plates.

As summarized in Tab. 3.2, several assumptions were made besides those pertaining to the basic capacitor model. All these parameters directly or indirectly affect the result, with most of them contributing linearly to the result. This means that the result is quite sensitive to the choice of the constants used in the parameterizations. As stated in section 3.1, the particular choices are based on a tuning procedure which was aimed at yielding "plausible" results for COSMO-DE cells. Although the qualitative behavior of the parameterized variables are basically known, as are their orders of magnitude, the particular choices for the constants remain uncertain. This follows from a lack of observations and from the complexity of the thunderstorms themselves. The path chosen to nonetheless find quantitative relationships was to run repeated simulations and to adjust the parameters until plausible results were achieved. In a next step, this parameterization was tested against independent data, which involved radar measurements[1].

In the light of the simplifications in developing the D10 method, it is somewhat surprising that it yields rather accurate results (section 5.1). There appear to be two explanations, i) the accurate predictions are a product of coincidence and ii) the bulk lightning activity is indeed obeying rather simple laws. Although only 14 cases were investigated, it is unlikely that the close agreements between observa-

---

[1]The intention at this stage was to refine the parameterization based on the information gleaned from radar measurements; it was not expected that the tuning based on model data would yield accurate predictions when applied to real-world storms. However, the resulting predictions (section 5.1) were satisfactory already, so the radar could directly be used to test the parameterization (rather than refining it).

tions and theoretical predictions are purely coincidental. This is because cases were selected that covered very different storm environments. These range from highly unstable and strongly sheared to minimally unstable and essentially unsheared ones. Intermediate cases were also considered. However, errors in the parameterization of, e.g., the lightning charge and the charge density in the generator current could compensate one another. E.g., measurements that relate storm size to discharge strength would be required to determine whether there are compensating errors in the parameterization.

The alternative is that the flash rate can indeed be determined with a rather simple model. It must me remembered that only the *bulk* electrical activity is diagnosed with the D10 approach. I.e., CG and IC discharges are not distinguished, and the polarity of the discharges is not considered, either. Clearly, if these details were to be predicted, the D10 approach would be insufficient. What the results based on the bulk flash rate support, on the one hand is that the charging rate is tied to the graupel mass. This is based on the graupel-ice mechanism and on the assumption that the fall velocity as well as the number of the graupel pellets increases with increasing graupel mass. On the other hand, the discharge strength[2] strongly depends on the geometry of the charge regions. Albeit simple, these assumptions have their foundation built upon basic microphysics and electrostatics, the general validity of which was tested in laboratory experiments. Thus, it is speculated that the bulk lightning rate of isolated thunderstorms may indeed be described using a simple dipole model.

Some uncertainties are involved in the method used to test the D10 predictions. Due in part to the principle incompleteness of radar data (no coherent spatio-temporal picture is provided), the parameters for the flash-rate equation were retrieved manually. This method is somewhat inaccurate and not reproducible in every small detail. However, rather large errors in determining the cross-sectional diameter of the graupel regions were included to account for these deficits. These became especially large with the high-flash-rate MCSs.

Altogether, it is concluded that the broad range from less than one flash per minute to one flash every other second *associated with isolated thunderstorm cells* is handled well by the D10 approach.

Most of the very-weakly flashing cells are also handled well, but cases exist where the approach misses weakly electrified cells. The lightning activity of the three MCSs contained in the data was captured quite poorly by the D10 approach. This is not surprising since the many simplifications are not applicable to MCSs in

---

[2]The discharge strength refers to the neutralization of Ψ, which depends on the lightning charge, ΔQ, as well as by the horizontal extent of the charge region. If $\Delta \Psi = \Delta Q$, then only the lightning charge determines the "discharge strength".

any meaningful way, given their complex charge structure (Stolzenburg and Marshall, 2009). Moreover, the lightning charge saturates at 25 C as the charge volume increases. In large MCSs however, charge-moment changes of 1,500 C km were observed[3] (Lu et al., 2009). This means that if more lightning charge was admitted in the parameterization for MCS cases, then the overestimation of the lightning rates may be reduced in these cases.

In Fig. 5.7, data are shown that were artificially corrected for MCS cases. This plot merely justifies the inclusion of the MCS correction. The only reason this was included is to render the simulations of the overall lightning activity in COSMO-DE more realistically. This correction is not proposed as a universal relation that remedies the inadequacies of the D10 model.

7.3 The PR92, YMUK09, and GR01 approaches

The PR92 parameterization for continental storms is based on results presented by Williams (1985). His plots show a good correlation between the 5th power of cloud-top height and a height-averaged lightning frequency. However, he states that "natural variability in these data was suppressed by the averaging..." (Williams, 1985, p. 6017). Though this variability is not specified, it implies that his correlation supporting the 5th-power law may be weaker than suggested. The data used in that study were retrieved from three earlier studies, i.e., Shackford (1960), Jacobson and Krider (1976), and Williams (1981), where observation periods in the late 1950's and early-mid 1970's were considered. The detection technique varied from visual observation by humans (Shackford, 1960) to a combination of surface-based field changes using a field-mill, TV records, and again eye observations by human observers (Jacobson and Krider, 1976). This means that the original purpose of the resulting parameterization was the application to individual convective clouds, as done in this study.

In order to test this parameterization, PR92 used an optical sensor on a satellite of NASA's "Defense Meteorological Satellite Program" (DMSP). Based on an estimated detection efficiency of only 2 %, they multiplied the measured flashes with a correction factor. PR92 report correlation coefficients between predicted and observed flash rates on the order of 0.6, but without a measure of spread of the individual data points.

The LINET data were filtered to yield temporal resolution of one second in a 10 km radius, so that an attempt was made to come close to the detection efficiency of other techniques. A quantitative estimate of how comparable these data are cannot

---

[3]The charge is removed from altitudes of order 10 km, so this corresponds to about 150 C of lightning charge.

be offered as LINET data were not compared with the methods used in Shackford (1960), Jacobson and Krider (1976), and Williams (1981). An artificial upward correction of PR92 predictions was carried out in section 5.1. However, unless a rigorous comparison between LINET data and the other methods is available, such a correction cannot be established for general application. Hence, the original PR92 parameterization was implemented in COSMO-DE. Also, with this approach the original idea (Williams, 1985) to apply the cloud-height dependence to individual clouds was realized.

YMUK09 used data from a space-borne optical sensor (Lightning Imaging Sensor, LIS) which has a detection efficiency of roughly 90 % during night, and about 70 % during day (Finke, 2009). Given the artificial reduction of LINET's resolution by grouping the signals into flashes, the LINET and LIS detection efficiencies are practically identical[4]. The detection efficiency thus cannot explain the strong underestimation of the flash rate by YMUK09. Since this underestimation is evident when applying YMUK09 to observed as well as to modeled storms, it does not depend on the definition of the cloud depth (reflectivity field and and vertical-velocity field, respectively). The errors are inherent to the parameterization, rather than to the measurement devices.

Another factor is that oceanic storms generally produce less lightning than continental storms (e.g., Price and Rind, 1992). If the YMUK09 parameterization is dominated by weakly-flashing oceanic storms, the application to central European (i.e., continental) storms results in an underestimation of the lightning rate. Yoshida et al. (2009) also offer "local" parameterizations to account for these differences between oceanic and continental storms. These local areas include mostly southern hemispheric and tropical regions. The respective parameterizations are not presented in terms of numbers in their work, but only the respective regression lines are plotted (their Fig. 6). To test whether the YMUK09 parameterization is dominated by oceanic storms, one of the local parameterization was also investigated. For this purpose, south Africa was chosen. Though climatologically, this part of the world does not compare to central Europe in every detail, a sense may be gained about how the YMUK09 parameterization behaves over continental regions. The y-intercept and the slope had to be retrieved manually, based on their Fig. 6. The y-intercept is not plotted and was extrapolated, which may have resulted in some error. To assess how large this error is, the original parameterization was also determined manually based on the regression line. The original parameterization is

$$f_{ymuk} = 10^{-6.1} \bar{H}^{4.9}, \tag{7.1}$$

---

[4]These results were presented at the Eumetsat Meteorological Satellite Conference 2009, by H. Höller, K. Schmidt, and H.-D. Betz.

while the manual retrieval of the global parameterization (f_{glob}) by this author leads to

$$f_{glob} = 10^{-6.4} \bar{H}^{5.1}. \qquad (7.2)$$

For the south-African parameterization (f_{SA}) it was found that

$$f_{SA} = 10^{-6.1} \bar{H}^{5.0}. \qquad (7.3)$$

The comparison between Eqs. (7.1) and (7.2) reveals the degree of accuracy in manually determining the parameterization. The difference is about 100 %, or a factor of two. More importantly, the difference between f_{SA} and f_{glob} is also about a factor of two. This means that the influence of oceanic storms can only explain a factor-two difference (rather than the observed factor of about 20; Fig. 5.11(a)).

The averaging does not explain the large differences, either. In section 5.2, average lightning frequencies have been calculated, but the order of magnitude is largely retained (except for the MCS on 26 May which was surrounded by weakly-flashing convection); See Tabs. 5.1 and 5.2. Moreover, averaged LINET measurements were compared to averaged D10 predictions in section 6.1, and the same order of magnitude was achieved in the investigated cases. This implies that even if the LINET data are averaged, YMUK09 strongly underestimates the lightning rates, (the YMUK09 predictions were lower those of D10).

Based on a reflectivity-based definition of a convective cell, *all* cells fulfilling the "convective" criterion are included in the dataset. This number of cells is then related to the number of LIS signals (Yoshida et al., 2009, p. 3). YMUK09 report that about 80 % of the detected convective cells were associated with lightning, so this cannot explain the strong underestimation, either.

Presently, no explanation can be offered that accounts for the large differences between observed flash rates and the flash-rate predictions based on YMUK09.

The mathematical model underlying the PR92 and YMUK09 parameterizations, is based on a constant electrostatic-energy neutralization. YMUK09 present calculations demonstrating that their approach is also consistent with the assumption of constant charge neutralization (see, however, section 2.5.2). The fact that there are only weak correlations between the cloud-top-based PR92 and YMUK09 predictions with observations is owed to the fact that the cloud-top height in the investigated cases did not vary substantially from storm to storm. I.e., isolated, disorganized convection with weak flash rates on 30 June 2009 had the same cloud-top height as the strongly flashing supercell on 22 August 2008 (13,000 m). The same holds for the YMUK09 parameterization. In the two-plate circular model the separation distance between the charge regions has no influence on the flash rate at all. So what skill may have been detected on a global scale in using the PR92 and YMUK09 parameterizations, probably stems from the assumption that wider

storms are deeper and shallower storms are more skinny (i.e., $h \propto R$, p. 31). On a global scale, this assumption may have some merit, as dynamic entrainment tends to increase with updraft velocity (Houze, 1993, p. 257). If in general, stronger updrafts are assumed to be deeper than their weak counterparts, then only the wide storms can be sustained against entrainment. This may be the reason that globally, the PR92 and YMUK09 parameterizations have some skill, though that skill is difficult to ascertain given the observational constraints these investigators were faced with. Applied to parameterized convection in global circulation models, Tost et al. (2007) found that the PR92 predictions did not reproduce observations satisfactorily. For individual storms, it is very unlikely that accurate predictions are achieved with these approaches, which is consistent with the results shown in the previous chapter.

If the lightning rate is increased artificially by multiplying the PR92 and YMUK09 flash rates with a constant factor, then it is seen that rough trends are reproduced. The scattering is rather substantial, however.

The GR01 approach inherits the nature – and also the problems – of the PR92 parameterization. The fact that the GR01 total lightning is somewhat higher than with the PR92 parameterization is directly evident when plotting the PR92 and GR01 predictions for the training data, see Fig. 7.1. The correlation coefficient is 0.75, with a regression-line slope of 0.82; RMSE is 1.3 min^{-1}, which all suggests that the GR01 approach reproduces the PR92 results rather well, which was the goal of GR01. However, from the slope of 0.82 it follows that there is a slight overestimation when using the GR01 approach compared to PR92.

Altogether, it has become clear that the YMUK09 parameterization does not yield meaningful results when applied to individual clouds, though their method suggests that it should be. PR92 derived their results based on observations of individual clouds and applied these result to the global scale. Whether the differences between LINET and PR92 are due to different detection efficiencies is not known.

7.4   D10 application: individual cells in COSMO-DE

All the above-mentioned limitations of each parameterization are directly inherited to the implementation in the COSMO-DE. The performance of the parameterization applied to modeled cumulonimbi does not test the accuracy of the approach itself. This was tested by applying it to observed clouds. Rather, the comparison of individual modeled convective clouds with observed ones, tests how well the properties of the graupel regions are represented in the model, and whether the
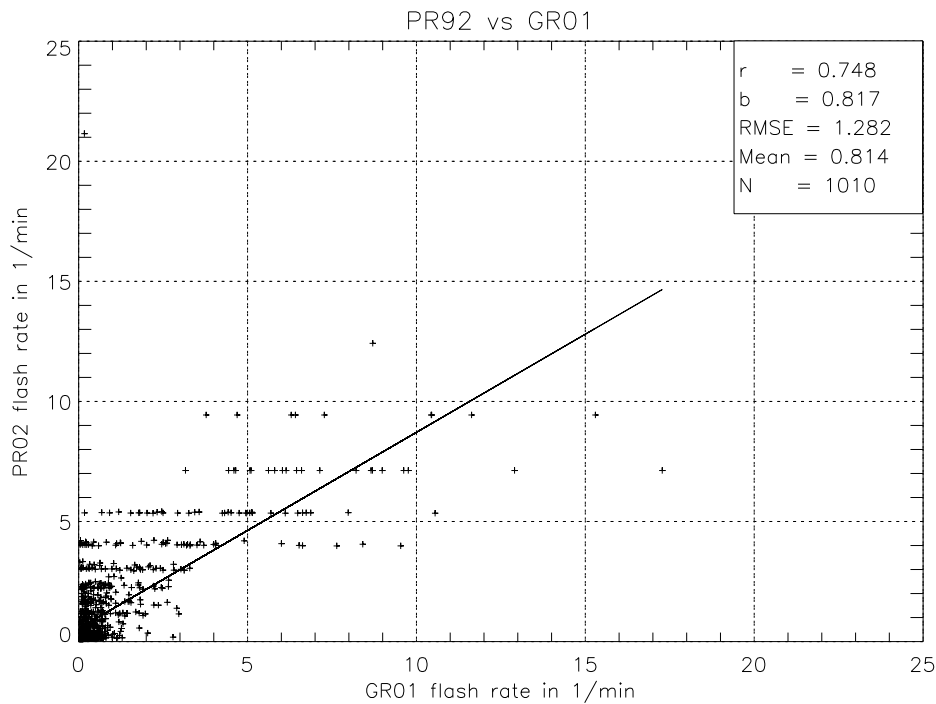
Figure 7.1: PR92 and GR01 lightning rates. Solid line is a least-square fit.

COSMO-DE-specific correction (section 4.3) yields realistic results.

The cases that were tested supported the findings based on measurements with radar. This means that the size and the graupel mass of the simulated convection was very similar to the observed convection, which justifies the COSMO-DE specific corrections. The fact that a simulated cloud produces the same lightning frequency as the observed cloud, is trivial if the cross-sectional areas and the graupel masses are equal.

It is open to question how many artificial modifications of the model fields are desirable in order to obtain realistic flash-rate results in the model. The main strength of the D10 parameterization is its physical foundation, which becomes corrupted if an increasing amount of model-dependent correction factors is included. Also, the D10 predictions should improve as the model convection becomes more realistic. If too much artificial model-specific tuning is applied, this property is lost.

7.5 COSMO-DE implementation - entire domain

The main question that one might ask is whether the discrepancies between observed and simulated lightning activity are due to erroneous lightning-frequency predictions while the convective cells are correctly simulated, or due to erroneous convective development in the model, while the lightning frequencies are correctly simulated. A definite answer to this question unfortunately cannot be provided, which is owed

to the fact that the model virtually never captures the exact convective evolution observed in the real world. As discussed in section 6.1, it usually is impossible to associate a particular observed cell (and its flash rate) with a particular simulated cell (and its flash rate). The few cases where such a comparison was attempted (sections 6.1), suggest that the lightning-frequency simulations are accurate for non-MCS storms. This implies that the bulk lightning forecasts would likely improve if the convection simulations become more accurate.

Altogether, it is not surprising that COSMO-DE does not capture every detail of the convective development, given the long lead times (usually more than 12 h), as well as the principle lack of understanding of convective initiation (e.g., Doswell et al., 2007). Hence, it is very unlikely that observed and modeled lightning swaths will exactly coincide anytime in the near future. One might thus reach the conclusion that forecasting lightning with COSMO-DE is not useful yet, and that it needs to await times when each thunderstorm cell is accurately simulated. However, there are at least two reasons that these forecasts are of value. It may be used as "quality-control" how well the model captures the timing and location of convective development. The results thus far imply that the predicted lightning rate of individual cells is reasonably realistic. This suggests that, e.g., too large a total number of discharges may reflect too large a number of simulated convective cells. The timing of convective initiation may also readily be compared. Even though this is mainly an additional tool for model developers, there also is a direct use in the forecasting process. Although the model is incapable of capturing every detail of the convective evolution, it may be considered to offer one possible scenario, given a certain environment. E.g., if the model simulates intensely-flashing storms, it is a hint to the forecaster that the environment on that day supports high flash rates. The exact time and location of convective initiation needs to be determined by nowcasting techniques (e.g., surface analyses, "clear-air mode" radar data, etc.). In the example of 22 August 2008, the message would have been that a long-lived, strongly flashing storm develops in the pre-Alpine region, which may not readily have been anticipated by inspecting the precipitation forecasts or the observed soundings from 12 UTC. This would certainly raise the forecaster's awareness that, e.g., severe convective weather such as large hail, damaging wind gusts, etc., may be imminent[5]. Though this information could generally have been retrieved by perusing environmental parameters and precipitation forecast fields, the lightning forecast yields a nice overall picture of the modeled convective potential. COSMO-DE handled 22 August 2008 quite well, in that it correctly anticipated the evolution

---

[5]The possibility of severe convective weather should not be inferred from the flash rate alone, of course. However, if much lightning is simulated in an inconspicuous environment, the forecaster may be prompted to inspect the situation for the possibility of severe weather.

of well-organized, strongly-electrified supercells. An interesting effect that is very
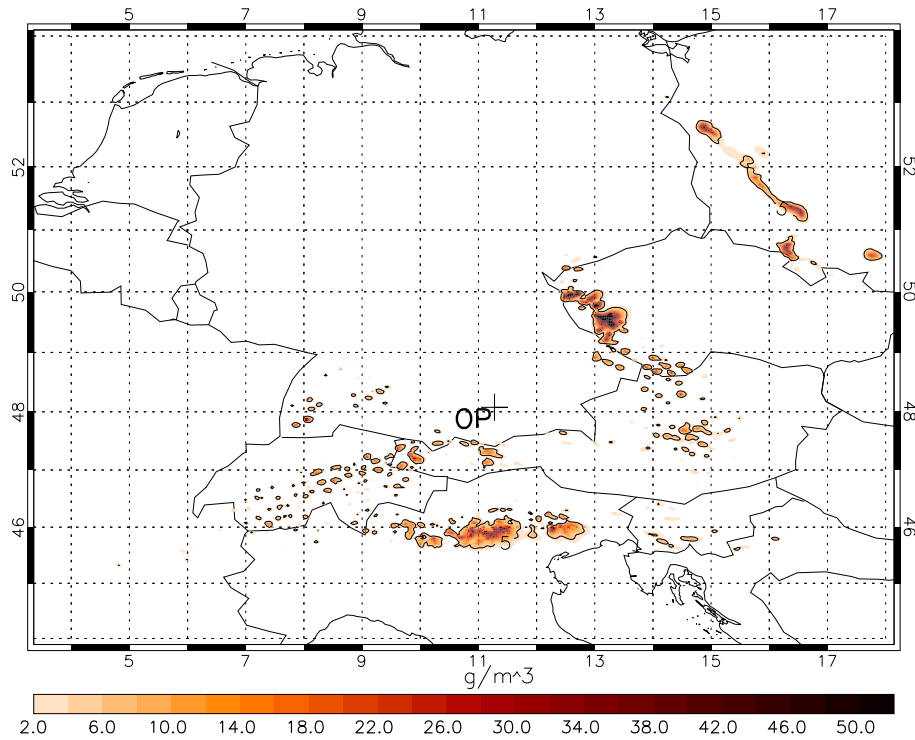
Figure 7.2: Vertically integrated COSMO-DE graupel mass in gm^{-3} one hour after initialization on 5 July 2009. The strong graupel accumulations are consistent with the simulated early-morning lightning activity on that day.

clearly shown by the lightning simulations is the extensive nocturnal convection that develops especially in weakly-forced, weakly unstable situations. Fig. (7.2) shows the simulated vertically-integrated graupel mass one hour after initialization on 5 July 2009. Widespread graupel areas are visible, consistent with the strong lightning activity. The reason for this development is likely tied to the latent-heat nudging used to assimilate radar data into the model (see, e.g., Stephan et al., 2008). This procedure modifies the latent heating profiles in the model in proportionality to the inferred rain rate. This imparted latent-heat release initiates the convection (see also Craig et al., 2009). Though no latent-heat nudging is done in the simulations in this study, the initial analysis field contains the assimilated radar data. Fig. (7.3) shows the observed reflectivity fields (left panel) and the ones produced by the operational COSMO-DE run (right panel) at 0000 UTC and 0100 UTC. The model was initialized at 0000 UTC. The inconsistencies between the modeled graupel field and the reflectivity field arise from the vertical integral that was taken over the graupel-mass field. Also, nudging is applied in the operational simulations, but not in this study. It may thus be advisable to use COSMO-DE lightning forecasts only after several hours into the simulation to avoid a misinterpretation.
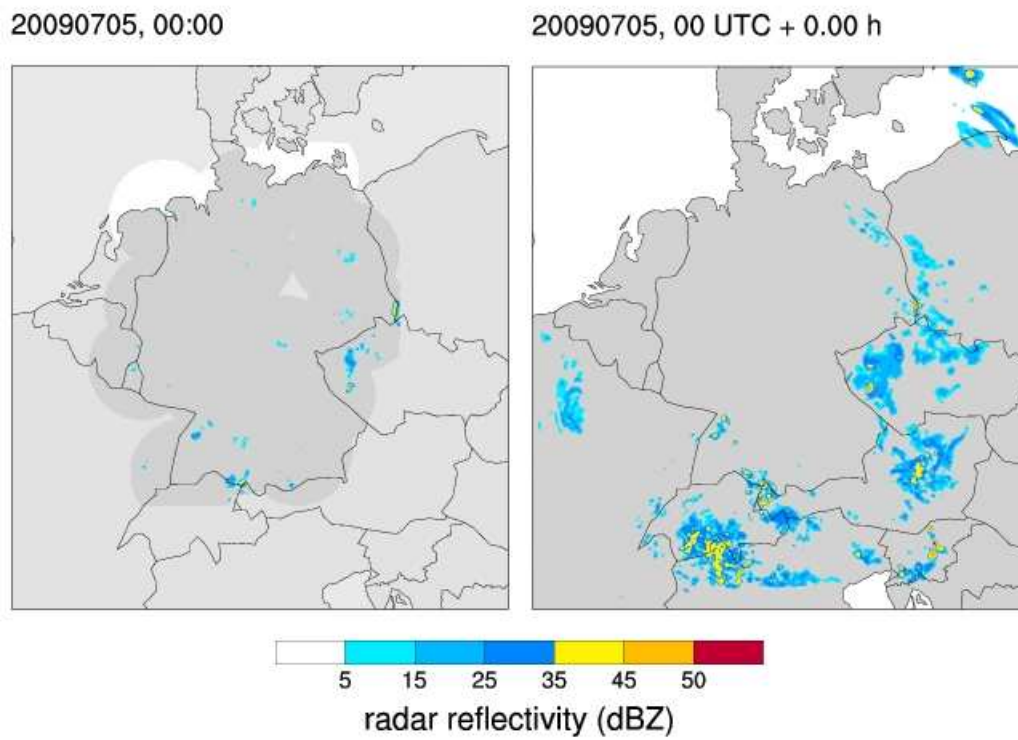
(a)
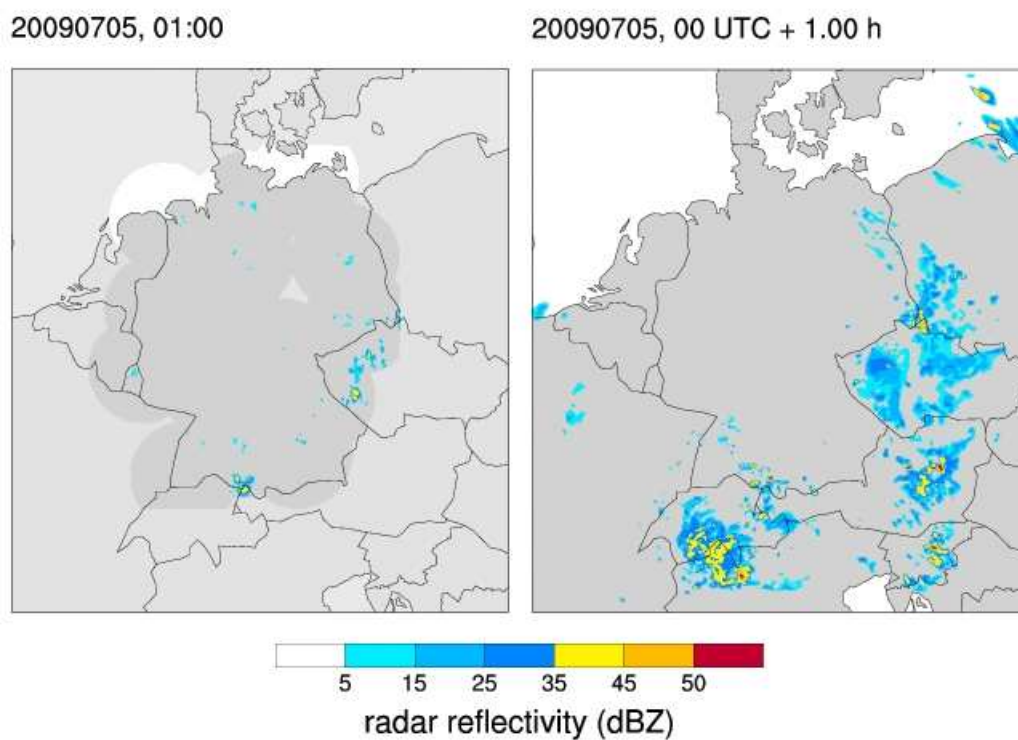
(b)

Figure 7.3: Observed (left) and modeled (right) reflectivity fields at 0000 UTC (a) and 0100 UTC (b) on 5 July 2009. Courtesy of A. Seifert (DWD).

As the number and the location of thunderstorms in the model usually differs from the observations, all of the parameterizations will fall short of capturing the correct lightning evolution. On some days, there may be too much convection, which may be compensated for by the PR92 and YMUK09 parameterization, which predict too little lightning per cell. However, if physical consistency is desired, the D10 approach should be the choice.

The displacement and amplitude score (DAS) supports the subjective assessment that COSMO-DE performed better on 22 August 2008 than on 5 July 2009. On that day, D10 results in a DAS of about 4.3, while the other parameterizations result in a DAS of about one. This is because in the simulations, the convection developed during the night rather than during the day, which means that the parameterizations yielding least lightning activity perform best (YMUK09). D10 produces most lightning, and hence falls off to the last rank.

On 22 August 2008, GR01 and PR92 yield a DAS of 0.6, with YMUK09 resulting in DAS = 1.2. The fact that PR92 and GR01 outperform D10 is probably due to modeled convection in the western part of the domain. D10 produces most lightning with this activity, which increases the DAS. Most of the observed lightning activity is missing in simulations using the YMUK09 parameterization, which is why in this case YMUK09 results in the highest DAS.

This shows that none of the parameterizations can be said to yield the "best" results if the convective activity over a large area is considered. Lightning is simulated inaccurately with all parameterizations, which is due mainly to problems of the model to handle the convective evolution itself properly.

7.6 Sounding-derived parameters

An alternative way to predict lightning is to inspect data from a rawinsonde ascent and estimate the lightning rate based on sounding-based environmental parameters. This method cannot reveal whether or not deep convection will form, but how much lightning a convective storm may produce once it developed. The correlations for the data used in this investigation are generally quite poor. This is not surprising. For example, MUCAPE and ICAPE only account for the strength of upward accelerations due to thermal buoyancy (Doswell and Markowski, 2004) for an undilute parcel. Real-world upward accelerations are strongly influenced by the perturbation pressure field, which is neglected in parcel theory. Also, precipitation load is neglected. Perturbation-pressure related upward motions may easily exceed buoyancy-related vertical velocities (Brooks and Wilhelmson, 1995), so that intense convection may result despite vanishing CAPE (e.g., Dahl 2006, p. 95).

Moreover, cases exist where thunderstorms developed in environments where

no positive CAPE existed (Colman, 1990). All these limitations explain why CAPE (and derived quantities) cannot be expected to be a good measure of updraft intensity. The strength of the updraft indirectly influences the lightning frequency: The stronger the upward motion, the higher the condensation rate, which leads to larger liquid-water contents and hence, to more riming (Zipser, 1994).

Among those parameters tested in this study, the best environmental predictor for the flash rate is the temperature at the equilibrium level. This may be due to the fact that the flash rate is dominated by geometry (section 2.4.1). In general, the lower the anvil-level temperature, the deeper the convective cloud. As hypothesized in section 7.3, deeper clouds tend to be wider than more shallow clouds which would support the tendency for deeper clouds to produce more lightning than shallow clouds. In fact, this is the basis for the PR92 and YMUK09 parameterizations.

The remaining predictors are practically uncorrelated with the flash rate. The low-level moisture may be considered as rough proxy for CAPE, and so inherits its shortcomings as lightning-rate predictor. The kinematic parameters, deep-layer shear and storm-relative helicity, have no skill in predicting the flash rate, either. This is due to three data points indicating flash rates below 2 min^{-1} with DLS > 25 ms^{-1}. These cases involved strongly-sheared but shallow graupel showers (2 April 2008), where the low lightning rate is dominated by geometry, and elevated convection (24 June 2008), for which the shear in the cloud-bearing layer would need to be considered (i.e., 0-6 km shear likely is an overestimation). The mean flash rate on 23 July 2009 was also only 0.1 min^{-1}, mainly because widespread but weak elevated convection developed ahead the large MCS that crossed the proximity area in the evening hours. If the MCS had reached the proximity box before the end of the 8 h time window, the flash rate would have been substantially higher.

Chapter 8

Conclusions and Outlook

In this work, a straightforward approach based on a physical model (abbreviated D10) was developed to describe the total (IC and CG) lightning rate of a thunderstorm. Lightning is described described as discharges between two oppositely-charged capacitor plates. The main idea behind this model is that the discharge frequency not only depends of the charging rate of the capacitor, but also on the strength of the discharges. In this approach, negative charge is associated with graupel and positive charge with ice particles, respectively. The area of the plates equals the equivalent circular diameter of the horizontal cross-sectional area through the graupel region. This cross section is taken at the height of the centroid position of the graupel area.

Only the graupel-mass field above the 263 K isotherm, as well as the ice-mass field need to be known to determine the flash rate. It was shown that the generator current density, the cross-sectional area of the graupel region, the lightning efficiency (i.e., the degree to which the lightning current contributes to the overall discharging process), as well as the lightning charge are required to determine the flash rate. The generator current density is parameterized using the maximum graupel mass and the lightning charge is parameterized using the volume of the space-charge regions. The parameterization was calibrated with the aid of modeled convective clouds, but it is directly applicable to observed clouds.

In addition to the new approach, the parameterizations by PR92, YMUK09, and GR01 have been investigated. These are based on a 5th-power dependence of the flash rate on the depth of the cloud (or a measure thereof).

All these approaches were implemented in the COSMO-DE model by introducing a new module, `src_lightning.f90`. An algorithm originally developed in the context of percolation theory determines cluster membership of each gridpoint: I.e., contiguous regions fulfilling certain criteria (e.g., the graupel mass exceeds 0.1 g m^{-3}) are assigned to a common cluster. This way the geometries of the cells, maximum graupel contents, and their centroid locations could be specified. With this

information, the flashes per cell were determined and randomly distributed around the centroids of the cells.

In order to test the flash-frequency predictions by PR92, YMUK09, and D10, the respective formulae were applied to measurements from a polarimetric doppler radar located at DLR-Oberpfaffenhofen. With this radar, not only the cloud depth but also details about the hydrometeors contained in this cloud, could be determined. Based on these measurements, the theoretical flash rate was determined using the three above-mentioned parameterizations. These predictions were compared with measurements from the lightning-detection network, LINET. For isolated thunderstorms, the results using the D10 approach are quite encouraging: The correlation coefficient between observed and predicted flash rates exceeds 0.9 with an RMSE of about four flashes per minute. The flash rates of the thunderstorms used for this test varied from one flash every few minutes to about one flash per second. If MCS cases are considered, the D10 approach results in a strong overestimation of the flash rate. Based on observed cases, an artificial downward correction was introduced for storms with large diameters.

It was shown that PR92, GR01, and YMUK09 do not capture the flash rate of individual thunderstorm cells satisfactorily, the main problem being a strong underestimation of the flash rates. At least for the YMUK09 approach, it could be demonstrated that this underestimation does not result from the dominance of (weakly flashing) oceanic storms. Nor is it due to different lightning-detection efficiencies of the different measuring platforms.

The new lightning scheme may be used to infer how realistically COSMO-DE simulates deep convection. The investigation of isolated cumulonimbus clouds in COSMO-DE simulations was aimed at the cloud physics. Using the D10 parameterization, this application revealed that the individual clouds in general exhibit flash rates close to measured ones. However, this required an artificial correction for the "too snowy" nature of the graupel, which primarily results in cells that are too large horizontally. The cases that were investigated included very different storm types and intensities, and good agreement was found between observations and simulations.

The comparison between observed and simulated lightning over a larger area, including southern Germany and parts of Austria, France, and the Czech Republic, reveals that none of the implemented parameterizations captures the observed lightning development in the investigated cases. The main reason is that COSMO-DE does not develop the observed number of cells at the observed times. To achieve consistent, and within the scope of the model realistic results, the D10 approach seems most appropriate. Most importantly, the lightning forecasts will improve as the model convection improves. This is not the case with either the PR92 or the

YMUK09 parameterization, as they do not capture the lightning activity of the individual cells. As PR92, GR01 and YMUK09 underestimate the individual flash rates, the total number of flashes is also lower than when using the D10 approach. All parameterizations inherit the problems of COSMO-DE regarding convective initiation and the coverage of the convection.

Using sounding-derived thermodynamic and kinematic parameters was shown not to be a promising tool to predict the flash rate.

The long-standing question about what determines the flash rate, generator power or generator current (see Boccippo, 2001, and also Yoshida et al., 2009) is answered with "neither". In general, any quantity uniquely describing a breakdown criterion, like the critical charge or the critical electric field, may to be used. The flash rate is then given by the rate of increase with time of this quantity, divided through the dissipation of this quantity during a discharge.[1]

The COSMO-DE model is now equipped with a lightning scheme, containing four parameterizations (D10, PR92, YMUK09, GR01). The main use of this application is a quick and complete overview of a given day's convective evolution. This aids in the evaluation of the lightning threat, and may indirectly reveal information about the severe convective weather potential. Neither precipitation fields, nor parameters characterizing the convective environment reveal as directly where the model anticipates convection. Also, the influence of environmental parameters on the lightning frequency may be studied with this new tool. Apart from these applications, the D10 lightning forecasts may serve as "quality control" of the modeled convection.

An important reason for simulating lightning is the assessment of lightning NO_x in global circulation models. However, neither is the graupel mass available in such models, nor can a width or diameter of the parameterized convective cells reasonably be defined. This means that the D10 scheme currently is not applicable to global circulation models. The COSMO model can be used for climate predictions, but in this setup also has its convection parameterized, which does not support the determination of the flash rate with the D10 method. However, the GR01 parameterization would be well suited for such an application. Although the flash rate based on this parameterization is generally underestimated, its application may reveal changes of thunderstorm activity (and NO_x production) in the future.

---

[1]If other discharging mechanisms than lightning are admitted in the model, then an additional factor, the "lightning efficiency" needs to be included.

8.1   Future work

A brief look at open questions that may be tackled in future work. An interesting
test would be to apply the D10 scheme to severe supercell thunderstorms in the
great plains of the USA. Despite their large size, these storms still are isolated, and
would thus provide a good test case. Another interesting storm type would be tall
– and in terms of convective rainfall – intense tropical-oceanic thunderstorms that
usually exhibit minimal lightning rates.

The main shortcoming of the D10 model is its inability to predict the flash
rates of MCSs realistically. Although the simple two-plate capacitor approach is
unlikely to capture the essence of the electrical structure of an MCS, the lightning
charge could be increased beyond 25 C for MCS cases, which would lower the flash
rate. This is the most straightforward remedy, which should at least reduce the
overestimation of the flash rate.

Further work may involve the refinement of the parameterization to yield more
details about the lightning discharges. An additional, positive charge layer could
be introduced near the 273 K isotherm. With the image charge at the surface,
altogether four charge layers would be obtained. This would allow for a distinction
between IC and CG discharges. As knowledge about the origin of the lower positive
charge region remains incomplete at the moment, empirical relations may be found
and used for this purpose. The height of the discharges could be retrieved by using
the initiation point between the main charge regions for IC discharges, and the
earth's surface for CG discharges.

It would be interesting to include the polarity of the flashes. One way to
incorporate e.g., positive CG discharges would be the assumption of an inverted
dipole charge structure (e.g., Williams, 2001). If cloud properties similar to those
found by Rust et al. (2005) are identified, the polarity of CG discharges could be
switched to positive.

Work by Huntrieser et al. (2008) suggests that the length of the lightning chan-
nel determines the amount of LNO_x that is produced during a discharge. Since the
channel length depends on the size of the space charge region, the LNO_x production
per flash could also be parameterized with the graupel-mass fields. Because espe-
cially tropical MCSs contribute to the global LNO_x production, such an application
requires that the flash rates associated with MCSs are simulated accurately. By
choosing the graupel region to parameterize lightning-channel lengths, the effect of
the vertical wind shear would not need to be considered, because the size of the
graupel region naturally depends on the vertical wind shear in the model. This is
because the organization of the convection is directly simulated (which, to a large
extent, depends on the vertical wind shear).

Appendix A

Mathematical Details

In this appendix, the calculations required to describe the electrostatic field between two capacitor plates as well as its temporal changes are presented.

A.1   The electrostatic field in a two-plate capacitor

The starting point is Gauss' law (e.g., Nolting, 2004, p. 63), which is given by

$$\nabla^2 \Phi = \frac{\rho}{\epsilon}, \tag{A.1}$$

where Φ is the electrostatic potential, ρ is the space-charge density, and ϵ is the permittivity. The solution of this equation is given by

$$\Phi(\mathbf{r}) = \frac{1}{4\pi\epsilon} \int d^3 r' \frac{\rho(\mathbf{r}')}{|\mathbf{r} - \mathbf{r}'|}, \tag{A.2}$$

where $\mathbf{r}'$ is a dummy integration variable and $\mathbf{r} = (x, y, z)$ is the position vector (Nolting, 2004; p. 104). The integral is taken over the entire space, with Φ decreasing to zero towards spatial infinity. Now

$$\mathbf{E} = -\nabla\Phi, \tag{A.3}$$

where $\mathbf{E}$ is the electrostatic field. With Eq. (A.2), Eq. (A.3) may be written as

$$\mathbf{E}(\mathbf{r}) = \frac{1}{4\pi\epsilon} \int d^3 r' \rho(\mathbf{r}') \frac{\mathbf{r} - \mathbf{r}'}{|\mathbf{r} - \mathbf{r}'|^3}, \tag{A.4}$$

where use of the fact was made that

$$\nabla |\mathbf{r} - \mathbf{r}'|^{-1} = -\frac{\mathbf{r} - \mathbf{r}'}{|\mathbf{r} - \mathbf{r}'|^3}. \tag{A.5}$$

In order to solve Eq. (A.4), the space-charge density distribution, $\rho(\mathbf{r}')$, needs to be specified. To describe the field inside a circular two-plate capacitor, the linear

nature of Eq. (A.1) will be used to superpose the solutions of the positively and the negatively charged plates. The first step is thus to solve Eq. (A.4) for a charged, horizontal, and infinitesimally thin circular plate. The charge distribution is then given by

$$\rho(\mathbf{r}) = \begin{cases} \sigma\delta(z - z_0) & \text{if } r \leq R \\ 0 & \text{if } r > R. \end{cases} \tag{A.6}$$

Here R is the plate's radius and r is the radial distance from the plate's center, σ is the charge per unit area, and δ is Dirac's delta distribution. z_0 is the vertical distance of the space-charge distribution from the coordinate system's origin. Only the non-trivial part of Eq. (A.6) contributes to Eq. (A.4), and the electrostatic field is given by

$$
\begin{aligned}
\mathbf{E}(\mathbf{r}) &= \frac{\sigma}{4\pi\epsilon} \int d^3 r' \delta(z' - z_0) \frac{\mathbf{r} - \mathbf{r}'}{|\mathbf{r} - \mathbf{r}'|^3} \\
&= \frac{\sigma}{4\pi\epsilon} \int\int dx' dy' \int dz' \begin{pmatrix} x - x' \\ y - y' \\ z - z' \end{pmatrix} \frac{\delta(z - z_0)}{[(x - x')^2 + (y - y')^2 + (z - z')^2]^{\frac{3}{2}}} \\
&= \frac{\sigma}{4\pi\epsilon} \int\int dx' dy' \begin{pmatrix} x - x' \\ y - y' \\ z - z_0 \end{pmatrix} \frac{1}{[(x - x')^2 + (y - y')^2 + (z - z_0)^2]^{\frac{3}{2}}},
\end{aligned}
\tag{A.7}
$$

where

$$\int_{-\infty}^{\infty} da' \delta(a' - a_0) f(a') = f(a_0), \tag{A.8}$$

was used, $(a \in \mathbb{R})$. Now the following substitutions are introduced:

$$\xi = x - x' \tag{A.9}$$
$$\eta = y - y' \tag{A.10}$$
$$\zeta = z - z_0, \tag{A.11}$$

so that

$$d\xi = -dx' \tag{A.12}$$
$$d\eta = -dy'. \tag{A.13}$$

Then,

$$r^2 = \xi^2 + \eta^2. \tag{A.14}$$

With this, Eq. (A.7) becomes

$$
\mathbf{E}(\mathbf{r}) \;=\; \frac{\sigma}{4\pi\epsilon} \int_{x-\infty}^{x+\infty} d\xi \int_{y-\infty}^{y+\infty} d\eta \begin{pmatrix} \xi \\ \eta \\ \zeta \end{pmatrix} \frac{1}{(\xi^2 + \eta^2 + \zeta^2)^{\frac{3}{2}}} \tag{A.15}
$$

$$
=\; \frac{\sigma}{4\pi\epsilon} \int_{x-\infty}^{x+\infty} d\xi \int_{y-\infty}^{y+\infty} d\eta \begin{pmatrix} \xi \\ \eta \\ \zeta \end{pmatrix} \frac{1}{(r^2 + \zeta^2)^{\frac{3}{2}}}. \tag{A.16}
$$

Since only the variations of $\mathbf{E}$ in the vertical are of interest, the horizonal dependencies are neglected by setting

$$
x \;=\; 0 \tag{A.17}
$$
$$
y \;=\; 0, \tag{A.18}
$$

so that

$$
\mathbf{E}(0,0,z) = \frac{\sigma}{4\pi\epsilon} \int_{-\infty}^{+\infty} d\xi \int_{-\infty}^{+\infty} d\eta \begin{pmatrix} \xi \\ \eta \\ \zeta \end{pmatrix} \frac{1}{(r^2 + \zeta^2)^{\frac{3}{2}}}. \tag{A.19}
$$

If the sheet of charge extends to infinity, $\mathbf{E}$ is horizontally homogeneous, and the restriction to $x = y = 0$ does not affect the result, as will be shown below. The next step involves a transformation to plane polar coordinates where,

$$
\xi \;=\; r\cos\phi \tag{A.20}
$$
$$
\eta \;=\; r\sin\phi \tag{A.21}
$$
$$
d\xi d\eta \;=\; r dr d\phi. \tag{A.22}
$$

Now the integral may be solved. Because the charge density is non-zero only where $0 \leq r \leq R$, the domain over which the integral is taken is finite. In plane polar coordinates, the intergal is taken over $r \in [0, R]$ and over $\phi \in [0, 2\pi]$. Because now

$$
r^2 = x'^2 + y'^2, \tag{A.23}
$$

this means that the solution is valid for the symmetry axis only (as desired). Eq. (A.19) may now be solved:

$$\mathbf{E}(0,0,z) = \frac{\sigma}{4\pi\epsilon} \int_0^R \frac{rdr}{(r^2+\zeta^2)^{\frac{3}{2}}} \int_0^{2\pi} d\phi \begin{bmatrix} r\cos\phi \\ r\sin\phi \\ \zeta \end{bmatrix} \tag{A.24}$$

$$= \frac{\sigma}{4\pi\epsilon} \int_0^R \frac{rdr}{(r^2+\zeta^2)^{\frac{3}{2}}} \begin{bmatrix} r\sin\phi \\ -r\cos\phi \\ \zeta\phi \end{bmatrix}_0^{2\pi} \tag{A.25}$$

$$= \frac{\sigma}{4\pi\epsilon} \int_0^R \frac{rdr}{(r^2+\zeta^2)^{\frac{3}{2}}} \begin{bmatrix} 0 \\ 0 \\ 2\pi\zeta \end{bmatrix} \tag{A.26}$$

$$= \frac{\sigma\zeta}{2\epsilon} \left[-\frac{1}{\sqrt{r^2+\zeta^2}} \right]_0^R \mathbf{e}_3 \tag{A.27}$$

$$= \frac{\sigma\zeta}{2\epsilon} \left[\frac{1}{\sqrt{\zeta^2}} - \frac{1}{\sqrt{R^2+\zeta^2}} \right] \mathbf{e}_3, \tag{A.28}$$

where $\mathbf{e}_3 = (0,0,1)$ is the vertical unit vector. Upon re-substitution of ζ, and observing that

$$\frac{\zeta}{\sqrt{\zeta^2}} = \frac{\zeta}{|\zeta|}, \tag{A.29}$$

one obtains the desired expression for the electrostatic field:

$$\mathbf{E}(z) = \frac{\sigma}{2\epsilon} \left[\frac{z-z_0}{|z-z_0|} - \frac{z-z_0}{\sqrt{R^2+(z-z_0)^2}} \right] \mathbf{e}_3. \tag{A.30}$$

The coordinate system may be translated such that

$$z_0 = 0; \tag{A.31}$$

then,

$$\mathbf{E}(z) = \frac{\sigma}{2\epsilon} \left[\frac{z}{|z|} - \frac{z}{\sqrt{R^2+z^2}} \right] \mathbf{e}_3. \tag{A.32}$$

If $R \gg z$, then the second term in Eq. (A.32) vanishes and

$$\mathbf{E}(z) = \frac{\sigma}{2\epsilon} \frac{z}{|z|} \mathbf{e}_3, \tag{A.33}$$

which is the well-known solution for a "charged-plate" with infinite horizontal extent (e.g., Nolting, 2004, p. 75). As alluded to above, this solution is independent of the horizontal coordinates.

Now two oppositely-charged plates are employed. The field is only considered between the plates where $0 \leq z \leq d$. The negatively-charged plate is located at $z_0 = 0$, so that

$$E^- = -\frac{\sigma}{2\epsilon}\left[1 - \frac{z}{\sqrt{R^2 + z^2}}\right].$$
(A.34)

The positively-charged plate is located at $z_0 = d$, yielding

$$E^+ = \frac{\sigma}{2\epsilon}\left[-1 - \frac{z - d}{\sqrt{R^2 + (z - d)^2}}\right].$$
(A.35)

The superposition of Eq. (A.34) and Eq. (A.35) results in

$$E = -\frac{\sigma}{\epsilon} + \frac{\sigma}{2\epsilon}\left[\frac{z}{\sqrt{R^2 + z^2}} - \frac{z - d}{\sqrt{R^2 + (z - d)^2}}\right].$$
(A.36)

This field has maximum magnitude at the plates, i.e., where $z = 0$ and $z = d$. For this application, the field in the middle between the plates is sought. This is because the "plates" in a convective storm have a finite thickness. If the oppositely-charged regions are staggered in a way that there is no deep neutral region between them, the field is maximum between the charge regions because in the interior of these regions the field is reduced ((e.g., Nolting, 2004, p. 61)). This is analogous to the representation of a charged sphere with finite radius by a point charge at the centroid location of the sphere. If this point charge carries the same amount of charge as the sphere, the electrostatic fields associated with both charge distributions are identical in the exterior of the sphere (see also Nolting, 2004, p. 61). So, upon setting $z = d/2$, one obtains

$$E = -\frac{\sigma}{\epsilon} + \frac{\sigma}{2\epsilon}\left[\frac{d}{\sqrt{R^2 + (\frac{d}{2})^2}}\right].$$
(A.37)

Upon re-arrangement of terms and introducing

$$G(R, d) = \left[\frac{d}{\sqrt{R^2 + (\frac{d}{2})^2}}\right],$$
(A.38)

Eq. (A.37) may be written as

$$E = \frac{\sigma}{2\epsilon}[G(R, d) - 2]$$
(A.39)

This result is consistent with Boccippio (2002) and is used in section 2.4.2.

A.2   The rate of change of the electrostatic field in a two-plate capacitor

The rate of change of E with respect to time is given by

$$\frac{\partial E}{\partial t} = \frac{\partial}{\partial t}\left[\frac{\sigma}{2\epsilon}[G(R,d)-2]\right] \tag{A.40}$$

$$= \frac{\partial \sigma}{\partial t}\frac{1}{2\epsilon}[G(R,d)-2]. \tag{A.41}$$

As the geometry of the capacitor is assumed to be constant in time, only the rate of change of σ matters. The charge density on both plates is given by $\rho = \sigma/h$, where h is the depth of the plates. Then,

$$\frac{\partial \sigma}{\partial t} = h\frac{\partial \rho}{\partial t}. \tag{A.42}$$

Integrating the charge-continuity equation, $\partial \rho/\partial t = -\nabla \cdot \mathbf{j}$, over the volume, V, of each plate yields

$$\int_V d^3r\frac{\partial \rho}{\partial t} = -\int_V d^3r\nabla \cdot \mathbf{j} \tag{A.43}$$

$$= \oint_{\partial V} d\mathbf{r} \cdot \mathbf{j}, \tag{A.44}$$

where $\mathbf{j}$ is the current density. If $\mathbf{j}$ is parallel to the plates' axes (i.e., charge is only transported vertically between the plates), then Eq. A.43 simplifies to

$$h\frac{\partial \rho}{\partial t} = j, \tag{A.45}$$

where $j = \|\mathbf{j}\|$. With $\sigma = \rho h$, this implies that

$$\frac{\partial \sigma}{\partial t} = j. \tag{A.46}$$

Hence,

$$\frac{\partial E}{\partial t} = \frac{j}{2\epsilon}[G(R,d)-2]. \tag{A.47}$$

This result is also used in section 2.4.2.

A.3   The charging current

The number, N_k, of hydrometeors of class k per volume is given by

$$N_k = \int_{-\infty}^{+\infty} f_k(D)dD, \tag{A.48}$$

where $f_k(D)$ is the particle-size distribution and D is the diameter of the particles. If the particles of class k carry the charge $q_k(D)$, then the total charge per volume (i.e., the charge density) is given by

$$\rho_k = \int_{-\infty}^{+\infty} \bar{\rho}_k(D)dD, \tag{A.49}$$

where $\bar{\rho}_k(D) = q_k(D)f_k(D)$ is the spectral charge density. In order to obtain the current density, the sedimentation velocity of the hydrometeors needs to be included:

$$j_k = -\int_{-\infty}^{+\infty} v_k(D)\bar{\rho}_k(D)dD, \tag{A.50}$$

where $v_k(D)$ is the magnitude of the terminal fall velocity of particles of class k and diameter D. The negative sign appears because the hydrometeors are falling downward (at the moment, it is assumed that there are no vertical motions of the ambient air). If the net effect of all hydrometeor classes is included, then

$$j = -\sum_k \int_{-\infty}^{+\infty} v_k(D)\bar{\rho}_k(D)dD. \tag{A.51}$$

This result corresponds to Boccippio (2002; p. 1096). Now only two classes shall be considered, ice crystals[1] and graupel. Moreover, the average diameter, $\bar{D}$, of the hydrometeors in each class is used and modeled by a delta distribution. In addition, the charge carried on the particles of each class does not depend on their size, so that

$$\bar{\rho}_k(D) = qf_k(D) = qn\delta(D - \bar{D}_k). \tag{A.52}$$

If the suffixes g and i pertain to graupel pellets and ice crystals, respectively, then Eq. (A.51) may be written as

$$j = -\int_{-\infty}^{+\infty} qn\delta(D - \bar{D}_g)v_g(D)dD - \int_{-\infty}^{+\infty} qn\delta(D - \bar{D}_i)v_i(D)dD. \tag{A.53}$$

Now the number of charged graupel pellets is assumed to be equal to the number of charged ice particles. In addition, the charge magnitude, q, carried on each hydrometeor class is identical but the signs are opposite, i.e.,

$$q_i = -q_g = q. \tag{A.54}$$

Then,

$$j = qnv_g - qnv_i = qn(v_g - v_i), \tag{A.55}$$

where n is the number of charged particles in each class, and $v_g \equiv v_g(\bar{D}_g)$ and $v_i \equiv v_i(\bar{D}_i)$. This means that only the *difference* between the terminal velocities

---

[1]These include cloud ice, which has zero sedimentation velocity and snow, which has non-zero sedimentation velocity.

of graupel and ice particles is relevant for determining the current density. This expression is Galilean invariant, as can be shown by imposing a vertical velocity, w:

$$j = qn[(w + v_g) - (w + v_i)] = qn(v_g - v_i). \tag{A.56}$$

Note that only the *magnitude* of the terminal fall velocities was considered, but this does not change the fact that Eq. (A.56) is Galilean invariant. The current density, j, is positive because $v_g > v_i$. Physically, this means that there always is an upward flux of positive charge. This corresponds to positive charging of the upper regions of a thunderstorm. Since $v_i \approx 0$ ms^{-1},

$$j = qnv_g = \rho v_g. \tag{A.57}$$

This result is used in section 3.1.3.

A.4   The generator power

The electrical power, P, is given by

$$P = \int_V d^3r \mathbf{E}(\mathbf{r}) \cdot \mathbf{j}(\mathbf{r}), \tag{A.58}$$

where V is the volume of the capacitor. In this application, the plates are vertically stacked and the current density is parallel to the electric field vectors. If A is the area of the plates and d their vertical separation distance, then

$$P = \int_A \int_d dA ds j \mathbf{s} \cdot \mathbf{E} \tag{A.59}$$

$$= \int_A dA dz j \mathbf{e_3} \cdot \mathbf{E} \tag{A.60}$$

$$= \int_A dA j \int_d dz \mathbf{e_3} \cdot \mathbf{E} \tag{A.61}$$

$$= I \int_d d\Phi \tag{A.62}$$

$$= IU. \tag{A.63}$$

I is the electric current, and U is the voltage between the plates. The electric current is simply

$$I = \pi R^2 j. \tag{A.64}$$

In order to determine the voltage, Gauss' law needs to be solved for the electrostatic potential, Φ. The procedure is identical to the determination of the electrostatic field in section A.1 except that the integral is somewhat simpler. Hence, the calculations shall not be repeated here. The solution for one positively-charged plate is given by

$$\Phi(z) = \frac{\sigma}{2\epsilon} \left[\sqrt{R^2 + (z - z_0)^2} - |z - z_0| \right]. \tag{A.65}$$

Superposing the solutions of the negative and positive plates, and taking the potential difference between the plates yields the voltage (see also Boccippio, 2002, p. 1097):

$$U = \Phi(z = 0) - \Phi(z = D) = \frac{\sigma}{\epsilon} \left[\sqrt{R^2 + d^2} - R - d \right].$$ (A.66)

This result is used to derive the 5th-power relation in section 2.5.2.

Appendix B

The COSMO-DE Model

In this appendix some details about the COMSO-DE model which is used in this work are presented. COSMO-DE was originally developed by the German weather service (DWD), where it was called "LMK"[1]. In 1998, the Consortium for Small-Scale Modeling (COSMO) was founded in order to develop the model in a pan-European effort[2]. At DWD, the model is run in two configurations: COSMO-EU covers most of Europe and is run at a horizontal resolution of about 7 km. COSMO-DE covers Germany and parts of the adjacent countries and is run at a horizontal resolution of about 2.8 km. COSMO-DE is nested in the COSMO-EU domain. The COSMO-EU and COSMO-DE domains are shown in Fig. B.1. COSMO-DE is a fully

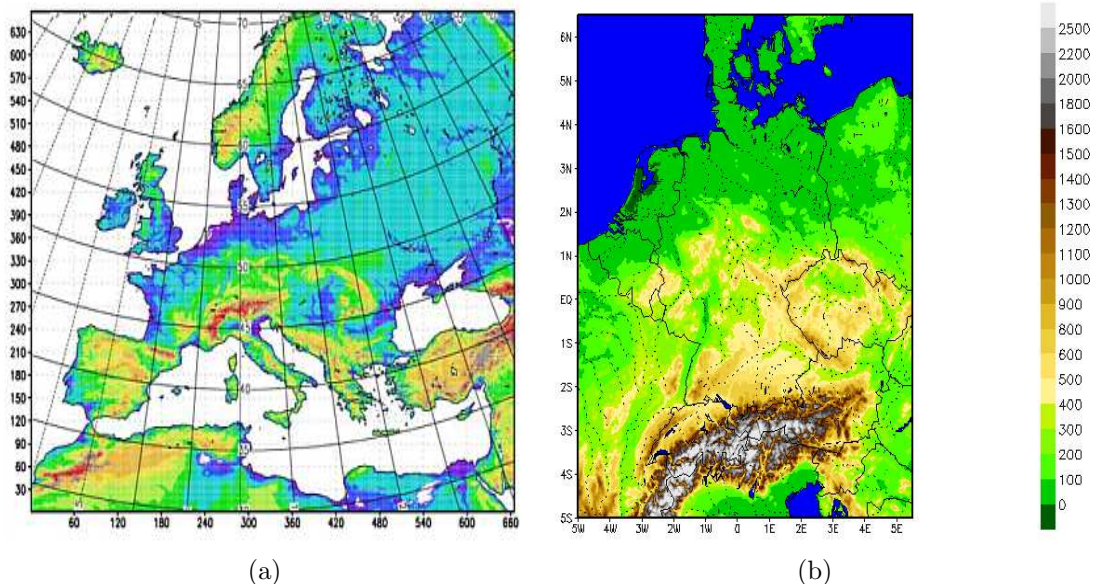(a)   (b)

Figure B.1: COSMO-EU domain (a) and the COSMO-DE domain (b). Images courtesy of DWD.

---

[1]LMK is a German acronym for "Lokal-Modell Kürzesfrist" (very-short range local model).
[2]For more information about this consortium, visit http://www.cosmo-model.org/.

compressible, non-hydrostatic numerical weather prediction model. A hydrostatic base state is assumed, and the prognostic variables are departures from this base state. These are the three velocity components, the perturbation pressure, the perturbation temperature, and the mass fractions of water vapor, cloud water, cloud ice, rain, snow, and graupel. The density is diagnosed using virtual temperature and pressure. The prognostic equations are discretized on an Arakawa-C grid, which is rotated in a way that the equator and the zero meridian are running through central Germany. The time-independent vertical grid is terrain-following, becoming quasi-horizontal with increasing altitude. The vertical resolution varies from about 50 m in thelowestt model layers to about 1,000 m towards the domain top, which is at 22,500 m. Altogether, there are $421 \times 461 \times 50$ gridpoints.

The time integration is performed using a two-time-level Runge-Kutta scheme with a time step of 25 s. Deep moist convection is explicitely resolved and shallow convection is parameterized using the Tiedke scheme.

In this study, the simulations were initialized with analysis fields that contain assimilated radar data. In the operational setup, these data are nudged into the simulation, which was not done in this study. Hourly boundary data from COSMO-EU were merely interpolated to the COSMO-DE grid. This partly resulted in significant spin-up effects during the first few hours into the simulation.

The model was run on a NEC SX-9E vector computer at DWD. Using one node (16 processors), the run time for 24 h was roughly 30 min. The lightning scheme was called every 15 min.

More information about the COSMO model can be found in Doms and Schaettler (2002), Steppeler et al. (2003), and the references therein. Extensive on-line documentation can be found on the COSMO website (http://www.cosmo-model.org).

Appendix C

List of Abbreviations and Symbols

ASCII	American Standard Code for Information Interchange
a	arbitrary variable
A	area of capacitor plates
b	slope of the regression line; arbitrary variable
C	arbitrary constant
CAPE	convective available potential energy
CAPPI	constant-altitude plan position indicator
CG	cloud-to-ground (lightning discharge)
$\pm$CG	positive/negative cloud-to-ground (lightning discharge)
CIN	convective inhibition
COSMO	consortium for small-scale modeling;
	the numerical model developed in this consortium
COSMO-DE	COSMO model with 2.8 km horizontal resolution
COSMO-EU	COSMO model with 7 km horizontal resolution
`csize`	array containing cluster information
d	plate separation distance; cloud depth
D	diameter; displacement error
D_g	diameter of graupel pellets
$\bar{D}_g$	mean diameter of graupel pellets
$\bar{D}_i$	mean diameter of hydrometeors of class i
$\bar{D}_{ice}$	mean diameter of ice pellets
DAS	displacement-amplitude score
DLR	Deutsches Zentrum für Luft- und Raumfahrt e.V.
	(German Aerospace Center)
DMSP	Defense Meteorological Satellites Program
D10	lightning-rate parameterization developed in this study

DWD   Deutscher Wetterdienst (German weather service)

ΔE electric field strength neutralized during a discharge

Δf difference between predicted and observed flash rates, $|f_p - f_L|$

$\Delta \Psi$ Ψ-strength neutralized during a discharge

ΔQ electric charge strength neutralized during a discharge

$\Delta \sigma$ charge per area neutralized during a discharge

ΔW electric energy strength neutralized during a discharge

E electric field strength

$\mathbf{E}(\mathbf{r})$ electrostatic field vector

E_c critical electric field strength

$\mathbf{e}_3$ vertical unit vector

$\bar{E}$ electric field strength after a discharge

ECHAM4   Global circulation model (MPI Hamburg)

EL   equilibrium level

ϵ permittivity

f discharge rate

f_g flash rate based on GETAL01

$f_i(D)$ size distribution function of particle class i

f_k flash rate of the cell labeled k

f_Q discharge rate if $Q = $ const

f_L observed flash rate (LINET)

f_p predicted flash rate

f_{pr} flash rate based on PR92

f_W discharge rate if $W = $ const

f_σ discharge rate if $\sigma = $ const

f_{ymuk} flash rate based on YMUK09

$G(R, d)$ geometric term

GR01   Grewe et al. (2001); their lightning-frequency parameterization

γ lightning efficiency

h plate thickness

H cloud-top height; breakdown altitude

$\bar{H}$ cold cloud depth

H^+ hydrogen cation

$H_2 0$ water

HK76   Hoshen and Kopelman (1976); their algorithm

i arbitrary index

I electric current

IC   intra-cloud (lightning discharge)

I_L	lightning current
j	magnitude of current density; arbitrary index
$\mathbf{j}$	current density
j_d	discharge current density
j_i	current density due to particles of class i
j_l	lightning current density
j^+	generator current with positive charge density
j^-	generator current with negative charge density
k	arbitrary index
l	length scale
LF	low frequency band
LFC	level of free convection
LINET	lightning network (NowCast GmbH)
LIS	lightning imaging sensor
LNO_x	lightning-produced nitrogen (di-)oxide
λ	longitude
m_i	ice-crystal mass (non-sedimenting)
m_g	graupel mass
m_{gc}	corrected graupel mass
m_{s+i}	sum of snow and ice mass
MCS	mesoscale convective system
MSL	mean seal level
n	number of charged particles
N	number of cases
N_i	number of hydrometeors of class i per volume
n_k	accumulated flashes of the cell labeled k
NASA	National Aeronautics and Space Administration
NEC	NEC Corporation (formerly: Nippon Electric Company)
NO_x	nitrogen (di-)oxide
OH^-	hydroxide anion
p	pressue
P	electric power
POLDIRAD	polarimetric diversity radar
PPI	plan position indicator
PR92	Price and Rind (1992); their approach
ϕ	latitude; azimuthal angle
Φ	electrostatic potential; convective mass flux
Ψ	Arbitrary variable uniquely describing a breakdown criterion

Ψ_c	Ψ at critical field strength
$\bar{\Psi}$	Ψ after a discharge
q	charge magnitude on individual hydrometeors
q_g	electric charge carried on a graupel pellet
$q_i(D)$	charge on hydrometeor of class i and diameter D
q_{ice}	electric charge carried on an ice crystal
Q	electric charge
r	Pearson's correlation coefficient; radial distance from plate center
$\mathbf{r} = (x, y, z)$	position vector
$\mathbf{r}' = (x', y', z')$	integration dummy variable
R	individual gas constant of dry air; plate radius
R_k	radius of the capacitor labeled k
RGR	relative growth rate
RHI	range height indicator
$RMSE$	root mean square error
ρ	charge density
ρ_c	charge density in the generator current
ρ_i	charge density due to charged particles of class i
$\bar{\rho}_i$	spectral charge density due to charged particles of class i
ρ^+	magnitude of positive charge density
ρ^-	magnitude of negative charge density
σ	electric charge per unit area; factor in Gauss function
t	time
T	temperature; time for initial charging
TOA	time of arrival
T_v'	perturbation virtual temperature
TRMM	Tropical Rainfall Measuring Mission
τ	time to replenish the electric fild after a discharge
U	voltage
UTC	universal time coordinated
v	charge velocity
v_g	terminal velocity of graupel; its magnitude
v_{ice}	magnitude of terminal velocity of ice crystals
VLF	very low frequency band
w	vertical velocity
W	electrostatic energy
x	zonal Cartesian coordinate
ξ	substitution for x

y	meridional Cartesian coordinate
YMUK09	Yoshida et al. (2009); their approach
η	field neutralization efficiency; substitution for y
η_Ψ	Ψ-neutralization efficiency
z	vertical Cartesian coordinate
z_1, z_2	integration boundaries
ζ	substitution for z

Bibliography

Aldridge, M. L.: 2008, *A finite state machine approach to cluster identification using the Hoshen-Kopelman algorithm*, Ph.D. Thesis, University of Tennessee, Knoxville.

Andrews, P., Cats, G., Dent, D., Gertz, M. and Ricard, J. L.: 1994, European Standards for Writing and Documenting Exchangeable Fortran 90 Code, ECMWF.

Baker, B., Baker, M. B., Jayaratne, E. R., Latham, J. and Saunders, C. P. R.: 1987, The influence of diffusional growth rates on the charge transfer accompanying rebounding collisions between ice crystals and soft hailstones, *Quart. J. Roy. Met. Soc* **113**, 1193–1215.

Barthe, C., Molinie, G. and Pinty, J.: 2005, Description and first results of an explicit electrical scheme in a 3D cloud resolving model, *Atmos. Res.* **76**, 95–113.

Betz, H., Schmidt, K. and Oettinger, P.: 2009, LINET – An International VLF/LF Lightning Detection Network in Europe, *Lightning: Principles, Instruments and Applications, Eds. H.-D. Betz, U. Schumann, and P. Laroche*, Springer, pp. 115–140.

Bluestein, H. B. and Parks, C. R.: 1983, A synoptic and photographic climatology of low-precipitation severe thunderstorms in the southern plains, *Mon. Weather Rev.* **111**, 2034–2046.

Blyth, A. M., Christian, H. J., Driscoll, K., Gadian, A. M. and Latham, J.: 2001, Determination of ice precipitation rates and thunderstorm anvil ice contents from satellite observations of lightning, *Atmos. Res.* **59**, 217–229.

Boccippio, D.: 2002, Lightning scaling relations revisited, *J. Atmos. Sci.* **59**, 1086–1104.

Bright, D. R., Jewell, R. E. and Weiss, S. J.: 2005, A physically based parameter for lightning prediction and its calibration in ensemble forecasts, *Preprints, Conf. on Meteorological Applications of Lightning Data, San Diego, CA, Amer. Meteor. Soc.*

Brooks, H. E. and Wilhelmson, R. B.: 1995, Hodograph curvature and updraft intensity in numerically modeled supercells, *J. Atmos. Sci.* **50**, 1824–1833.

Byers, H. and Braham, R.: 1949, *The thunderstorm*, US Dept. of Commerce, Weather Bureau.

Cheze, J. and Sauvageot, H.: 1997, Area-average rainfall and lightning activity, *J. Geophys. Res.* **102**, 1707–1716.

Coleman, L., Marshall, T., Stolzenburg, M., Hamlin, T., Krehbiel, P., Rison, W. and Thomas, R.: 2003, Effects of charge and electrostatic potential on lightning propagation, *J. Geophys. Res.* **108**, 4298.

Colman, B. R.: 1990, Thunderstorms above frontal surfaces in environments without positive CAPE. Part II: Organization and instability mechanisms, *Mon. Weather Rev.* **118**, 1123–1144.

Constantin, J., Berry, M. and Vander Zanden, B.: 1997, Parallelization of the Hoshen-Kopelman algorithm using a finite state machine, *Int. J. High. Perform. C.* **11**, 34.

Cooke, C. M., Williams, E. R. and Wright, E. A.: 1982, Electrical discharge propagation in space-charged PMMA, *Conference on Electrical Insulation, Inst. Electron. Eng., Philadelphia* pp. 6059–6070.

Cooray, V.: 1997, Energy dissipation in lightning flashes, *J. Geophys. Res.* **102**, 21401–21410.

Craig, G. C., Keil, C. and Leuenberger, D.: 2009, Impact of radar rainfall data assimilation on forecasts of cumulus convection, *Quart. J. Roy. Meteor. Soc., in revision* .

Dahl, J. M. L.: 2006, Supercells - Their Dynamics and Prediction, *M.Sc. Thesis, Free University of Berlin, Germany, 121 pp* .

Dash, J. G., Mason, B. L. and Wettlaufer, J. S.: 2001, Theory of charge and mass transfer in ice-ice collisions, *J. Geophys. Res.* **106**, 20395–20402.

Davies-Jones, R.: 2002, Linear and nonlinear propagation of supercell storms, *Journal of the Atmospheric Sciences* **59**, 3178–3205.

Davies-Jones, R. P., Burgess, D. and Foster, M.: 1990, Test of helicity as a tornado forecast parameter, *Preprints, 16th Conf. on Severe Local Storms, Kananaskis Park, AB, Canada, Amer. Meteor. Soc.*, pp. 588–592.

Deierling, W., Petersen, W., Latham, J., Ellis, S. and Christian, H.: 2008, The relationship between lightning activity and ice fluxes in thunderstorms, *J. Geophys. Res.* **113**, D15210.

Doms, G. and Schaettler, U.: 2002, A description of the nonhydrostatic regional model LM, *Part I: Dynamics and numerics. Deutscher Wetterdienst (German Weather Service); available online at http://cosmo-model* .

Doms, G. and Schaettler, U.: 2004, *COSMO-DE Documentations. Deutscher Wetterdienst, Offenbach*, available from: http://www.cosmo-model.org/public/documentation.htm.

Doswell, C. A.: 1987, The distinction between large-scale and mesoscale contribution to severe convection: A case study example, *Wea. Forecasting* **2**, 3–16.

Doswell, C. A. and Burgess, D.: 1993, *Tornadoes and tornadic storms: A review of conceptual models*, Vol. 79, AGU.

Doswell, C. A. and Markowski, P.: 2004, Is buoyancy a relative quantity?, *Mon. Weather Rev.* **132**, 853–863.

Doswell, C. A., Weber, D. B., Loftus, A. M., Baranowski, B. C. and DuFran, Z. M.: 2007, Preliminary results: Environmental controls on updraft regeneration frequency in numerically-simulated, isolated multicellular convection, *Extended abstracts, 4th European Conf. on Severe Storms, Trieste, Italy*.

Driscoll, K., Blakeslee, R. and Baginski, M.: 1992, A modeling study of the time-averaged electric currents in the vicinity of isolated thunderstorms, *J. Geophys. Res.* **97**.

Fehr, T.: 2000, *Meskalige Modellierung der Produktion und des dreidimensionalen Transports von Stickoxiden durch Gewitter*, Forschungsbericht, Deutsches Zentrum für Luft- und Raumfahrt e.V.

Finke, U.: 2009, Optical detection of lightning from space, *Lightning: Principles, Instruments and Applications, Eds. H.-D. Betz, U. Schumann, and P. Laroche*, Springer, pp. 271–286.

Finkelstein, D. and Powell, J. R.: 1970, Earthquake prediction: Electromagnetic emissions before earthquakes, *Nature* **301**, 377.

Grewe, V.: 2009, Impact of lightning on air chemistry and climate, *Lightning: Principles, Instruments and Applications, Eds. H.-D. Betz, U. Schumann, and P. Laroche*, Springer, pp. 537–549.

Gurevich, A., Milikh, G. and Roussel-Dupre, R.: 1992, Runaway electron mechanism of air breakdown and preconditioning during a thunderstorm, *Phys. Lett. A* **165**, 463–468.

Helsdon, J. H. J. and Farley, R. D.: 1987, A numerical modeling study of a Montana thunderstorm: 2. Model results versus observations involving electrical aspects, *J. Geophys. Res.* **92**, 5661–5675.

Heymsfield, A. and Kajikawa, M.: 1987, An improved approach to calculating terminal velocities of plate-like crystals and graupel, *J. Atmos. Sci.* **44**, 1088–1099.

Höller, H., Hagen, M., Meischner, P. F., Bringi, V. N. and Hubbert, J.: 1994, Life cycle and precipitation formation in a hybrid-type hailstorm revealed by polarimetric and doppler radar measurements, *J. Atmos. Sci.* **51**, 2500–2522.

Hoshen, J. and Kopelman, R.: 1976, Percolation and cluster distribution. I. Cluster multiple labeling technique and critical concentration algorithm, *Phys. Rev. B* **14**, 3438–3445.

Houze, R.: 1993, *Cloud Dynamics*, Academic Press.

Huntrieser, H., Schumann, U., Schlager, H., Höller, H., Giez, A., Betz, H. D., Brunner, D., Forster, C., Pinto Jr, O. and Calheiros, R.: 2008, Lightning activity in Brazilian thunderstorms during TROCCINOX: implications for NOx production, *Atmos. Chem. Phys.* **8**, 921–953.

Jacobson, E. and Krider, E.: 1976, Electrostatic field changes produced by Florida lightning, *J. Atmos. Sci.* **33**, 103–117.

Jayaratne, E.: 1998, Density and surface temperature of graupel and the charge separation during ice crystal interactions, *J. Geophys. Res.* **103**, 13,957–13,961.

Johns, R. and Doswell, C. I.: 1992, Severe local storms forecasting, *Weather Forecast.* **7**, 588–612.

Keil, C. and Craig, G. C.: 2007, A displacement-based error measure applied in a regional ensemble forecasting system, *Mon. Weather Rev.* **135**, 3248–3259.

Keil, C. and Craig, G. C.: 2009, A displacement and amplitude error based score employing an optical flow technique, *Weather Forecast., submitted* .

Klemp, J. B. and Wilhelmson, R. B.: 1978, The simulation of three-dimensional convective storm dynamics, *J. Atmos. Sci.* **35**, 1070–1096.

Larsen, H. and Stansbury, E.: 1974, Association of lightning flashes with precipitation cores extending to height 7 km, *J. Atmos. Terr. Phys.* **36**, 1547.

Lilly, D.: 1986, The structure, energetics and propagation of rotating convective storms. Part II: Helicity and storm stabilization, *J. Atmos. Sci.* **43**, 126–140.

Lu, G., Cummer, S. A., Li, J., Han, F., Blakeslee, R. J. and Christian, H. J.: 2009, Charge transfer and in-cloud structure of large-charge-moment positive lightning strokes in a mesoscale convective system, *Geophysical Research Letters* **36**, L15805.

MacGorman, D. R. and Rust, W. D.: 1998, *The electrical nature of storms*, Oxford University Press, USA.

MacGorman, D., Straka, J. and Ziegler, C.: 2001, A lightning parameterization for numerical cloud models, *J. Appl. Met.* **40**, 459–478.

Maggio, C., Marshall, T. and Stolzenburg, M.: 2009, Estimations of charge transferred and energy released by lightning flashes, *J. Geophys. Res.* **114**, D14203.

Mansell, E.: 2000, *Electrification and lightning in simulated supercell and non-supercell thunderstorms*, Ph.D. Thesis, University of Oklahoma.

Mapes, B. E. .: 1993, Gregarious tropical convection, *J. Atmos. Sci.* **50**, 2026–2037.

Marshall, T., McCarthy, M. and Rust, W.: 1995, Electric field magnitudes and lightning initiation in thunderstorms, *J. Geophys. Res.* **100**.

Marshall, T., Stolzenburg, M., Maggio, C., Coleman, L., Krehbiel, P., Hamlin, T., Thomas, R. and Rison, W.: 2005, Observed electric fields associated with lightning initiation, *Geophys. Res. Lett.* **32**.

Meschede, D. and Vogel, H.: 2006, *Gerthsen Physik*, 23 edn, Springer.

NCAR: 1984, *The National STORM-Program: STORM-central phase*, Interagency team for STORM-central, NCAR, Boulder, CO.

Nolting, W.: 2004, *Grundkurs Theoretische Physik 3: Elektrodynamik*, Springer.

Ogawa, T.: 1995, Lightning currents, *Handbook of Atmospheric Electrodynamics* **1**, 93–136.

Petersen, D., Bailey, M., Beasley, W. and Hallett, J.: 2008, A brief review of the problem of lightning initiation and a hypothesis of initial lightning leader formation, *J. Geophys Res.* **113**, D17205.

Phelps, C.: 1974, Positive streamer system intensification and its possible role in lightning initiation, *J. Atmos. Terr. Phys.* **36**, 103–111.

Pickering, K., Huntrieser, H. and Schumann, U.: 2009, Lightning and NO_x production in global models, *Lightning: Principles, Instruments and Applications, Eds. H.-D. Betz, U. Schumann, and P. Laroche*, Springer, pp. 551–571.

Price, C. and Rind, D.: 1992, A simple lightning parameterization for calculating global lightning distributions, *J. Geophys. Res.* **97**.

Pruppacher, H. R. and Klett, J. D.: 1997, *Microphysics of clouds and precipitation, 2nd edition*, Kluwer Academic Publishers.

Rakov, V. and Uman, M.: 2003, *Lightning: physics and effects*, Cambridge Univ. Pr.

Rawlins, F.: 1982, A numerical study of thunderstorm electrification using a three dimensional model incorporating the ice phase, *Quart. J. Roy. Meteor. Soc.* **108**, 779–800.

Rotunno, R.: 1993, Supercell thunderstorm modeling and theory, *The Tornado: Its Structure, Dynamics, Prediction, and Hazards* pp. 57–73.

Rotunno, R. and Klemp, J.: 1982, The influence of the shear-induced pressure gradient on thunderstorm motion, *Mon. Weather Rev.* **110**, 136–151.

Rust, W., MacGorman, D., Bruning, E., Weiss, S., Krehbiel, P., Thomas, R., Rison, W., Hamlin, T. and Harlin, J.: 2005, Inverted-polarity electrical structures in thunderstorms in the severe thunderstorm electrification and precipitation study (steps), *Atmos. Res.* **76**, 247–271.

Saunders, C. P. R.: 2008, Charge separation mechanisms in clouds, *Space Sci. Rev.* **137**, 335–353.

Saunders, C. P. R. and Peck, S.: 1998, Laboratory studies of the influence of the rime accretion rate on charge transfer during crystal/graupel collisions, *J. Geophys. Res.* **103**.

Schmidt, K.: 2007, Ortung und Analyse von Blitz-Entladungen mittels Registrierung von VLF-Atmospherics innerhalb eines Messnetzes.

Schroth, A. C., Chandra, M. S. and Meischner, P. F.: 1988, A C-Band coherent polarimetric radar for propagation and cloud physics research, *J. Atmos. Ocean. Tech.* **5**, 803–822.

Schumann, U. and Huntrieser, H.: 2007, The global lightning-induced nitrogen oxides source, *Atmos. Chem. Phys* **7**, 3823–3907.

Shackford, C. R.: 1960, Radar indications of a precipitation-lightning relationship in New England thunderstorms, *J. Atmos. Sci.* **17**, 15–19.

Shao, X. M., Stanley, M., Regan, A., Harlin, J., Pongratz, M. and Stock, M.: 2006, Total lightning observations with the new and improved Los Alamos Sferic Array (LASA), *J. of Atmos. Ocean. Tech.* **23**, 1273–1288.

Solomon, R., Schroeder, V. and Baker, M. B.: 2001, Lightning initiation - conventional and runaway-breakdown hypotheses, *Quart. J. Roy. Meteor. Soc.* **127**, 2683–2704.

Stephan, K., Klink, S. and Schraff, C.: 2008, Assimilation of radar-derived rain rates into the convective-scale model COSMO-DE at DWD, *Quart. J. Roy. Meteor. Soc.* **134**, 1315–1326.

Steppeler, J., Doms, G., Schaettler, U., Bitzer, H. W., Gassmann, A., Damrath, U. and Gregoric, G.: 2003, Meso-gamma scale forecasts using the nonhydrostatic model LM, *Meteorol. and Atmos. Phys.* **82**, 75–96.

Stolzenburg, M. and Marshall, T. C.: 2009, *Electric field and charge structure in lightning-producing clouds.*

Stolzenburg, M., Rust, W., Smull, B. and Marshall, T.: 1998, Electrical structure in thunderstorm convective regions 1. Mesoscale convective systems, *J. Geophys. Res.* **103**.

Takahashi, T.: 1978, Riming electrification as a charge generation mechanism in thunderstorms, *J. Atmos. Sci.* **35**, 1536–1548.

Tapia, A., Smith, J. and Dixon, M.: 1998, Estimation of convective rainfall from lightning observations, *J. Appl. Met.* **37**, 1497–1509.

Tost, H., Jockel, P. and Lelieveld, J.: 2007, Lightning and convection parameterisations–uncertainties in global modelling, *Atmos. Chem. Phys* **7**, 4553–4568.

Trapp, R. and Weisman, M.: 2003, Low-level mesovortices within squall lines and bow echoes. Part II: Their genesis and implications, *Mon. Weather Rev.* **131**, 2804–2823.

Uman, M. A.: 2001, *The lightning discharge*, Dover.

Vonnegut, B.: 1963, *Some facts and speculations concerning the origin and role of thunderstorm electricity*, Vol. 5.

Weisman, M., Klemp, J. and Rotunno, R.: 1988, Structure and evolution of numerically simulated squall lines, *J. Atmos. Sci.* **45**, 1990–2013.

Weisman, M. L.: 2001, Bow echoes: A tribute to T. T. Fujita, *B. Am. Meteorol. Soc.* **82**, 97–116.

Williams, E.: 1981, Thunderstorm electrification: precipitation versus convection, *Ph.D. Thesis, Massachussets Institute of Technology* .

Williams, E., Cooke, C. and Wright, K.: 1985, Electrical discharge propagation in and around space charge clouds, *J. Geophys. Res.* **90**, 6059–6070.

Williams, E. R.: 1985, Large-scale charge separation in thunderclouds, *J. Geophys. Res.* **90**, 6013–6025.

Williams, E. R.: 1989, The tripole structure of thunderstorms, *J. Geophys. Res.* **94**, 13151–13167.

Williams, E. R.: 2001, The electrification of severe storms, *Severe Convective Storms, Meteor. Monogr. 28, No. 50*, Amer. Met. Soc., pp. 527–561.

Yoshida, S., Morimoto, T., Ushio, T. and Kawasaki, Z.: 2009, A fifth-power relationship for lightning activity from Tropical Rainfall Measuring Mission satellite observations, *J. Geophys. Res.* **114**, D09104.

Zinner, T., Mannstein, H. and Tafferner, A.: 2008, Cb-TRAM: Tracking and monitoring severe convection from onset over rapid development to mature phase using multi-channel Meteosat-8 SEVIRI data, *Meteorol. Atmos. Phys.* **101**, 191–210.

Zipser, E. J.: 1994, Deep cumulonimbus cloud systems in the tropics with and without lightning, *Mon. Weather Rev.* **122**, 1837–1851.

Acknowledgments

I would like to thank Prof. Ulrich Schumann for having advised this work, as well as for his helpful suggestions, his motivation, and his kind support during the course of this study.

I'm also grateful to Prof. George Craig for the many discussions that not only helped improving this work, but also deepened my understanding about atmospheric physics and about scientific writing. Also, he co-examined this work, which is gratefully acknowledged.

Prof. H.-D. Betz kindly provided the LINET data, without which this study could not have been carried out.

Discussions with Hartmut Höller, Kersten Schmidt, and Vera Meyer helped me deepen my understanding of atmospheric electricity. Hartmut also provided valuable suggestions especially towards the end of the study.

Christian Keil patiently supported me especially during the familiarization with the COSMO source code.

Axel Seifert and Ulrich Schättler (both DWD) helped out whenever I encountered technical problems (especially with the new vector processors at DWD). Furthermore, conversations with Axel deepened my knowledge about the microphysics scheme in COSMO-DE and about cloud microphysics in general. The computations were performed at DWD, which is gratefully acknowledged.

Whenever technical problems arose at DLR, Winfried Beer found a quick solution.

Dennis Boccippio, Ted Mansell, Earle Williams, Cathan Cooke, and Rohan Jayaratne engaged in very helpful discussions with me about atmospheric electricity.

Volker Grewe kindly helped me with fitting COSMO-DE data into his flash-rate

parameterization from 2001, making its application to COSMO-DE possible.

Apart from these contributions, more indirect factors were of great help while working on this study:

My room mates Jana and Christian, and my next-door neighbor Andreas, maintained a very nice and relaxed atmosphere, which made it easy to come to the office even in exhausting periods.

My colleagues and fellow students, especially Kirstin, Julia, Helge, and many others (too numerous to acknowledge individually), always endured me when I needed a break and kept them from working.

My family and friends always believed in me and provided support in many ways, which was indispensable during the course of this work.

Finally, I would like to thank the late Albert Ammons and Franz Liszt for having composed such inspiring music, which often provided the energy to focus on this work.

Curriculum Vitae

Johannes M. L. Dahl, Munich

Born on 29 April 1980 in Berlin, Germany

EDUCATION AND PROFESSIONAL TRAINING:

2007–2010	Ph.D. student at DLR-Oberpfaffenhofen (German Aerospace Center) Institute of Atmospheric Physics (IPA)
2000–2006	Study of meteorology at the Free University of Berlin
1999–2000	Community service at Caritas, Berlin
1992–1999	Schadow-Gymnasium Berlin-Zehlendorf (high school)